Supporting Information

Position of substituents directs the electron transfer properties of entatic state complexes: new insights from guanidine-quinoline copper complexes

Joshua Heck,[a] Anastasia Kucenko,[a] Alexander Hoffmann[a] and Sonja Herres-Pawlis*[a]

a. Institute of Inorganic Chemistry, RWTH Aachen University, Landoltweg 1a, 52074 Aachen, Germany. E-mail: sonja.herres-pawlis@ac.rwth-aachen.de

Table of contents

1 Experimental Part

1.1 General aspects, chemicals and solvents

All reactions and manipulations that require inert conditions were carried out under nitrogen atmosphere. Nitrogen was dried by passage through a column filled with SICAPENT®. If necessary, the solvents were dried by standard literature procedures and degassed by three circles of freeze pump thaw.[1] [Cu(MeCN)$_4$]PF$_6$, [Cu(MeCN)$_4$](OTf)$_2$ and the Vilsmeier salt chloro-*N,N,N',N'*-tetramethylformamidinium chloride (TMG-VS) were synthesized according to the literature.[2,3] All other chemicals were purchased from commercial suppliers and used without further purification.

1.2 Analytics and compound purification

1.2.1 Nuclear magnetic resonance spectroscopy

The nuclear magnetic resonance (NMR) spectra were recorded on a Bruker Avance III HD 400 or a Bruker Avance II 400 nuclear resonance spectrometer at 25 °C. The ^{1}H NMR spectra were referenced to the solvent residual signal and the ^{13}C{^{1}H} NMR spectra were referenced to the solvent signal. The solvent signals in the ^{1}H and ^{13}C{^{1}H} NMR spectra were defined relative to the external standard tetramethylsilane (TMS) as reported in the literature.[4] The chemical shifts of the compounds were assigned with the use of two-dimensional NMR spectroscopic experiments (COSY, HSQC, HMBC, APT). For the Bruker Avance III HD 400, the software Topspin (Version 3.5 pl 7) from Bruker Corporation and for the Bruker Avance II 400, the software TopSpin (Version 2.1) from Bruker Corporation were used for data acquisition. For visualization and examination of the NMR spectra the software MestReNova (Version 12.0.1-20560) from Mestrelab Research was used. Selected NMR spectroscopic data were deposited as original data in the Chemotion Repository and are published under an Open Access model.[5,6] The link to the original data is given in the analytical description.

1.2.2 Electron spray ionization high resolution mass spectrometry

The electron spray ionization (ESI) high-resolution (HR) mass spectra were recorded on an UHR-TOF Bruker Daltonik maXis II or a ThermoFisher Scientific LTQ Orbitrap XL. The measurements were performed on an UHR-TOF Bruker Daltonik maXis II, an ESI-quadrupole time-of-flight (qToF) mass spectrometer capable of a resolution of at least 80.000 FWHM.

Detection was either in positive or in the negative ion mode. The mass spectrometer was calibrated subsequently to every experiment via direct infusion of a L-proline sodium salt solution, which provided a *m/z* range of singly charged peaks up to 3000 Da in both ion modes. For the ThermoFisher Scientific LTQ Orbitrap XL the source voltage was 4.49 kV and the capillary temperature was 299.54 °C. The tube lens voltage was set between 110 and 130 V. For the Bruker Daltonik maXis II, the software otofControl (Version 6.3, Build 0.5) and Compass DataAnalysis (Version 5.3, Build 556.396.6383) from Bruker Corporation and for the ThermoFisher Scientific LTQ Orbitrap XL, the software Thermo Xcalibur (Version 4.5.445.18) were used for data acquisition and examination. Selected ESI-HRMS data were deposited as original data in the Chemotion Repository and are published under an Open Access model.[5,6] The link to the original data is given in the analytical description.

1.2.3 Fourier transform infrared spectroscopy

The Fourier transform infrared (FTIR) spectra were recorded on a Shimadzu IRTracer 100 using a CsI beam splitter in combination with an attenuated total reflectance (ATR) unit (Quest model from Specac utilising a robust monolithic crystalline diamond) in a resolution of 2 cm^{-1}. For data acquisition, the software LabSolution IR (Version 2.15) from Shimadzu Corporation was used. Selected FTIR spectroscopic data were deposited as original data in the Chemotion Repository and are published under an Open Access model.[5,6] The link to the original data is given in the analytical description.

1.2.4 Thin layer chromatography

Thin layer chromatography (TLC) was performed with TLC sheets from MACHEREY-NAGEL pre-coated with a layer of silica gel 60 with a thickness of 0.20 mm and a fluorescent indicator.

1.2.5 Column chromatography

Column chromatography was performed with Geduran® Si 60 (40-63 μm) from Merck or with MP Alumina B - Super I from MP Biomedicals.

1.2.6 Single-crystal X-ray diffraction

The ellipsoid plots and crystallographic data of **L7**, **C11−PF₆**, **(C12+OTf)−OTf**, **C13−PF₆** and **C14−OTf** are presented in Fig. S1 to S5 and in Table S1 and S2. The data were collected with a four-circle goniometer Stoe Stadivari with Dectris Pilatus3 R 200 K hybrid pixel detector using GeniX 3D high flux Mo-K$_\alpha$ radiation (λ = 0.71073 Å; **L7**, **C11−PF₆**, **(C12+OTf)−OTf** and **C13−PF₆**,)

or GeniX 3D high flux Cu-K$_\alpha$ radiation (λ = 1.54186 Å; **C14−OTf**) at 100 K. The temperature was controlled by an Oxford Cryostream 800. Crystals were mounted on cryoloops with perfluorinated oil. Data were collected with X-Area Pilatus[7], indexed with X-Area Recipe[8] and integrated with X-Area Integrate.[9] A spherical absorption correction was performed with STOE X-Red32 followed by a multi-scan absorption correction and scaling of reflections with X-Area LANA.[10]

The structures were solved by intrinsic phasing (ShelXT[11]) or direct methods (ShelXS[12]) and refined against F^2 with the full-matrix least-square method of ShelXL[13] using the graphical user interface ShelXle.[14] Non-hydrogen atoms were refined with anisotropic displacement parameters. All hydrogen atoms were localized at idealized positions and refined with isotropic displacement parameters. All methyl groups were allowed to rotate but not to tip.

In **C14−OTf**, it was not possible to model the disordered molecule diethyl ether per asymmetric unit (162 Å^3, 42 electrons) adequately and the data sets were treated with the SQUEEZE routine as implemented in PLATON.[15,16]

Full crystallographic data of **L7**, **C11−PF$_6$**, **(C12+OTf)−OTf**, **C13−PF$_6$** and **C14−OTf** have been deposited with the Cambridge Crystallographic Data Centre as supplementary no. CCDC−2358203 for **L7**, CCDC − 2358204 for **C11−PF$_6$**, CCDC − 2358205 for **(C12+OTf)−OTf**, CCDC − 2358206 for **C13−PF$_6$** and CCDC − 2358207 for **C14−OTf**. Copies of the data can be obtained free of charge on application to CCDC, 12 Union Road, Cambridge CB2 1EZ, UK (fax: (+44)1223-336-033; e-mail: deposit@ccdc.cam.ac.uk).

1.2.7 Cyclic voltammetry

The cyclic voltammetry (CV) measurements were performed with a Metrohm Autolab PGSTAT 101 potentiostat using a three-electrode arrangement with a Pt disc working electrode (1 mm diameter), a Pt wire as counter electrode and an Ag/AgCl reference electrode. The measurements were performed in MeCN containing 100 mM NBu$_4$PF$_6$ with a sample concentration of 1 mM at room temperature. The redox potentials of the copper complex redox pairs [Cu(TMG4Rqu)$_2$]$^{+/2+}$ (**R6** and **R7**) were measured starting from the corresponding Cu(I) complexes [Cu(TMG4Rqu)$_2$]PF$_6$ and the redox potential of [Co(bpy)$_3$]$^{2+/3+}$ was measured starting from [Co(bpy)$_3$](PF$_6$)$_3$. Ferrocene was added as an internal standard after the measurements of the sample and all potentials are referenced relative to the Fc/Fc$^+$ potential.

Cyclic voltammograms were measured with 200 mV s^{-1}, 100 mV s^{-1}, 50 mV s^{-1} and 20 mV s^{-1}. For data acquisition and examination, the software NOVA 2.1.5 (Build 7691) from Metrohm Autolab was used. For visualization of the cyclic voltammograms, the software OriginPro 2021b (Version 9.8.5.212) from OriginLab was used.

The cyclic voltammograms of **R1**-**R7** are available via the Chemotion Repository.

[Cu(TMGqu)$_2$]$^{+/2+}$ (**R1**): https://dx.doi.org/10.14272/UVLHGRADYISRGZ-UHFFFAOYSA-N.1

[Cu(TMG2Mequ)$_2$]$^{+/2+}$ (**R2**): https://dx.doi.org/10.14272/DMWOEMCLSHNHOH-UHFFFAOYSA-N.2

[Cu(TMG2^{c}Hexqu)$_2$]$^{+/2+}$ (**R3**): https://dx.doi.org/10.14272/GCLZBRQZKMRROK-UHFFFAOYSA-N.2

[Cu(TMG2Meequ)$_2$]$^{+/2+}$ (**R4**): https://dx.doi.org/10.14272/JBXRXORXEOBVKS-UHFFFAOYSA-N.2

[Cu(TMG4NMe$_2$qu)$_2$]$^{+/2+}$ (**R5**): https://dx.doi.org/10.14272/AAVQNGKZFKMISP-UHFFFAOYSA-N.1

[Cu(TMG4Mequ)$_2$]$^{+/2+}$ (**R6**): https://dx.doi.org/10.14272/reaction/SA-FUHFF-UHFFFADPSC-UXMQGFPLGU-UHFFFADPSC-NUHFF-NUHFF-NUHFF-ZZZ

[Cu(TMG4Meequ)$_2$]$^{+/2+}$ (**R7**): https://dx.doi.org/10.14272/reaction/SA-FUHFF-UHFFFADPSC-YUTCBXVUPC-UHFFFADPSC-NUHFF-NUHFF-NUHFF-ZZZ

1.2.8 UV/Vis spectroscopy

The UV/Vis spectra were recorded with a Cary 60 spectrophotometer from Agilent Technologies in combination with quartz glass cuvettes (1 mm, QS) at room temperature. The solutions of the copper complexes (**C11−PF$_6$**-**C14−OTf**) in MeCN (c = 1 mM) were prepared *in situ* with one equiv. of [Cu(MeCN)$_4$]PF$_6$ for the Cu(I) complexes or one equiv. of [Cu(MeCN)$_4$](OTf)$_2$ for the Cu(II) complexes, respectively, and two equiv. of the appropriate ligand. For data acquisition, the software Cary WinUV (Version 5.1.3.1042) from Agilent Technologies was used. For visualization of the UV/Vis spectra, the software OriginPro 2021b (Version 9.8.5.212) from OriginLab was used.

1.2.9 Stopped-flow UV/Vis spectroscopy

The stopped-flow UV/Vis spectroscopic measurements were performed with a HI-TECH Scientific SF-61SX2 device with a diode array detector. The optical light path for transmission of the quartz glass cuvette was 10 mm. The mixing time is given by HI-TECH to amount to 2 ms.

UV/Vis spectra in a wavelength range of 300 nm to 800 nm were detected with a temporal resolution of 1.5 ms. The analyses were carried out with the TgK Scientific program Kinetic Studio 4.0.8.18533. For visualization and examination of the results, the software OriginPro 2021b (Version 9.8.5.212) from OriginLab was used.

The cross reactions of the Cu(I) complexes (**C11−PF₆** and **C13−PF₆**) with the counter complex [Co(bpy)₃](PF₆)₃ were monitored. To measure the kinetic of the cross reaction, a solution of each Cu(I) complex (**C11−PF₆** and **C13−PF₆**) in MeCN ($c = 0.2$ mM) was mixed with five differently concentrated solutions of [Co(bpy)₃](PF₆)₃ in MeCN ($c = 1$ mM, 1.5 mM, 2 mM, 2.5 mM, 3 mM). The solutions of the Cu(I) complexes were prepared *in situ* with one equiv. of [Cu(MeCN)₄]PF₆ and two equiv. of the corresponding ligand. For every concentration of [Co(bpy)₃](PF₆)₃, 15 measurements were performed. The whole measurement was repeated twice for each Cu(I) complex.

Due to the five differently concentrated solutions of the counter complex [Co(bpy)₃](PF₆)₃, the ionic strength was not the same for all analyzed cross reactions and varied depending on the concentration of the counter complex. The ionic strength influences the activity coefficients of the reactants. However, the influence on the activity coefficient is not significant for the determination of k_{12}. Therefore, for simplification, the concentrations and not the activity coefficients were considered for the determination of k_{12}.
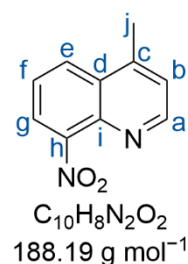
1.3 Ligand synthesis

1.3.1 Synthesis of TMG4Mequ (L7) and corresponding precursors

1.3.1.1 Resynthesis of 4-methyl-8-nitroquinoline (4-Me-8-NO₂-qu)

The synthesis was performed following a modified procedure of the literature.[17,18]

4-Methylquinoline (20.0 g, 18.5 mL, 139.7 mmol, 1 equiv.) was dissolved in conc. H₂SO₄ (30 mL). A mixture of fuming HNO₃ (22.0 g, 14.6 mL, 349.2 mmol, 2.5 equiv.) and conc. H₂SO₄ (15 mL) was added dropwise under stirring over a period of 30 min at 0 °C. The reaction mixture was stirred for 18 h at room temperature and then poured on ice. The mixture was neutralized (pH ≈ 7) with an aqueous NaOH solution (15 M). The formed solid was filtered off, washed with water and then dissolved in DCM (650 mL). The organic layer was dried over Na₂SO₄ and filtered. The solvent was removed under reduced pressure. The resulting solid was purified by column

chromatography (isohexane:ethyl acetate = 3:2, Geduran, R_f = 0.57). 4-Methyl-8-nitroquinoline was obtained as a colorless solid (11.71 g, 62.2 mmol, 44.6 %).

¹H NMR (400 MHz, CDCl₃): δ = 8.88 (d, J = 4.4 Hz, 1H, a), 8.19 (dd, J = 8.5, 1.4 Hz, 1H, e), 7.96 (dd, J = 7.5, 1.3 Hz, 1H, g), 7.61 (dd, J = 8.5, 7.5 Hz, 1H, f), 7.36 (dd, J = 4.4, 1.1 Hz, 1H, b), 2.75 (d, J = 1.0 Hz, 3H, j) ppm.

¹³C{¹H} NMR (101 MHz, CDCl₃): δ = 152.3 (a), 149.1 (h), 144.9 (c), 139.5 (i), 129.3 (d), 128.0 (e), 125.1 (f), 123.6 (b), 123.1 (g), 19.0 (j) ppm.

FTIR (ATR, neat): $\tilde{v}$ = 3066 (vw, v(C-H$_{arom}$)), 1592 (w), 1569 (w), 1525 (vs, v(C-NO₂)), 1449 (w), 1409 (w), 1371 (s), 1305 (w), 1251 (w), 1233 (w), 1213 (w), 1170 (w), 1123 (w), 1089 (w), 1035 (w), 1001 (w), 983 (w), 894 (w), 850 (s), 825 (m), 810 (vw), 776 (s), 766 (vs), 713 (m), 593 (m), 511 (w), 492 (w), 465 (m) cm^{-1}.

HRMS (ESI+, MeOH): m/z (found) = 189.06568 (100 %), 190.06895 (11 %), 191.07091 (>1 %), 211.04753 (100 %), 212.05067 (12 %), 213.05291 (1 %); m/z (calc.) = 189.06585 (100 %, $^{12}C_{10}{}^{1}H_{9}{}^{14}N_{2}{}^{16}O_{2}{}^{+}$), 190.06921 (11 %, $^{12}C_{9}{}^{13}C^{1}H_{9}{}^{14}N_{2}{}^{16}O_{2}{}^{+}$), 191.07010 (>1 %, $^{12}C_{10}{}^{1}H_{9}{}^{14}N_{2}{}^{16}O^{18}O$), 191.07256 (>1 %, $^{12}C_{8}{}^{13}C_{2}{}^{1}H_{9}{}^{14}N_{2}{}^{16}O_{2}$), 211.04780 (100 %, $^{23}Na^{12}C_{10}{}^{1}H_{8}{}^{14}N_{2}{}^{16}O_{2}$), 212.05115 (11 %, $^{23}Na^{12}C_{9}{}^{13}C^{1}H_{8}{}^{14}N_{2}{}^{16}O_{2}$), 213.05451 (>1 %, $^{23}Na^{12}C_{8}{}^{13}C_{2}{}^{1}H_{8}{}^{14}N_{2}{}^{16}O_{2}$), 213.05204 (>1 %, $^{23}Na^{12}C_{10}{}^{1}H_{8}{}^{14}N_{2}{}^{16}O^{18}O$).

Additional information on the synthesis of the target compound and original analysis data files are available via Chemotion Repository: https://dx.doi.org/10.14272/reaction/SA-FUHFF-UHFFFADPSC-ZNGIJEBXIR-UHFFFADPSC-NUHFF-NUHFF-NUHFF-ZZZ

1.3.1.2 Resynthesis of 4-methyl-8-aminoquinoline (4-Me-8-NH₂-qu)

This molecule has been synthesized before.[18] The performed procedure was inspired by the literature.[19]

4-Methyl-8-nitroquinoline (7.51 g, 39.9 mmol, 1 equiv.) and palladium on active charcoal (10 w% Pd, 210 mg Pd/C, 0.197 mmol Pd, 0.005 equiv. Pd) were suspended in methanol (300 mL) under nitrogen. Then the gas phase was exchanged by hydrogen. The reaction mixture was stirred for 5 hours at room temperature. The solvent was removed under reduced pressure. The resulting solid was dissolved in DCM and the solution was filtered through Geduran with DCM

C₁₀H₁₀N₂
158.20 g mol⁻¹
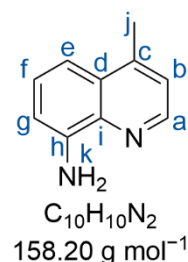
as eluent. The solvent was removed under reduced pressure. 4-Methyl-8-aminoquinoline was obtained as a yellow crystalline solid (5.48 g, 34.6 mmol, 86.8 %).

1H NMR (400 MHz, CDCl$_3$): δ = 8.62 (d, J = 4.3 Hz, 1H, a), 7.35 (dd, J = 8.4, 7.2 Hz, 1H, f), 7.29 (dd, J = 8.4, 1.5 Hz, 1H, e), 7.20 (dd, J = 4.4, 1.0 Hz, 1H, b), 6.93 (dd, J = 7.2, 1.5 Hz, 1H, g), 5.01 (s, 2H, k), 2.65 (d, J = 0.9 Hz, 3H, j) ppm.

13C{1H} NMR (101 MHz, CDCl$_3$): δ = 147.1 (a), 144.6 (h), 144.5 (c), 138.1 (i), 128.9 (d), 127.2 (f), 122.3 (b), 112.2 (e), 110.1 (g), 19.1 (j) ppm.

FTIR (ATR, neat): $\tilde{v}$ = 3460 (w, v(N-H)), 3442 (m, v(N-H)), 3315 (w), 3285 (w), 3155 (w), 3034 (vw, v(C-H$_{arom}$)), 2982 (vw, v(C-H$_{aliph}$)), 2918 (vw, v(C-H$_{aliph}$)), 1613 (s), 1590 (m), 1516 (vs), 1473 (s), 1449 (m), 1436 (w), 1407 (m), 1366 (m), 1318 (s), 1285 (w), 1246 (m), 1211 (w), 1159 (m), 1056 (w), 1032 (w), 1005 (vw), 963 (vw), 914 (vw), 862 (m), 838 (m), 832 (m), 813 (m), 802 (m), 749 (vs), 646 (w), 608 (w), 540 (m), 496 (w) cm^{-1}.

HRMS (ESI+, MeOH): m/z (found) = 159.09211 (100 %), 160.09538 (12 %), 161.09869 (>1 %); m/z (calc.) = 159.09167 (100 %, $^{12}C_{10}{}^{1}H_{11}{}^{14}N_2{}^{+}$), 160.09503 (11 %), 161.09838 (>1 %, $^{12}C_8{}^{13}C_2{}^{1}H_{11}{}^{14}N_2{}^{+}$).

Additional information on the synthesis of the target compound and original analysis data files are available via Chemotion Repository: https://dx.doi.org/10.14272/reaction/SA-FUHFF-UHFFFADPSC-JRIMCEIADA-UHFFFADPSC-NUHFF-NUHFF-NUHFF-ZZZ

1.3.1.3 Synthesis of TMG4Mequ (L7)

The guanidine synthesis was performed following a slightly modified procedure of Herres-Pawlis *et al.* which bases on the procedure of Kantlehner *et al.*[3,20] The synthesis and purification were modified compared to TMG2Mequ from the previous study.[21]

4-Methyl-8-aminoquinoline (5.00 g, 31.6 mmol, 1 eq.) and TMG-VS (6.49 g, 37.9 mmol, 1.2 eq.) were dissolved in MeCN (80 mL) and triethylamine (6.40g, 8.76 mL, 63.2 mmol, 2 eq.) was added. The reaction mixture was heated to reflux for 30 min under stirring. After cooling to room temperature, an aqueous KOH solution (25 mL, 50 w%) was added and the aqueous layer was extracted with MeCN (3x 100 mL). The combined organic layer was dried over Na$_2$SO$_4$ and filtered. The solvent was removed under reduced
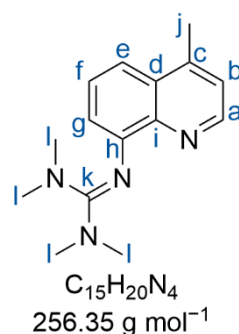
C$_{15}$H$_{20}$N$_4$
256.35 g mol^{-1}

pressure and the contained 1,1,3,3-tetramethylurea was removed in vacuum (<10^{-1} mbar) at 100 °C. The crude product was dissolved in DCM and the solution was filtered through alumina with DCM as eluent. The solvent was removed under reduced pressure. TMG4Mequ was obtained as a yellow oil that turns into yellow solid after a few months (7.72 g, 30.1 mmol, 95.3 %).

¹H NMR (400 MHz, CDCl₃): δ = 8.48 (d, J = 4.3 Hz, 1H, a), 7.20 (dd, J = 8.3, 1.8 Hz, 1H, e), 7.16 (dd, J = 8.3, 7.0 Hz, 1H, f), 6.87 (dd, J = 4.3, 1.1 Hz, 1H, b), 6.64 (dd, J = 7.0, 1.8 Hz, 1H, g), 2.47 (s, 12H, l), 2.39 (d, J = 1.0 Hz, 3H, j) ppm.

¹³C{¹H} NMR (101 MHz, CDCl₃): δ = 160.9 (k), 150.2 (h), 147.6 (a), 143.1 (c), 142.2 (i), 128.8 (d), 126.3 (f), 121.0 (b), 118.3 (g), 114.1 (e), 39.0 (l), 18.6 (j) ppm.

FTIR (ATR, neat): $\tilde{\nu}$ = 3067 (vw, ν(C-H$_{arom}$)), 3025 (vw, ν(C-H$_{arom}$)), 2997 (vw, ν(C-H$_{aliph}$)), 2924 (w, ν(C-H$_{aliph}$)), 2876 (w, ν(C-H$_{aliph}$)), 2791 (vw, ν(C-H$_{aliph}$)), 1599 (m), 1577 (s), 1554 (vs, ν(C-N$_{gua}$)), 1502 (vs), 1473 (m), 1453 (s), 1423 (m), 1402 (m), 1371 (s), 1348 (m), 1291 (w), 1277 (w), 1223 (m), 1180 (w), 1137 (vs), 1106 (w), 1086 (vw), 1061 (w), 1022 (s), 999 (m), 930 (w), 905 (m), 854 (w), 833 (m), 824 (m), 806 (m), 747 (s), 728 (m), 680 (w), 635 (w), 587 (w), 558 (w), 544 (w), 506 (m), 493 (w), 447 (w) cm^{-1}.

HRMS (ESI+, MeOH): m/z (found) = 257.17608 (100 %), 258.17924 (17 %), 259.18238 (1 %); m/z (calc.) = 257.17607 (100 %, $^{12}C_{15}{}^{1}H_{21}{}^{14}N_4{}^+$), 258.17943 (16 %, $^{12}C_{14}{}^{13}C^{1}H_{21}{}^{14}N_4{}^+$), 259.18278 (1 %, $^{12}C_{13}{}^{13}C_2{}^{1}H_{21}{}^{14}N_4{}^+$).

Additional information on the synthesis of the target compound and original analysis data files are available via Chemotion Repository: https://dx.doi.org/10.14272/reaction/SA-FUHFF-UHFFFADPSC-RTVLWQCONC-UHFFFADPSC-NUHFF-NUHFF-NUHFF-ZZZ

1.3.2 Synthesis of TMG4Meequ (L8) and corresponding precursors

1.3.2.1 Synthesis of methyl quinoline-4-carboxylate (4-Mee-qu)

Quinoline-4-carboxylic acid (20.00 g, 115.5 mmol, 1 equiv.) was dissolved in MeOH (300 mL) and conc. H₂SO₄ (19 mL) was added under stirring at 0 °C. The reaction mixture was heated to reflux for 22 h. After cooling to room temperature, the reaction mixture was poured in water (300 mL) under stirring and DCM (300 mL) was added. A saturated aqueous Na₂CO₃ solution

C₁₁H₉NO₂
187.20 g mol⁻¹
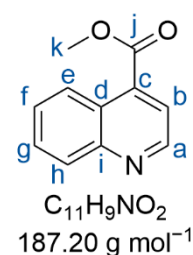
was added slowly under stirring until pH ≈ 5 was reached. The organic layer was separated and the aqueous layer was extracted with DCM (6x 150 mL). The combined organic layer was dried over Na_2SO_4 and filtered. The solution was concentrated under reduced pressure and filtered through Geduran with DCM as eluent. The solvent was removed under reduced pressure. Methyl quinoline-4-carboxylate was obtained as an orange oil (16.38 g, 87.5 mmol, 75.8 %).

^{1}H NMR (400 MHz, $CDCl_3$): δ = 9.02 (d, J = 4.4 Hz, 1H, a), 8.77 (ddd, J = 8.5, 1.4, 0.6 Hz, 1H, e), 8.18 (ddd, J = 8.4, 1.4, 0.7 Hz, 1H, h), 7.91 (d, J = 4.4 Hz, 1H, b), 7.78 (ddd, J = 8.4, 6.9, 1.4 Hz, 1H, g), 7.67 (ddd, J = 8.4, 6.8, 1.4 Hz, 1H, f), 4.05 (s, 3H, k) ppm.

^{13}C{^{1}H} NMR (101 MHz, $CDCl_3$): δ = 166.8 (j), 149.9 (a), 149.3 (i), 135.0 (c), 130.2 (h), 129.9 (g), 128.4 (f), 125.8 (e), 125.3 (d), 122.4 (b), 52.9 (k) ppm.

FTIR (ATR, neat): $\tilde{v}$ = 3063 (vw, v(C-H$_{arom}$)), 3035 (vw, v(C-H$_{arom}$)), 3002 (vw, v(C-H$_{arom}$)), 2952 (vw, v(C-H$_{aliph}$)), 1722 (s, v(C=O)), 1616 (vw), 1584 (m), 1567 (vw), 1507 (m), 1462 (w), 1436 (m), 1390 (vw), 1353 (w), 1311 (m), 1273 (vs), 1250 (vs), 1198 (s), 1180 (m), 1147 (s), 1136 (m), 1072 (m), 1031 (m), 1015 (m), 947 (m), 880 (w), 859 (w), 849 (w), 815 (vw), 794 (s), 771 (vs), 743 (w), 715 (w), 654 (m), 629 (w), 578 (vw), 533 (w), 522 (w), 464 (w), 412 (w) cm^{-1}.

HRMS (ESI+, MeOH): m/z (found) = 188.07014 (100 %), 189.07346 (12 %), 190.07591 (>1 %); m/z (calc.) = 188.07060 (100 %, $^{12}C_{11}{}^1H_{10}{}^{14}N^{16}O_2{}^+$), 189.07396 (12 %, $^{12}C_{10}{}^{13}C^1H_{10}{}^{14}N^{16}O_2{}^+$), 190.07485 (>1 %, $^{12}C_{11}{}^1H_{10}{}^{14}N^{16}O^{18}O^+$), 190.07731 (>1 %, $^{12}C_9{}^{13}C_2{}^1H_{10}{}^{14}N^{16}O_2{}^+$).

Additional information on the synthesis of the target compound and original analysis data files are available via Chemotion Repository: https://dx.doi.org/10.14272/reaction/SA-FUHFF-UHFFFADPSC-KPZUGRPXEZ-UHFFFADPSC-NUHFF-NUHFF-NUHFF-ZZZ

1.3.2.2 Synthesis of methyl 8-nitroquinoline-4-carboxylate (4-Mee-8-NO₂-qu) and methyl 5-nitroquinoline-4-carboxylate (4-Mee-5-NO₂-qu)

Methyl quinoline-4-carboxylate (15.86 g, 84.7 mmol, 1 equiv.) was dissolved in conc. H_2SO_4 (75 mL). A mixture of fuming HNO_3 (13.3 g, 8.8 mL, 212 mmol, 2.5 equiv.) and conc. H_2SO_4 (8.8 mL) was added dropwise under stirring at 0 °C. The reaction mixture was stirred for 6 h at 0 °C and then poured in water (400 mL) under stirring and DCM (400 mL) was added. First an aqueous NaOH

$C_{11}H_8N_2O_4$
232.20 g mol^{-1}
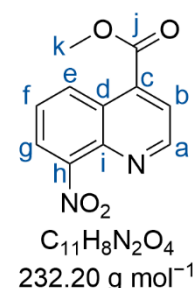
solution (15 M) and then a saturated aqueous Na_2CO_3 solution were added slowly until pH ≈ 5 was reached. The organic layer was separated and the aqueous layer was extracted with DCM (4x 300 mL). The combined organic layer was dried over Na_2SO_4 and filtered. The solvent was removed under reduced pressure. The resulting oil was purified by column chromatography (isohexane:ethyl acetate = 2:1, Geduran, R_f(4-Mee-8-NO$_2$-qu) = 0.31, R_f(4-Mee-5-NO$_2$-qu) = 0.16). Methyl 8-nitroquinoline-4-carboxylate was obtained as a pale yellow crystalline solid (2.72 g, 11.7 mmol, 13.8 %) and methyl 5-nitroquinoline-4-carboxylate was obtained as a pale yellow solid (13.61 g, 58.6 mmol, 69.2 %).

Characterization of 4-Mee-8-NO$_2$-qu:

^{1}H NMR (400 MHz, CDCl$_3$): δ = 9.16 (d, J = 4.4 Hz, 1H, a), 9.05 (dd, J = 8.8, 1.3 Hz, 1H, e), 8.06 (d, J = 4.4 Hz, 1H, b), 8.04 (dd, J = 7.5, 1.3 Hz, 1H, g), 7.73 (dd, J = 8.8, 7.5 Hz, 1H, f), 4.07 (s, 3H, k) ppm.

^{13}C{^{1}H} NMR (101 MHz, CDCl$_3$): δ = 165.8 (j), 152.2 (a), 149.1 (h), 140.5 (i), 135.0 (c), 129.9 (e), 127.0 (f), 126.0 (d), 124.0 (b), 123.6 (g), 53.3 (k) ppm.

FTIR (ATR, neat): $\tilde{\nu}$ = 3119 (vw, ν(C-H$_{arom}$)), 3083 (vw, ν(C-H$_{arom}$)), 3055 (vw, ν(C-H$_{arom}$)), 3012 (vw, ν(C-H$_{arom}$)), 2965 (w, ν(C-H$_{aliph}$)), 2868 (vw, ν(C-H$_{aliph}$)), 1724 (vs, ν(C=O)), 1619 (w), 1586 (m), 1569 (vw), 1559 (vw), 1522 (vs, ν(C-NO$_2$)), 1503 (s), 1464 (w), 1424 (m), 1413 (w), 1355 (s), 1307 (vw), 1261 (s), 1247 (m), 1217 (m), 1194 (s), 1152 (m), 1098 (m), 1069 (m), 1057 (m), 989 (vw), 966 (m), 935 (w), 921 (vw), 880 (vs), 875 (s), 850 (w), 827 (s), 811 (w), 792 (m), 767 (s), 759 (vs), 729 (m), 698 (m), 636 (w), 578 (m), 543 (m), 526 (w), 485 (vw), 457 (w) cm^{-1}.

HRMS (ESI+, MeOH): m/z (found) = 233.05547 (100 %), 234.05874 (12 %), 235.06057 (2 %); m/z (calc.) = 233.05568 (100 %, $^{12}C_{11}{}^1H_9{}^{14}N_2{}^{16}O_4{}^+$), 234.05904 (12 %, $^{12}C_{10}{}^{13}C^1H_9{}^{14}N_2{}^{16}O_4{}^+$), 235.05993 (>1 %, $^{12}C_{11}{}^1H_9{}^{14}N_2{}^{16}O_3{}^{18}O^+$), 235.06239 (>1 %, $^{12}C_9{}^{13}C_2{}^1H_9{}^{14}N_2{}^{16}O_4{}^+$).

Characterization of 4-Mee-5-NO$_2$-qu:

^{1}H NMR (400 MHz, CDCl$_3$): δ = 9.12 (d, J = 4.3 Hz, 1H, a), 8.44 (dd, J = 8.6, 1.2 Hz, 1H, h), 8.22 (dd, J = 7.6, 1.3 Hz, 1H, f), 7.89 (d, J = 4.3 Hz, 1H, b), 7.84 (dd, J = 8.5, 7.6 Hz, 1H, g), 3.93 (s, 3H, k) ppm.

^{13}C{^{1}H} NMR (101 MHz, CDCl$_3$): δ = 166.3 (j), 151.5 (a), 148.9 (i), 147.0 (e), 136.2 (c), 136.0 (h), 128.3 (g), 125.3 (f), 123.9 (b), 117.1 (d), 52.8 (k) ppm.

FTIR (ATR, neat): $\tilde{v}$ = 3105 (vw, v(C-H$_{arom}$)), 3102 (vw, v(C-H$_{arom}$)), 3046 (vw, v(C-H$_{arom}$)), 3041 (vw, v(C-H$_{arom}$)), 3031 (vw, v(C-H$_{arom}$)), 2961 (vw, v(C-H$_{aliph}$)), 1722 (vs, v(C=O)), 1684 (vw), 1583 (w), 1566 (vw), 1559 (vw), 1522 (vs, v(C-NO$_2$)), 1505 (m), 1473 (vw), 1457 (w), 1435 (m), 1409 (m), 1385 (w), 1342 (s), 1314 (w), 1274 (s), 1242 (w), 1229 (m), 1206 (s), 1176 (m), 1087 (m), 1043 (vw), 1020 (m), 982 (m), 928 (w), 915 (m), 877 (m), 869 (m), 837 (m), 826 (m), 809 (w), 797 (s), 773 (vs), 747 (m), 739 (s), 690 (m), 643 (m), 616 (w), 612 (w), 577 (m), 543 (m), 502 (w), 466 (w), 453 (m), 437 (w) cm^{-1}.

HRMS (ESI+, MeOH): m/z (found) = 255.03823 (100 %), 256.04147 (12 %), 257.04340 (1 %); m/z (calc.) = 255.03763 (100 %, ^{23}Na^{12}C$_{11}^{1}$H$_8^{14}$N$_2^{16}$O$_4^+$), 256.04098 (12 %, ^{23}Na^{12}C$_{10}^{13}$C^{1}H$_8^{14}$N$_2^{16}$O$_4^+$), 257.04187 (>1 %, ^{23}Na^{12}C$_{11}^{1}$H$_8^{14}$N$_2^{16}$O$_3^{18}$O$^+$), 257.04434 (>1 %, ^{23}Na^{12}C$_9^{13}$C$_2^{1}$H$_8^{14}$N$_2^{16}$O$_4^+$).

Additional information on the synthesis of the target compound and original analysis data files are available via Chemotion Repository: https://dx.doi.org/10.14272/reaction/SA-FUHFF-UHFFFADPSC-RXJOVRJXAW-UHFFFADPSC-NUHFF-NUHFF-NUHFF-ZZZ

1.3.2.3 Synthesis of methyl 8-aminoquinoline-4-carboxylate (4-Mee-8-NH$_2$-qu)

The performed procedure was inspired by the literature.[19]

Methyl 8-nitroquinoline-4-carboxylate (2.20 g, 9.47 mmol, 1 equiv.) and palladium on active charcoal (10 w% Pd, 50.4 mg Pd/C, 0.047 mmol Pd, 0.005 equiv. Pd) were suspended in methanol (100 mL) under nitrogen. Then the gas phase was exchanged by hydrogen. The reaction mixture was stirred for 24 hours at rt. The solvent was removed under reduced pressure. The resulting solid was purified by column chromatography (isohexane:ethyl acetate = 7:3, Geduran, R_f = 0.71). The solvent was removed under reduced pressure. Methyl 8-aminoquinoline-4-carboxylate was obtained as an orange crystalline solid (1.90 g, 9.40 mmol, 99.2 %).

C$_{11}$H$_{10}$N$_2$O$_2$
202.21 g mol^{-1}
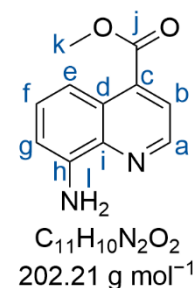
^{1}**H NMR** (400 MHz, CDCl$_3$): δ = 8.83 (d, J = 4.3 Hz, 1H, a), 8.00 (dt, J = 8.6, 1.0 Hz, 1H, e), 7.87 (d, J = 4.5 Hz, 1H, b), 7.44 (t, J = 8.1 Hz, 1H, f), 6.98 (dd, J = 7.6, 1.0 Hz, 1H, g), 5.23 (s, 2H, l), 4.03 (s, 3H, k) ppm.

13C{1H} NMR (101 MHz, CDCl₃): δ = 167.1 (j), 146.4 (a), 144.4 (h), 139.3 (i), 135.2 (c), 129.4 (f), 125.9 (d), 122.6 (b), 113.8 (e), 110.6 (g), 52.8 (k) ppm.

FTIR (ATR, neat): $\tilde{v}$ = 3470 (m, v(N-H)), 3362 (m, v(N-H)), 3224 (vw), 3179 (vw), 3087 (vw, v(C-H$_{arom}$)), 3033 (vw, v(C-H$_{arom}$)), 2954 (w, v(C-H$_{aliph}$)), 1710 (vs, v(C=O)), 1673 (w), 1615 (s), 1586 (m), 1563 (m), 1517 (m), 1471 (m), 1456 (w), 1434 (m), 1411 (w), 1404 (w), 1346 (m), 1320 (m), 1270 (vs), 1252 (s), 1232 (m), 1211 (m), 1196 (m), 1179 (m), 1136 (m), 1107 (m), 1038 (w), 980 (m), 899 (w), 872 (m), 852 (w), 814 (s), 800 (w), 773 (m), 755 (s), 745 (m), 657 (w), 617 (m), 555 (w), 529 (w), 504 (w) cm⁻¹.

HRMS (ESI+, MeOH): *m/z* (found) = 203.07826 (100 %), 204.08154 (12 %), 205.08380 (1 %); *m/z* (calc.) = 203.08150 (100 %, $^{12}C_{11}^{1}H_{11}^{14}N_2^{16}O_2^+$), 204.08486 (12 %, $^{12}C_{10}^{13}C^{1}H_{11}^{14}N_2^{16}O_2^+$), 205.08575 (>1 %, $^{12}C_{11}^{1}H_{11}^{14}N_2^{16}O^{18}O^+$), 205.08821 (>1 %, $^{12}C_9^{13}C_2^{1}H_{11}^{14}N_2^{16}O_2^+$).

Additional information on the synthesis of the target compound and original analysis data files are available via Chemotion Repository: https://dx.doi.org/10.14272/reaction/SA-FUHFF-UHFFFADPSC-ZPAJMNYHAI-UHFFFADPSC-NUHFF-NUHFF-NUHFF-ZZZ

1.3.2.4   Synthesis of TMG4Meequ (L8)

The guanidine synthesis was performed following a slightly modified procedure of Herres-Pawlis *et al.* which bases on the procedure of Kantlehner *et al.*[3,20] Due to the sensitivity of the methyl ester substituent against bases and high temperatures, the purification was slightly modified compared to TMG4Mequ and is similar to TMG2Meequ from the previous study.[21]

Methyl 8-aminoquinoline-4-carboxylate (1.76 g, 8.70 mmol, 1 equiv.) and TMG-VS (1.79 g, 10.4 mmol, 1.2 equiv.) were dissolved in MeCN (30 mL) and triethylamine (2.4 mL, 17.4 mmol, 2 equiv.) was added. The reaction mixture was heated to reflux for 30 min under stirring. After cooling to room temperature, an aqueous KOH solution (10 mL, 33 w%) was added and the mixture was mixed for several seconds. The aqueous layer was extracted with MeCN (2x 50 mL). The combined organic layer

C₁₆H₂₀N₄O₂
300.36 g mol⁻¹
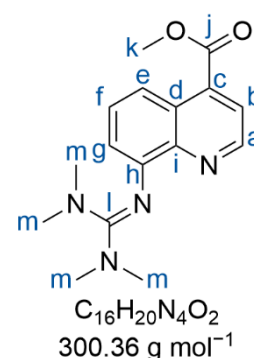
was dried over Na₂SO₄ and filtered. The solvent was removed under reduced pressure and the contained 1,1,3,3-tetramethylurea was removed in vacuum (<10⁻¹ mbar) at 80 °C. The resulting red oil was dissolved in a few mL of DCM and the solution was filtered through

alumina with DCM as eluent. The solvent was removed under reduced pressure. TMG4Meequ was obtained as a red oil (1.40 g, 4.66 mmol, 53.6 %).

^{1}H NMR (400 MHz, CDCl$_3$): δ = 8.90 (d, J = 4.3 Hz, 1H, a), 8.11 (dd, J = 8.5, 1.3 Hz, 1H, e), 7.75 (d, J = 4.3 Hz, 1H, b), 7.47 (dd, J = 8.5, 7.5 Hz, 1H, f), 6.90 (dd, J = 7.5, 1.3 Hz, 1H, g), 4.00 (s, 3H, k), 2.70 (s, 12H, m) ppm.

^{13}C{^{1}H} NMR (101 MHz, CDCl$_3$): δ = 167.5 (j), 161.9 (l), 150.8 (h), 147.6 (a), 144.0 (i), 134.9 (c), 129.0 (f), 126.2 (d), 121.8 (b), 119.4 (g), 116.2 (e), 52.6 (k), 39.6 (m) ppm.

FTIR (ATR, neat): $\tilde{\nu}$ = 3011 (vw, ν(C-H$_{arom}$)), 3003 (w, ν(C-H$_{arom}$)), 2998 (w, ν(C-H$_{aliph}$)), 2946 (w, ν(C-H$_{aliph}$)), 2929 (w, ν(C-H$_{aliph}$)), 2885 (w, ν(C-H$_{aliph}$)), 2873 (w, ν(C-H$_{aliph}$)), 2856 (w, ν(C-H$_{aliph}$)), 2813 (vw, ν(C-H$_{aliph}$)), 2791 (vw, ν(C-H$_{aliph}$)), 1723 (s, ν(C=O)), 1574 (s, ν(C-N$_{gua}$)), 1549 (vs, ν(C-N$_{gua}$)), 1502 (s), 1474 (m), 1453 (s), 1437 (m), 1423 (m), 1406 (w), 1374 (s), 1330 (m), 1261 (vs), 1224 (s), 1195 (s), 1173 (w), 1139 (s), 1113 (s), 1079 (w), 1061 (w), 1018 (m), 976 (m), 924 (w), 893 (m), 866 (w), 845 (w), 824 (s), 807 (m), 780 (m), 755 (s), 702 (s), 674 (w), 624 (vw), 601 (vw), 565 (w), 547 (vw), 541 (vw), 533 (w), 529 (w), 515 (vw), 505 (vw), 501 (vw), 495 (vw), 481 (w), 448 (w) cm^{-1}.

HRMS (ESI+, MeOH): m/z (found) = 301.16133 (100 %), 302.16447 (17 %), 303.16715 (2 %); m/z (calc.) = 301.16590 (100 %, ^{12}C$_{16}$^{1}H$_{21}$^{14}N$_4$^{16}O$_2$$^+$), 302.16926 (17 %, ^{12}C$_{15}$^{13}C^{1}H$_{21}$^{14}N$_4$^{16}O$_2$$^+$), 303.16629 (>1 %, ^{12}C$_{15}$^{13}C^{1}H$_{21}$^{14}N$_3$^{15}N^{16}O$_2$$^+$), 303.17015 (>1%, ^{12}C$_{16}$^{1}H$_{21}$^{14}N$_4$^{16}O^{18}O$^+$), 303.17261 (1 %, ^{12}C$_{14}$^{13}C$_2$^{1}H$_{21}$^{14}N$_4$^{16}O$_2$$^+$).

Additional information on the synthesis of the target compound and original analysis data files are available via Chemotion Repository: https://dx.doi.org/10.14272/reaction/SA-FUHFF-UHFFFADPSC-QTCGOPPBRA-UHFFFADPSC-NUHFF-NUHFF-NUHFF-ZZZ

1.4 Complex synthesis

1.4.1 Synthesis of copper complexes with TMG4Mequ (L7)

1.4.1.1 Synthesis of [Cu(TMG4Mequ)$_2$]PF$_6$ (C11−PF$_6$)

To a solution of TMG4Mequ (25.6 mg, 0.1 mmol, 2 equiv.) in DCM (1 mL) a solution of [Cu(MeCN)$_4$]PF$_6$ (18.6 mg, 0.05 mmol, 1 equiv.) in DCM (1 mL) was added. The resulting solution became instantly dark red. By slow diffusion of pentane, the compound [Cu(TMG4Mequ)$_2$]PF$_6$ crystallized after a few days as dark red crystals.


C$_{30}$H$_{40}$CuF$_6$N$_8$P
721.22 g mol^{-1}

^{1}H NMR (400 MHz, MeCN-d_3): δ = 8.39 (s, 2H, a), 7.74 – 7.46 (m, 4H, e, f), 7.34 (s, 2H, b), 6.89 (s, 2H, g), 2.69 (s, 6H, j), 2.49 (s, 24H, l) ppm.

^{13}C{^{1}H} NMR (101 MHz, MeCN-d_3): δ = 163.6 (k), 148.8 (h), 147.6 (a), 146.7 (c), 141.8 (i), 130.6 (d), 128.6 (f), 123.9 (b), 118.3 (g), 116.1 (e), 39.7 (l), 19.3 (j) ppm.

Due to the limited solubility in MeCN and other solvents, it was not possible to measure NMR spectra with a better S/N ratio.

FTIR (ATR, neat): $\tilde{\nu}$ = 2952 (w, ν(C-H$_{aliph}$)), 2943 (w, ν(C-H$_{aliph}$)), 2922 (w, ν(C-H$_{aliph}$)), 2870 (vw, ν(C-H$_{aliph}$)), 2795 (vw, ν(C-H$_{aliph}$)), 1592 (w), 1565 (w), 1527 (m, ν(C-N$_{gua}$)), 1502 (m), 1466 (m), 1459 (m), 1423 (m), 1404 (m), 1394 (s), 1385 (m), 1364 (m), 1338 (w), 1302 (w), 1278 (w), 1231 (w), 1207 (vw), 1181 (vw), 1153 (m), 1142 (m), 1109 (w), 1098 (w), 1067 (w), 1062 (w), 1036 (m), 1007 (w), 933 (vw), 908 (w), 902 (w), 876 (w), 841 (vs, ν(PF$_6$)), 831 (vs, ν(PF$_6$)), 827 (vs, ν(PF$_6$)), 802 (vs), 788 (m), 769 (m), 726 (m), 689 (w), 654 (vw), 589 (vw), 556 (s), 543 (w), 523 (vw), 516 (vw), 501 (m), 487 (w), 471 (w), 468 (w), 419 (vw) cm^{-1}.

HRMS (ESI+, MeCN): m/z (found) = 575.26751 (100 %), 576.27048 (35 %), 577.26638 (49 %), 578.26886 (14 %), 579.27194 (2%); m/z (calc.) = 575.26664 (100 %, ^{12}C$_{30}$^{1}H$_{40}$^{63}Cu^{14}N$_8$$^+$), 576.26368 (3 %, ^{12}C$_{30}$^{1}H$_{40}$^{63}Cu^{14}N$_7$^{15}N$^+$) 576.27000 (32 %, ^{12}C$_{29}$^{13}C^{1}H$_{40}$^{63}Cu^{14}N$_8$$^+$), 577.26483 (45 %, ^{12}C$_{30}$^{1}H$_{40}$^{65}Cu^{14}N$_8$$^+$), 577.27335 (5 %, ^{12}C$_{28}$^{13}C$_2$^{1}H$_{40}$^{63}Cu^{14}N$_8$$^+$), 578.26819 (14 %, ^{12}C$_{29}$^{13}C^{1}H$_{40}$^{65}Cu^{14}N$_8$$^+$), 579.27154 (2 %, ^{12}C$_{28}$^{13}C$_2$^{1}H$_{40}$^{65}Cu^{14}N$_8$$^+$).
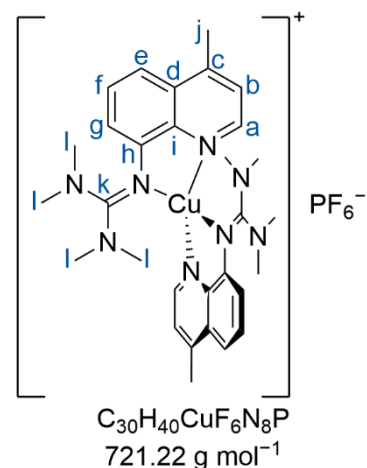
Additional information on the synthesis of the target compound and original analysis data files are available via Chemotion Repository: https://dx.doi.org/10.14272/reaction/SA-FUHFF-UHFFFADPSC-UXMQGFPLGU-UHFFFADPSC-NUHFF-NUHFF-NUHFF-ZZZ

1.4.1.2 Synthesis of [Cu(TMG4Mequ)$_2$(OTf)]OTf·MeOH ((C12+OTf)−OTf)

To a solution of TMG4Mequ (25.6 mg, 0.1 mmol, 2 equiv.) in MeOH (1 mL) a solution of [Cu(MeCN)$_4$](OTf)$_2$ (26.3 mg, 0.05 mmol, 1 equiv.) in MeOH (1 mL) was added. The resulting solution became instantly dark green. By slow diffusion of Et$_2$O, the compound [Cu(TMG4Mequ)$_2$(OTf)]OTf·MeOH crystallized after a few days as dark green orange crystals.

C$_{32}$H$_{40}$CuF$_6$N$_8$O$_6$S$_2$
874.38 g mol^{-1}
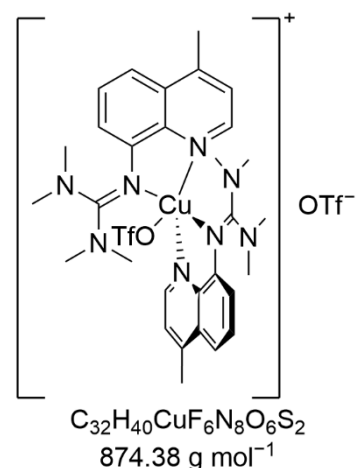
FTIR (ATR, neat): $\tilde{v}$ = 3079 (vw, v(C-H$_{arom}$)), 2936 (vw, v(C-H$_{aliph}$)), 1576 (m), 1521 (m), 1507 (s, v(C-N$_{gua}$)), 1469 (m), 1423 (m), 1402 (s), 1393 (m), 1371 (m), 1325 (m), 1308 (w), 1264 (s, v(OTf)), 1250 (s), 1224 (s), 1162 (m), 1142 (s), 1112 (w), 1086 (vw), 1066 (vw), 1044 (w), 1027 (vs, v(OTf)), 959 (vw), 934 (w), 894 (m), 875 (vw), 857 (w), 835 (m), 814 (w), 805 (m), 773 (m), 756 (m), 748 (m), 735 (w), 680 (w), 636 (vs, v(OTf)), 602 (w), 573 (m), 544 (w), 517 (m), 504 (m), 492 (w), 471 (w) cm^{-1}.

HRMS (ESI+, MeCN): m/z (found) = 287.63361 (100 %), 288.13499 (45 %), 288.63294 (61 %), 289.13416 (20 %), 289.63558 (3 %), 290.13698 (>1 %), 724.21989 (100 %), 725.22277 (36 %), 726.21860 (50 %), 727.22108 (17 %), 728.22074 (4 %); m/z (calc.) = 287.63305 (100 %, $^{12}C_{30}{}^{1}H_{40}{}^{63}Cu^{14}N_8{}^{2+}$), 288.13472 (32 %, $^{12}C_{29}{}^{13}C^{1}H_{40}{}^{63}Cu^{14}N_8{}^{2+}$), 288.63214 (45 %, $^{12}C_{30}{}^{1}H_{40}{}^{65}Cu^{14}N_8{}^{2+}$), 289.13382 (14 %, $^{12}C_{29}{}^{13}C^{1}H_{40}{}^{65}Cu^{14}N_8{}^{2+}$), 289.63550 (2 %, $^{12}C_{28}{}^{13}C_2{}^{1}H_{40}{}^{65}Cu^{14}N_8{}^{2+}$), 290.13402 (>1 %, $^{12}C_{28}{}^{13}C_2{}^{1}H_{40}{}^{65}Cu^{14}N_7{}^{15}N^+$), 290.13718 (>1 %, $^{12}C_{27}{}^{13}C_3{}^{1}H_{40}{}^{65}Cu^{14}N_8{}^+$), 724.21867 (100 %, $^{19}F_3{}^{12}C_{31}{}^{1}H_{40}{}^{63}Cu^{14}N_8{}^{16}O_3{}^{32}S^+$), 725.22202 (34 %, $^{19}F_3{}^{12}C_{30}{}^{13}C^{1}H_{40}{}^{63}Cu^{14}N_8{}^{16}O_3{}^{32}S^+$), 726.21686 (45 %, $^{19}F_3{}^{12}C_{31}{}^{1}H_{40}{}^{65}Cu^{14}N_8{}^{16}O_3{}^{32}S^+$), 726.22538 (5 %, $^{19}F_3{}^{12}C_{29}{}^{13}C_2{}^{1}H_{40}{}^{63}Cu^{14}N_8{}^{16}O_3{}^{32}S^+$), 727.22021 (15 %, $^{19}F_3{}^{12}C_{30}{}^{13}C^{1}H_{40}{}^{65}Cu^{14}N_8{}^{16}O_3{}^{32}S^+$), 728.21265 (2 %, $^{19}F_3{}^{12}C_{31}{}^{1}H_{40}{}^{65}Cu^{14}N_8{}^{16}O_3{}^{34}S^+$), 728.22357 (2 %, $^{19}F_3{}^{12}C_{29}{}^{13}C_2{}^{1}H_{40}{}^{65}Cu^{14}N_8{}^{16}O_3{}^{32}S^+$).

EA: calc. (%) for C$_{32}$H$_{40}$CuF$_6$N$_8$O$_6$S$_2$: C: 43.96, H: 4.61, N: 12.82; found: C: 43.98, H: 4.65, N: 12.83.

Additional information on the synthesis of the target compound and original analysis data files are available via Chemotion Repository: https://dx.doi.org/10.14272/reaction/SA-FUHFF-UHFFFADPSC-BPURWTHBGZ-UHFFFADPSC-NUHFF-LUHFF-NUHFF-ZZZ

1.4.2 Synthesis of copper complexes with TMG4Meequ (L8)

1.4.2.1 Synthesis of [Cu(TMG4Meequ)$_2$]PF$_6$ (C13−PF$_6$)

To a solution of TMG4Meequ (30.0 mg, 0.1 mmol, 2 equiv.) in DCM (1 mL) a solution of [Cu(MeCN)$_4$]PF$_6$ (18.6 mg, 0.05 mmol, 1 equiv.) in DCM (1 mL) was added. The resulting solution became instantly dark violet. By slow evaporation of the solvent, the compound [Cu(TMG4Meequ)$_2$]PF$_6$ crystallized after a few days as dark green crystals.

C$_{32}$H$_{40}$CuF$_6$N$_8$O$_4$P
809.23 g mol^{-1}

^{1}H NMR (400 MHz, MeCN-d_3): δ = 8.59 (s, 2H, a), 8.19 (d, J = 8.5 Hz, 2H, e), 7.97 − 7.88 (m, 2H, b), 7.64 (t, J = 8.1 Hz, 2H, f), 6.97 (d, J = 7.6 Hz, 2H, g), 4.00 (s, 6H, k), 2.52 (s, 24H, m) ppm.
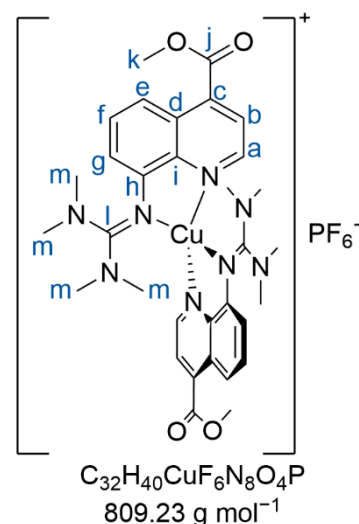
^{13}C{^{1}H} NMR (101 MHz, MeCN-d_3): δ = 167.4 (j), 164.0 (l), 148.7 (h), 146.9 (a), 143.1 (i), 136.3 (c), 130.5 (f), 127.8 (d), 124.8 (b), 118.9 (g), 117.3 (e), 53.6 (k), 39.9 (m) ppm.

FTIR (ATR, neat): $\tilde{\nu}$ = 3082 (vw, ν(C-H$_{arom}$)), 3018 (vw, ν(C-H$_{arom}$)), 2958 (vw, ν(C-H$_{aliph}$)), 2883 (vw, ν(C-H$_{aliph}$)), 2802 (vw, ν(C-H$_{aliph}$)), 1722 (m, ν(C=O)), 1583 (w), 1558 (m), 1526 (m, ν(C-N$_{gua}$)), 1505 (m), 1472 (w), 1456 (m), 1443 (w), 1425 (m), 1409 (m), 1397 (m), 1343 (w), 1295 (w), 1280 (m), 1259 (m), 1229 (s), 1212 (m), 1199 (m), 1186 (m), 1173 (m), 1159 (m), 1145 (m), 1119 (s), 1096 (m), 1067 (m), 1029 (w), 978 (m), 926 (vw), 902 (w), 878 (m), 831 (vs, ν(PF$_6$)), 823 (vs, ν(PF$_6$)), 805 (s), 796 (m), 773 (m), 763 (s), 751 (m), 741 (m), 706 (m), 673 (w), 640 (w), 605 (vw), 586 (vw), 556 (s), 488 (w), 467 (w) cm^{-1}.
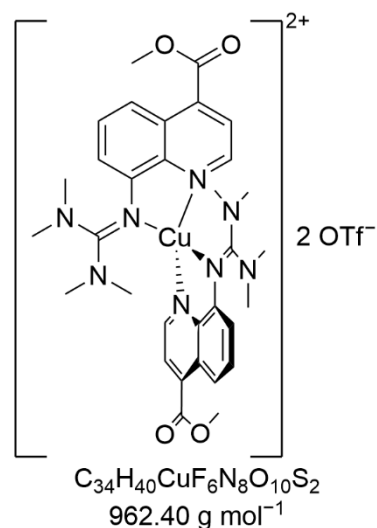
HRMS (ESI+, MeCN): m/z (found) = 663.24608 (100 %), 664.24910 (37 %), 665.24508 (48 %), 666.24762 (17 %), 667.25040 (3 %); m/z (calc.) = 663.24630 (100 %, ^{12}C$_{32}$^{1}H$_{40}$^{63}Cu^{14}N$_8$^{16}O$_4$$^+$), 664.24966 (35 %, ^{12}C$_{31}$^{13}C^{1}H$_{40}$^{63}Cu^{14}N$_8$^{16}O$_4$$^+$), 665.24449 (45 %, ^{12}C$_{32}$^{1}H$_{40}$^{65}Cu^{14}N$_8$^{16}O$_4$$^+$), 666.24785 (15 %, ^{12}C$_{31}$^{13}C^{1}H$_{40}$^{65}Cu^{14}N$_8$^{16}O$_4$$^+$), 667.25120 (3 %, ^{12}C$_{30}$^{13}C$_2$^{1}H$_{40}$^{65}Cu^{14}N$_8$^{16}O$_4$$^+$).

Additional information on the synthesis of the target compound and original analysis data files are available via Chemotion Repository: https://dx.doi.org/10.14272/reaction/SA-FUHFF-UHFFFADPSC-YUTCBXVUPC-UHFFFADPSC-NUHFF-NUHFF-NUHFF-ZZZ

1.4.2.2 Synthesis of [Cu(TMG4Meequ)$_2$](OTf)$_2$·Et$_2$O (C14–OTf)

To a solution of TMG4Meequ (30.0 mg, 0.1 mmol, 2 equiv.) in MeOH (1 mL) a solution of [Cu(MeCN)$_4$](OTf)$_2$ (26.3 mg, 0.05 mmol, 1 equiv.) in MeOH (1 mL) was added. The resulting solution became instantly dark red. By slow evaporation of the solvent, the compound [Cu(TMG4Meequ)$_2$](OTf)$_2$·Et$_2$O crystallized after a few days as dark green crystals.

C$_{34}$H$_{40}$CuF$_6$N$_8$O$_{10}$S$_2$
962.40 g mol^{-1}

FTIR (ATR, neat): $\tilde{\nu}$ = 3113 (vw, v(C-H$_{arom}$)), 3075 (vw, v(C-H$_{arom}$)), 3034 (vw, v(C-H$_{arom}$)), 2949 (w, v(C-H$_{aliph}$)), 2806 (vw, v(C-H$_{aliph}$)), 1740 (m, v(C=O)), 1723 (m), 1573 (m), 1521 (m, v(C-N$_{gua}$)), 1509 (m), 1465 (m), 1433 (vw), 1424 (w), 1416 (w), 1404 (m), 1366 (vw), 1355 (w), 1331 (w), 1303 (vw), 1258 (s, v(OTf)), 1226 (m), 1205 (w), 1169 (w), 1143 (m), 1121 (m), 1103 (w), 1084 (vw), 1068 (w), 1058 (w), 1041 (w), 1027 (s, v(OTf)), 982 (m), 929 (w), 905 (w), 883 (vw), 877 (vw), 854 (w), 834 (m), 823 (m), 807 (w), 802 (w), 774 (m), 771 (m), 757 (w), 752 (w), 717 (m), 681 (vw), 672 (vw), 666 (vw), 636 (vs, v(OTf)), 605 (vw), 589 (vw), 571 (m), 548 (vw), 540 (vw), 516 (m), 494 (w), 491 (w), 487 (w), 475 (w), 474 (w) cm^{-1}.

HRMS (ESI+, MeCN): *m/z* (found) = 331.62287 (100 %), 332.12439 (36 %), 332.62242 (49 %), 333.12363 (18 %), 663.24605 (100 %), 664.24909 (37 %), 665.24511 (50 %), 666.24767 (18 %), 667.25044 (4 %); *m/z* (calc.) = 331.62288 (100 %, $^{12}C_{32}{}^{1}H_{40}{}^{63}Cu^{14}N_8{}^{16}O_4{}^{2+}$), 332.12455 (35 %, $^{12}C_{31}{}^{13}C^1H_{40}{}^{63}Cu^{14}N_8{}^{16}O_4{}^{2+}$), 332.62197 (45 %, $^{12}C_{32}{}^{1}H_{40}{}^{65}Cu^{14}N_8{}^{16}O_4{}^{2+}$), 333.12365 (15 %, $^{12}C_{31}{}^{13}C^1H_{40}{}^{65}Cu^{14}N_8{}^{16}O_4{}^{2+}$), 663.24630 (100 %, $^{12}C_{32}{}^{1}H_{40}{}^{63}Cu^{14}N_8{}^{16}O_4{}^{+}$), 664.24966 (35 %, $^{12}C_{31}{}^{13}C^1H_{40}{}^{63}Cu^{14}N_8{}^{16}O_4{}^{+}$), 665.24449 (45 %, $^{12}C_{32}{}^{1}H_{40}{}^{65}Cu^{14}N_8{}^{16}O_4{}^{+}$), 666.24785 (15 %, $^{12}C_{31}{}^{13}C^1H_{40}{}^{65}Cu^{14}N_8{}^{16}O_4{}^{+}$), 667.25120 (3 %, $^{12}C_{30}{}^{13}C_2{}^{1}H_{40}{}^{65}Cu^{14}N_8{}^{16}O_4{}^{+}$).

EA: calc. (%) for C$_{34}$H$_{40}$CuF$_6$N$_8$O$_{10}$S$_2$: C: 42.43, H: 4.19, N: 11.64; found: C: 42.53, H: 4.28, N: 11.80.

Additional information on the synthesis of the target compound and original analysis data files are available via Chemotion Repository: https://dx.doi.org/10.14272/reaction/SA-FUHFF-UHFFFADPSC-FCSSWXJXSK-UHFFFADPSC-NUHFF-LUHFF-NUHFF-ZZZ

1.5 Theoretical calculations

1.5.1 Density functional theory calculations

Density functional theory (DFT) calculations were performed with Gaussian 16, Revision B.01, using the default UltraFine grid (a 99,590 grid).[22] The TPSSh functional[23] and the Ahlrichs type basis set def2-TZVP[24–26] were applied as implemented in Gaussian 16, Revision B.01.[22] As solvent model for MeCN, the polarizable continuum model (PCM) was used as implemented in Gaussian 16, Revision B.01.[22] As empirical dispersion correction, the D3 version of Grimme's dispersion with Becke-Johnson damping (GD3BJ) was used as implemented in Gaussian16, Revision B.01.[22,27] The structure optimizations were started from the solid state structures, if available. All subsequent calculations were performed based on the results of the optimization calculations. Frequency calculations did not show imaginary values. NBO calculations were accomplished using the program NBO 6.0 delivering the NBO charges and the charge-transfer energies E_{CT} by second-order perturbation theory.[28] For visualization and extraction of the calculated structural information, GaussView (Version 6.0.16) was used. Calculated energy values and NBO results were extracted directly from the output files using notepad++ (Version 7.8.1).

1.5.2 Conformer-rotamer ensemble sampling tool calculations

To verify the found minima of the DFT optimization calculations of **C11**-**C14**, conformer-rotamer ensemble sampling tool (CREST) calculations were performed.[29] The applied theory level was GFN2-xTB.[30] The minimum structures of the CREST calculations of **C11**-**C14** confirm the found structures of the DFT optimization calculations.

1.5.3 Domain-based local pair natural orbital coupled cluster calculations

Domain-based local pair natural orbital coupled cluster with singles, doubles and perturbative triples excitations (DLPNO-CCSD(T)) calculations were performed with ORCA 5.0.3.[31,32,33] The Ahlrichs type basis set def2-TZVP[24–26] and the auxiliary basis set def2-TZVP/C[34] were applied as implemented in ORCA 5.0.3.[31,32] The SCF convergence tolerance was set to TightSCF. As solvent model for MeCN, the conductor-like polarizable continuum model (C-PCM)[35] was

used as implemented in ORCA 5.0.3.[31,32] The calculations were performed based on the structures obtained from the DFT optimization calculations.

2 Results

2.1 SCXRD measurements

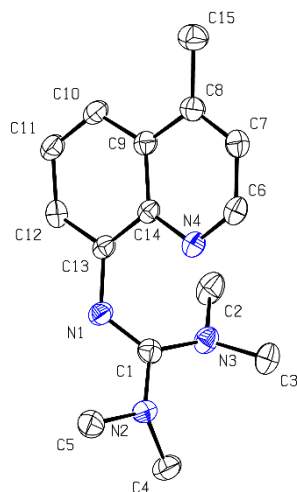### 2.1.1 Crystallographic data

Fig. S1 Displacement ellipsoid plot of TMG4Mequ (**L7**) (50 % probability level, asymmetric unit, H atoms are omitted for clarity).
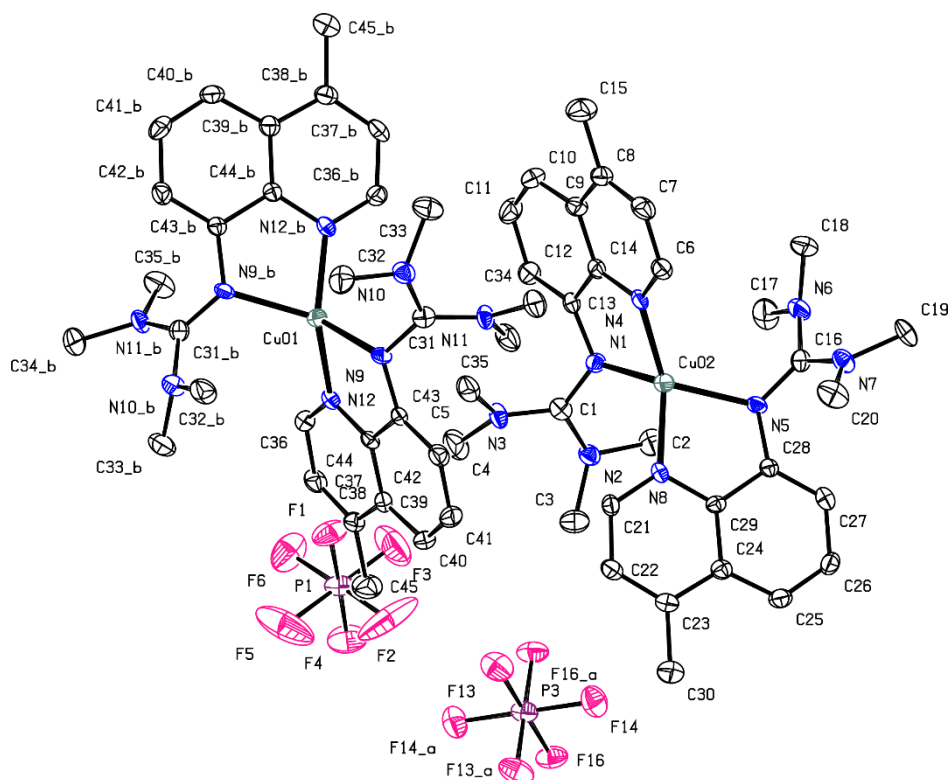

Fig. S2: Displacement ellipsoid plot of [Cu(TMG4Mequ)$_2$]PF$_6$ (**C11−PF$_6$**) (50 % probability level, H atoms are omitted for clarity).
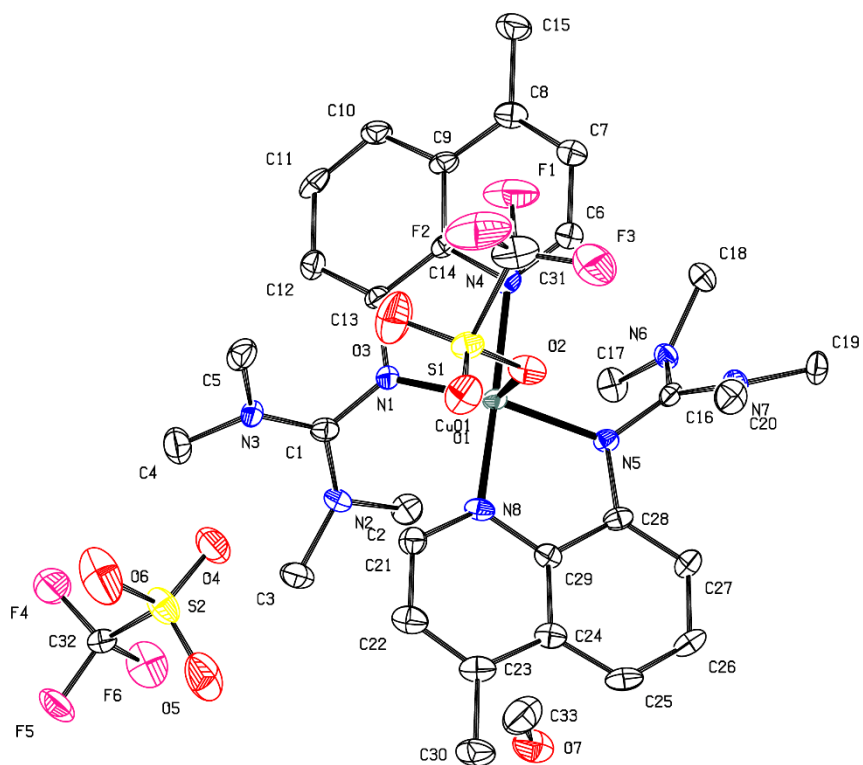
Fig. S3: Displacement ellipsoid plot of [Cu(TMG4Mequ)$_2$(OTf)]OTf·MeOH (**(C12+OTf)−OTf**) (50 % probability level, asymmetric unit, H atoms are omitted for clarity).

Table S1: Crystallographic data of TMG4Mequ (**L7**), [Cu(TMG4Mequ)₂]PF₆ (**C11−PF₆**) and [Cu(TMG4Mequ)₂(OTf)]OTf·MeOH (**(C12+OTf)−OTf**).

|	L7	C11−PF₆	(C12+OTf)−OTf
Empirical formula	$C_{15}H_{20}N_4$	$C_{30}H_{40}CuF_6N_8P$	$C_{33}H_{44}CuF_6N_8O_7S_2$
Formula weight [g mol⁻¹]	256.35	721.21	906.42
Crystal size [mm]	0.190 x 0.130 x 0.030	0.170 x 0.133 x 0.080	0.130 x 0.100 x 0.070
T [K]	100	100	100
Crystal system	monoclinic	monoclinic	monoclinic
Space group	$P2_1/c$	$C2/c$	$P2_1$
a [Å]	11.930(2)	19.080(6)	10.694(2)
b [Å]	14.545(3)	20.425(6)	16.698(3)
c [Å]	8.3850(17)	27.495(6)	11.055(2)
α [°]	90	90	90
β [°]	103.26(3)	108.59(3)	91.61(3)
γ [°]	90	90	90
V [Å³]	1416.3(5)	10156(5)	1973.3(7)
Z	4	12	2
$\rho_{calc.}$ [g cm⁻³]	1.202	1.415	1.526
μ [mm⁻¹]	0.074	0.759	0.744
λ [Å]	0.71073	0.71073	0.71073
$F(000)$	552	4488	938
hkl range	±15, ±18, −8 ≤ l ≤ 10	−15 ≤ h ≤ 23, ±24, ±33	−15 ≤ h ≤ 16, ±25, −16 ≤ l ≤ 14
Reflections collected	21802	89475	80492
Independent reflections	3094	9436	13802
$R_{int.}$	0.1195	0.1621	0.0712
Number of parameters	177	638	528
R_1 ($I \geq 2\sigma(I)$)	0.0504	0.0470	0.0464
wR_2 (all data)	0.1060	0.0988	0.1011
Abs. structure parameter	–	–	−0.003(10)
Goodness-of-fit	0.836	0.846	0.918
Largest diff. peak, hole [e Å⁻³]	0.175; −0.194	0.468; −0.399	0.823; −0.539
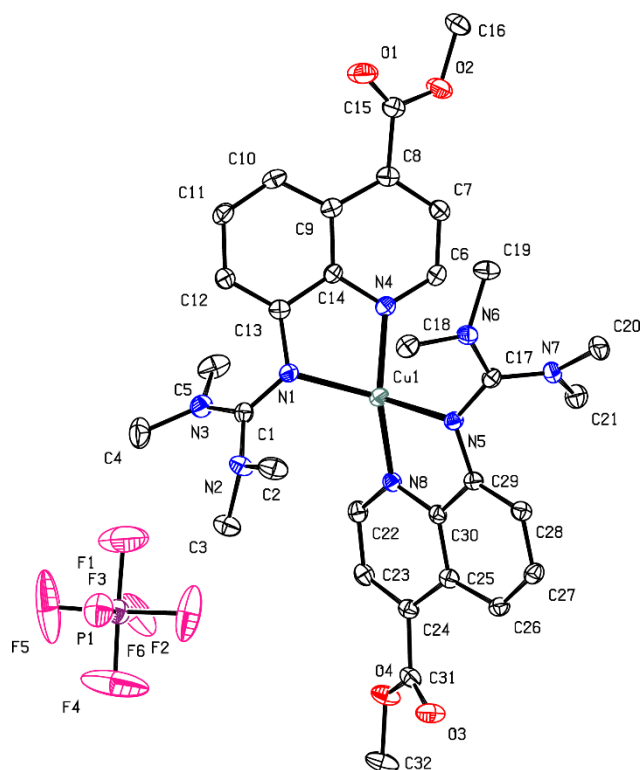
Fig. S4: Displacement ellipsoid plot of [Cu(TMG4Meequ)$_2$]PF$_6$ (**C13−PF$_6$**) (50 % probability level, asymmetric unit, H atoms are omitted for clarity).
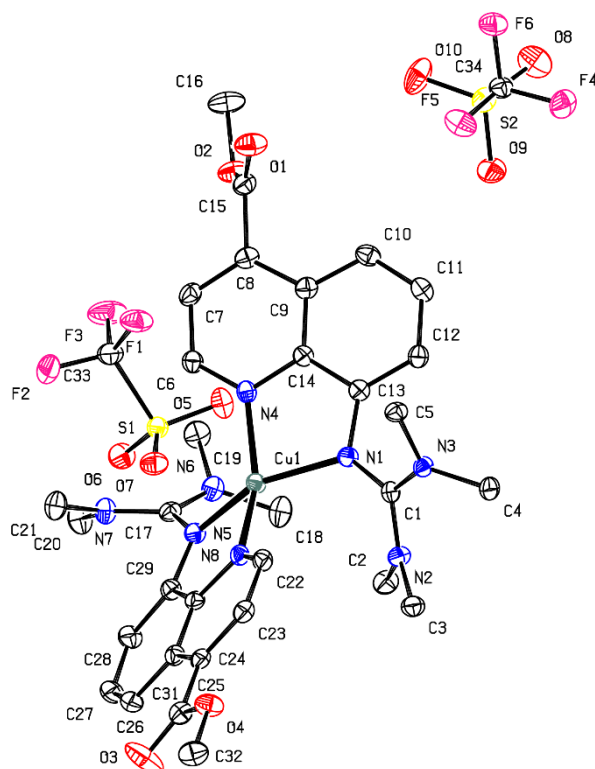

Fig. S5: Displacement ellipsoid plot of [Cu(TMG4Meequ)$_2$](OTf)$_2$·Et$_2$O (**C14−OTf**) (50 % probability level, asymmetric unit, H atoms are omitted for clarity). In **C14−OTf**, it was not possible to model the disordered molecule diethyl ether per asymmetric unit (162 Å³, 42 electrons) adequately and the data sets were treated with the SQUEEZE routine as implemented in PLATON.[15,16]

Table S2: Crystallographic data of [Cu(TMG4Meequ)$_2$]PF$_6$ (**C13−PF$_6$**) and [Cu(TMG4Meequ)$_2$](OTf)$_2$·Et$_2$O (**C14−OTf**).). In **C14−OTf**, it was not possible to model the disordered molecule diethyl ether per asymmetric unit (162 Å^3, 42 electrons) adequately and the data sets were treated with the SQUEEZE routine as implemented in PLATON.[15,16]

	C13−PF$_6$	C14−OTf
Empirical formula	C$_{32}$H$_{40}$CuF$_6$N$_8$O$_4$P	C$_{34}$H$_{40}$CuF$_6$N$_8$O$_{10}$S$_2$ [+ Et$_2$O]
Formula weight [g mol$^{−1}$]	809.23	962.40
Crystal size [mm]	0.190 x 0.150 x 0.090	0.190 x 0.120 x 0.050
T [K]	100	100
Crystal system	orthorhombic	triclinic
Space group	*Pbca*	*P$\bar{1}$*
a [Å]	9.5788(19)	9.5696(19)
b [Å]	25.802(5)	11.329(2)
c [Å]	28.714(6)	20.814(4)
α [°]	90	83.74(3)
β [°]	90	78.53(3)
γ [°]	90	73.62(3)
V [Å^3]	7097(2)	2118.4(8)
Z	8	2
$\rho_{calc.}$ [g cm$^{−3}$]	1.515	1.509
μ [mm$^{−1}$]	0.742	2.446
λ [Å]	0.71073	1.54186
F(000)	3344	990
hkl range	−13 ≤ h ≤ 14, −39 ≤ k ≤ 34, −30 ≤ l ≤ 44	−8 ≤ h ≤ 11, −13 ≤ k ≤ 12, −22 ≤ l ≤ 25
Reflections collected	178749	51599
Independent reflections	13239	7854
$R_{int.}$	0.1450	0.0391
Number of parameters	479	560
R_1 ($I \geq 2\sigma(I)$)	0.0427	0.0417
wR_2 (all data)	0.1022	0.1201
Goodness-of-fit	0.857	1.048
Largest diff. peak, hole [e Å$^{−3}$]	0.766; −0.689	0.996; −0.864

2.1.2 Structural properties of C11

Table S3: Selected bond lengths, bond angles and structure parameters of the two independent molecules of [Cu(TMG4Mequ)$_2$]$^+$ (**C11**) in the unit cell.

	[Cu(TMG4Mequ)$_2$]$^+$ (**C11**)	
	C11–1	**C11–2**
	Bond lengths [Å]	
Cu−N$_{gua,1/2}$	2.082(3), 2.055(3)	2.075(3), 2.075(3)
Cu−N$_{qu,1/2}$	1.970(3), 1.993(3)	1.998(3), 1.998(3)
	Bond angles [°]	
N$_{gua,1/2}$−Cu−N$_{qu,1/2}$	82.8(2), 82.5(2)	82.1(2), 82.1(2)
N$_{gua,1}$−Cu−N$_{gua,2}$	127.5(2)	129.2(2)
N$_{gua,1/2}$−Cu−N$_{qu,2/1}$	111.3(2), 120.9(2)	117.0(2), 117.0(2)
N$_{qu,1}$−Cu−N$_{qu,2}$	138.1(2)	136.6(2)
	Structure parameters	
τ_4 [ ]$^{[a]}$	0.67	0.67
∢ (CuN$_2$, CuN'$_2$) [°]	74.2	75.1
RMSD [Å]$^{[b]}$	0.148	

[a] $\tau_4 = \frac{360° - (\alpha + \beta)}{141°}$.[36]

[b] Considers inversion of one independent molecule.

2.2 Theoretical calculations

2.2.1 Optimization calculations

Table S4: Selected calculated bond lengths, bond angles and structure parameters of **C1**-**C4**, **C11** and **C12** (TPSSh, def2-TZVP, GD3BJ, PCM (MeCN); values of **C1**-**C4** from previous study).[21]

	TMGqu (**L1**)		TMG2Mequ (**L2**)		TMG4Mequ (**L7**)	
	C1	**C2**	**C3**	**C4**	**C11**	**C12**
	Bond lengths [Å]					
$Cu-N_{gua,1/2}$	2.066, 2.066	1.975, 1.975	2.083, 2.084	1.987, 1.987	2.065, 2.065	1.974, 1.974
$Cu-N_{qu,1/2}$	1.997, 1.997	1.979, 1.979	2.001, 2.001	1.987, 1.987	1.996, 1.996	1.974, 1.974
	Bond angles [°]					
$N_{gua,1/2}-Cu-N_{qu,1/2}$	82.3, 82.3	83.4, 83.4	81.9, 81.9	83.3, 83.3	82.06, 82.06	83.29, 83.29
$N_{gua,1}-Cu-N_{gua,2}$	129.3	149.4	124.6	136.2	129.21	149.48
$N_{gua,1/2}-Cu-N_{qu,2/1}$	114.3, 114.3	104.6, 104.6	115.9, 115.8	107.9, 107.9	114.54, 114.54	104.72, 104.73
$N_{qu,1}-Cu-N_{qu,2}$	142.2	149.8	143.1	150.4	142.28	149.75
	Structure parameters					
τ_4 [ ][a]	0.63	0.43	0.65	0.52	0.63	0.43
$\Delta\tau_4$ [ ]	0.20		0.13		0.20	
$\varnothing\tau_4$ [ ]	0.53		0.59		0.53	
∡(CuN$_2$, CuN'$_2$) [°]	70.3	46.5	74.4	57.3	70.5	46.5
Δ∡ [°]	23.8		17.1		24.0	
ρ [ ][b]	0.98, 0.98	1.00, 1.00	0.97, 0.97	1.00, 1.00	0.97, 0.97	1.00, 1.00

[a] $\tau_4 = \frac{360° - (\alpha + \beta)}{141°}$.[36]

[b] $\rho = \frac{2 \cdot a}{b + c}$ with $a = d(C_{gua}-N_{gua})$, $b = d(C_{gua}-N_{amine,1})$ and $c = d(C_{gua}-N_{amine,2})$.[37]

Table S5: Selected calculated bond lengths, bond angles and structure parameters of **C1**, **C2**, **C7**, **C8**, **C13** and **C14** (TPSSh, def2-TZVP, GD3BJ, PCM (MeCN); values of **C1**, **C2**, **C7** and **C8** from previous study).[21]

	TMGqu (**L1**)		TMG2Meequ (**L5**)		TMG4Meequ (**L8**)	
	C1	**C2**	**C7**	**C8**	**C13**	**C14**
Bond lengths [Å]						
Cu-N$_{gua,1/2}$	2.066, 2.066	1.975, 1.975	2.064, 2.045	2.120, 2.120	2.051, 2.051	1.979, 1.979
Cu-N$_{qu,1/2}$	1.997, 1.997	1.979, 1.979	2.024, 2.044	1.951, 1.951	1.988, 1.988	1.968, 1.968
Cu-O$_{carb,1/2}$	–	–	3.001, 4.524	2.407, 2.407	–	–
Cu-O$_{alc,1/2}$	–	–	4.448, 2.935	4.306, 4.306	–	–
Bond angles [°]						
N$_{gua,1/2}$-Cu-N$_{qu,1/2}$	82.3, 82.3	83.4, 83.4	81.7, 81.9	80.7, 80.7	82.10, 82.10	83.18, 83.18
N$_{gua,1}$-Cu-N$_{gua,2}$	129.3	149.4	119.6	110.0	129.95	149.69
N$_{gua,1/2}$-Cu-N$_{qu,2/1}$	114.3, 114.3	104.6, 104.6	137.7, 136.8	105.6, 105.6	114.43, 114.43	104.88, 104.88
N$_{qu,1}$-Cu-N$_{qu,2}$	142.2	149.8	108.0	169.3	141.89	149.38
Structure parameters						
τ_4 [ ][a]	0.63	0.43	0.61	0.60[c]	0.63	0.43
$\Delta\tau_4$ [ ]	0.20		0.00[c]		0.19	
$\varnothing\tau_4$ [ ]	0.53		0.61[c]		0.53	
∡(CuN$_2$, CuN'$_2$) [°]	70.3	46.5	66.8	74.3	70.1	46.6
Δ∡ [°]	23.8		−7.5		23.4	
ρ [ ][b]	0.98, 0.98	1.00, 1.00	0.98, 0.98	0.99, 0.99	0.98, 0.98	1.00, 1.00

[a] $\tau_4 = \frac{360° - (\alpha + \beta)}{141°}$.[36]

[b] $\rho = \frac{2 \cdot a}{b + c}$ with $a = d(C_{gua}–N_{gua})$, $b = d(C_{gua}–N_{amine,1})$ and $c = d(C_{gua}–N_{amine,2})$.[37]

[c] The comparability of this value is limited due to the 4+2 coordination motif.

2.2.2 NBO calculations

Table S6: Selected calculated NBO charges, charge-transfer energies E_{CT} and bond lengths of **C1**-**C4**, **C11** and **C12** (NBO6.0, TPSSh, def2-TZVP, GD3BJ, PCM (MeCN); values of **C1**-**C4** from previous study).[21]

	TMGqu (**L1**)		TMG2Mequ (**L2**)		TMG4Mequ (**L7**)	
	C1	**C2**	**C3**	**C4**	**C11**	**C12**
	NBO charges [e units]					
Cu	0.95	1.30	0.94	1.30	0.95	1.30
$N_{gua,1/2}$	−0.69, −0.69	−0.71, −0.71	−0.69, −0.69	−0.71, −0.71	−0.69, −0.69	−0.71, −0.71
$N_{qu,1/2}$	−0.53, −0.53	−0.52, −0.52	−0.54, −0.54	−0.53, −0.53	−0.53, −0.53	−0.53, −0.53
	Charge-transfer energies E_{CT} [kcal mol^{-1}]					
$N_{gua,1/2} \rightarrow Cu$	20.3, 20.3	48.7, 48.7	18.4, 18.4	41.0, 41.0	20.1, 20.1	47.4, 47.3
$N_{qu,1/2} \rightarrow Cu$	29.6, 29.6	52.8, 52.8	26.7, 26.7	51.1, 51.1	29.9, 29.9	54.0, 54.0
	Bond lengths [Å]					
$Cu-N_{gua,1/2}$	2.066, 2.066	1.975, 1.975	2.083, 2.084	1.987, 1.987	2.065, 2.065	1.974, 1.974
$Cu-N_{qu,1/2}$	1.997, 1.997	1.979, 1.979	2.001, 2.001	1.987, 1.987	1.996, 1.996	1.974, 1.974

Table S7: Selected calculated NBO charges, charge-transfer energies E_{CT} and bond lengths of **C1**, **C2**, **C7**, **C8**, **C13** and **C14** (NBO6.0, TPSSh, def2-TZVP, GD3BJ, PCM (MeCN); values of **C1**, **C2**, **C7** and **C8** from previous study).[21]

	TMGqu (**L1**)		TMG2Meequ (**L5**)		TMG4Meequ (**L8**)	
	C1	**C2**	**C7**	**C8**	**C13**	**C14**
NBO charges [e units]						
Cu	0.95	1.30	1.00	1.37	0.99	1.30
$N_{gua,1/2}$	−0.69, −0.69	−0.71, −0.71	−0.69, −0.69	−0.69, −0.69	−0.69, −0.69	−0.71, −0.71
$N_{qu,1/2}$	−0.53, −0.53	−0.52, −0.52	−0.49, −0.48	−0.47, −0.47	−0.51, −0.51	−0.50, −0.50
$O_{acyl,1/2}$	–	–	−0.58, −0.60	−0.61, −0.61	–	–
$O_{alc,1/2}$	–	–	−0.46, −0.45	−0.43, −0.43	–	–
Charge-transfer energies E_{CT} [kcal mol^{-1}]						
$N_{gua,1/2} \rightarrow Cu$	20.3, 20.3	48.7, 48.7	21.5, 22.3	26.9, 26.9	21.6, 21.6	49.4, 49.4
$N_{qu,1/2} \rightarrow Cu$	29.6, 29.6	52.8, 52.8	20.3, 19.4	64.2, 64.2	29.5, 29.5	51.5, 51.5
$O_{acyl,11/12} \rightarrow Cu$	–	–	2.6, –	14.1, 14.1	–	–
$O_{alc,1/2} \rightarrow Cu$	–	–	0.1, 2.5	–	–	–
Bond lengths [Å]						
$Cu-N_{gua,1/2}$	2.066, 2.066	1.975, 1.975	2.064, 2.045	2.120, 2.120	2.051, 2.051	1.968, 1.968
$Cu-N_{qu,1/2}$	1.997, 1.997	1.979, 1.979	2.024, 2.044	1.951, 1.951	1.988, 1.988	1.979, 1.979
$Cu-O_{acyl,1/2}$	–	–	3.001, 4.524	2.407, 2.407	–	–
$Cu-O_{alc,1/2}$	–	–	4.448, 2.935	4.306, 4.306	–	–

Table S8: Calculated charge-transfer energies $E_{CT,total}$, $E_{CT,gua}$ and $E_{CT,qu}$ of **C1**-**C14** and charge-transfer energy differences $\Delta E_{CT,total}$, $\Delta E_{CT,gua}$ and $\Delta E_{CT,qu}$ between the related Cu(I) and Cu(II) complexes ($E_{CT,total}$ and $\Delta E_{CT,total}$ values of **C7** and **C8** that include the O donors are marked red; NBO6.0, TPSSh, def2-TZVP, GD3BJ, PCM (MeCN); values of **C1**-**C10** from previous study).[21]

		Total		Gua		Qu	
		$E_{CT,total}$ [kcal mol^{-1}]	$\Delta E_{CT,total}$ [kcal mol^{-1}]	$E_{CT,gua}$ [kcal mol^{-1}]	$\Delta E_{CT,gua}$ [kcal mol^{-1}]	$E_{CT,qu}$ [kcal mol^{-1}]	$\Delta E_{CT,qu}$ [kcal mol^{-1}]
C1	**R1**	99.7	101.2	40.6	54.7	59.1	46.5
C2		200.9		95.3		105.6	
C3	**R2**	90.2	92.7	36.8	43.9	53.4	48.8
C4		183.0		80.8		102.2	
C5	**R3**	77.5	86.7	42.0	33.7	35.5	53.1
C6		164.2		75.7		88.6	
C7	**R4**	83.4 (88.6)	98.7 (121.6)	43.8	10.0	39.6	88.7
C8		182.1 (210.3)		53.8		128.3	
C9	**R5**	99.6	105.4	36.8	52.8	62.8	52.6
C10		205.0		89.6		115.4	
C11	**R6**	100.0	102.7	40.3	54.4	59.8	48.2
C12		202.7		94.7		108.0	
C13	**R7**	102.3	99.6	43.3	55.6	59.0	43.9
C14		201.9		98.9		103.0	

2.2.3 Ground state energies

Table S9: Calculated ground state energies $E_{GS,DFT/CCSD(T)}$ of **C1**-**C14** and ground state energy differences $\Delta E_{GS,DFT/CCSD(T)}$ of **R1-R7** (DFT: TPSSh, def2-TZVP, GD3BJ, PCM (MeCN); DLPNO-CCSD(T): def2-TZVP, def2-TZVP/C, C-PCM (MeCN)).[21]

		DFT			DLPNO-CCSD(T)		
		$E_{GS,DFT}$ [Hartree]	$\Delta E_{GS,DFT}$ [Hartree]	$\Delta E_{GS,DFT}$ [kJ mol^{-1}]	$E_{GS,CCSD(T)}$ [Hartree]	$\Delta E_{GS,CCSD(T)}$ [Hartree]	$\Delta E_{GS,CCSD(T)}$ [kJ mol^{-1}]
C1	**R1**	−3167.950965	0.155933	409.403	−3163.272869	0.137190	360.193
C2		−3167.795032			−3163.135679		
C3	**R2**	−3246.638749	0.160757	422.067	−3241.758956	0.142964	375.352
C4		−3246.477992			−3241.615992		
C5	**R3**	−3637.583401	0.164822	432.741	−3631.709921	0.150203	394.358
C6		−3637.418579			−3631.559718		
C7	**R4**	−3623.924555	0.155463	408.168	−3618.351410	0.142446	373.992
C8		−3623.769092			−3618.208964		
C9	**R5**	−3436.027554	0.145199	380.957	−3430.709141	0.131653	345.654
C10		−3435.882455			−3430.577488		
C11	**R6**	−3246.630632	0.153487	402.980	−3241.748947	0.135638	356.118
C12		−3246.477145			−3241.613309		
C13	**R7**	−3623.915109	0.161590	424.254	−3618.334396	0.139586	366.484
C14		−3623.753519			−3618.194810		

2.2.4 Reorganization energies

Table S10: Calculated energies of the Cu complexes for different charge, structure and solvent configurations and resulting total, internal and solvent reorganization energies of **R6** and **R7** (TPSSh, def2-TZVP, GD3BJ, PCM (MeCN)).

	[Cu(TMG4Mequ)$_2$]$^{+/2+}$ (**R6**)		[Cu(TMG4Meequ)$_2$]$^{+/2+}$ (**R7**)	
	C11	**C12**	**C13**	**C14**
	Total reorganization energy $\lambda_{11,T}$			
$E_{Cu(X)L(I)S(I)}$ [Hartree]	−3246.630632	−3246.439174	−3623.915109	−3623.717272
$E_{Cu(X)L(II)S(II)}$ [Hartree]	−3246.591907	−3246.477145	−3623.877370	−3623.753519
$\lambda_{Cu(X),T}$ [Hartree]	0.0387	0.0380	0.0377	0.0362
$\lambda_{11,T}$ [kJ mol^{-1}]	201.4		194.2	
	Internal reorganization energy $\lambda_{11,I}$			
$E_{Cu(X)L(I)S(X)}$ [Hartree]	−3246.630632	−3246.46438	−3623.915109	−3623.741585
$E_{Cu(X)L(II)S(X)}$ [Hartree]	−3246.617313	−3246.477145	−3623.902249	−3623.753519
$\lambda_{Cu(X),I}$ [Hartree]	0.0133	0.0128	0.0129	0.0119
$\lambda_{11,I}$ [kJ mol^{-1}]	68.5		65.1	
	Solvent reorganization energy $\lambda_{11,S}$			
$\lambda_{11,S}$ [kJ mol^{-1}]	132.9		129.2	

2.3 Cyclic voltammograms
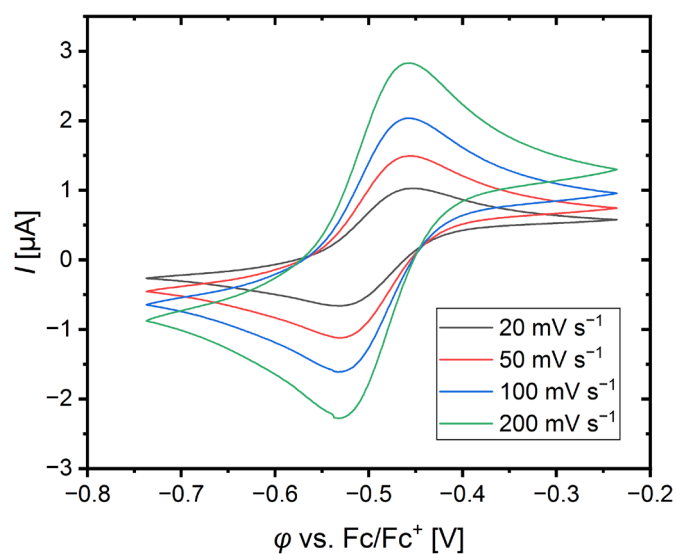
Fig. S6: Cyclic voltammogram of [Cu(TMG4Mequ)$_2$]$^{+/2+}$ (**R6**) starting from [Cu(TMG4Mequ)$_2$]PF$_6$ (**C11−PF$_6$**) (c = 1 mM) in MeCN solution with NBu$_4$PF$_6$ (c = 100 mM).
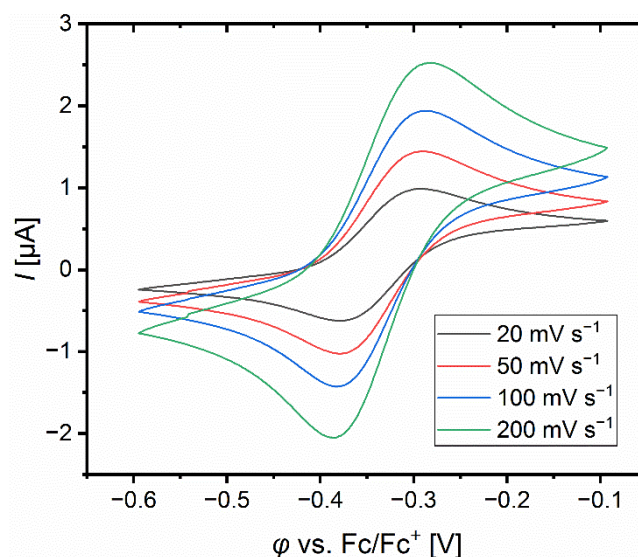
Fig. S7: Cyclic voltammogram of [Cu(TMG4Meequ)$_2$]$^{+/2+}$ (**R7**) starting from [Cu(TMG4Meequ)$_2$]PF$_6$ (**C13−PF$_6$**) (c = 1 mM) in MeCN solution with NBu$_4$PF$_6$ (c = 100 mM).

2.4 UV/Vis spectra
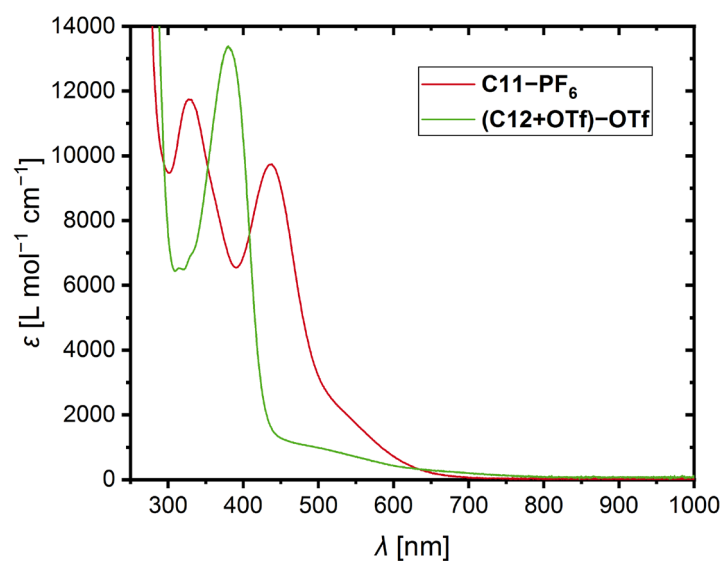
Fig. S8: UV/Vis spectra of [Cu(TMG4Mequ)$_2$]PF$_6$ (**C11−PF$_6$**) and [Cu(TMG4Mequ)$_2$](OTf)$_2$ (**(C12+OTf)−OTf**) in MeCN at room temperature.
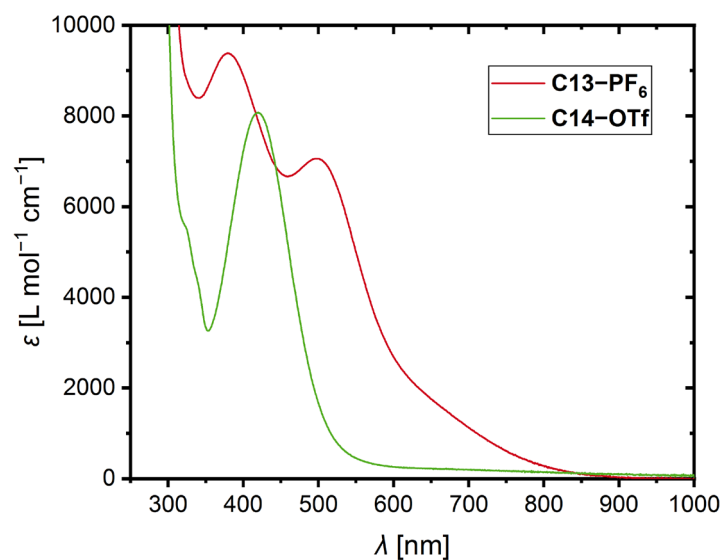
Fig. S9: UV/Vis spectra of [Cu(TMG4Meequ)$_2$]PF$_6$ (**C13−PF$_6$**) and [Cu(TMG4Meequ)$_2$](OTf)$_2$ (**C14−OTf**) in MeCN at room temperature.

2.5 Stopped-flow UV/Vis measurements

$k_{12} = (4.90 \pm 0.19) \cdot 10^4 \text{ L mol}^{-1} \text{ s}^{-1}$

$R^2 = 0.9942$
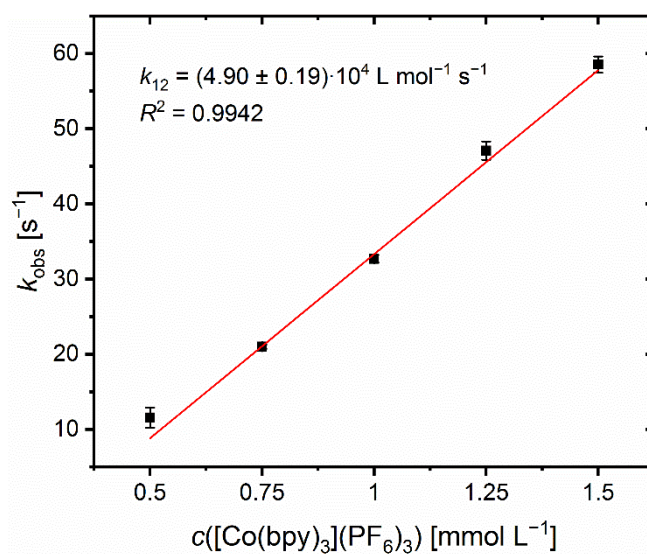
Fig. S10: Plot of the reaction rate k_{obs} of the cross reaction between [Cu(TMG4Mequ)$_2$]PF$_6$ (**C11–PF$_6$**) and [Co(bpy)$_3$](PF$_6$)$_3$ in MeCN at 298 K against the concentration of [Co(bpy)$_3$](PF$_6$)$_3$ (some error bars are too small to be visualized properly).

$k_{12} = (3.88 \pm 0.16) \cdot 10^3 \text{ L mol}^{-1} \text{ s}^{-1}$

$R^2 = 0.9939$
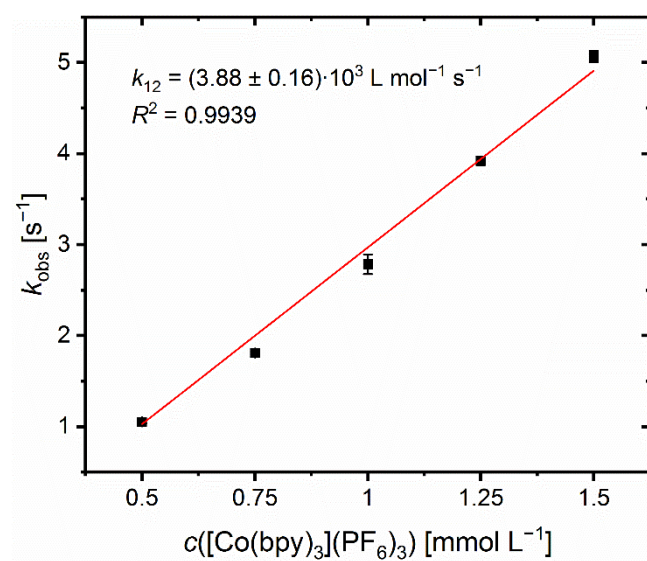
Fig. S11: Plot of the reaction rate k_{obs} of the cross reaction between [Cu(TMG4Meequ)$_2$]PF$_6$ (**C13–PF$_6$**) and [Co(bpy)$_3$](PF$_6$)$_3$ in MeCN at 298 K against the concentration of [Co(bpy)$_3$](PF$_6$)$_3$ (some error bars are too small to be visualized properly).

2.6 NMR spectra

2.6.1 TMG4Mequ (L7) and corresponding precursors and Cu(I) complex

2.6.1.1 4-Methyl-8-nitroquinoline (4-Me-8-NO₂-qu)
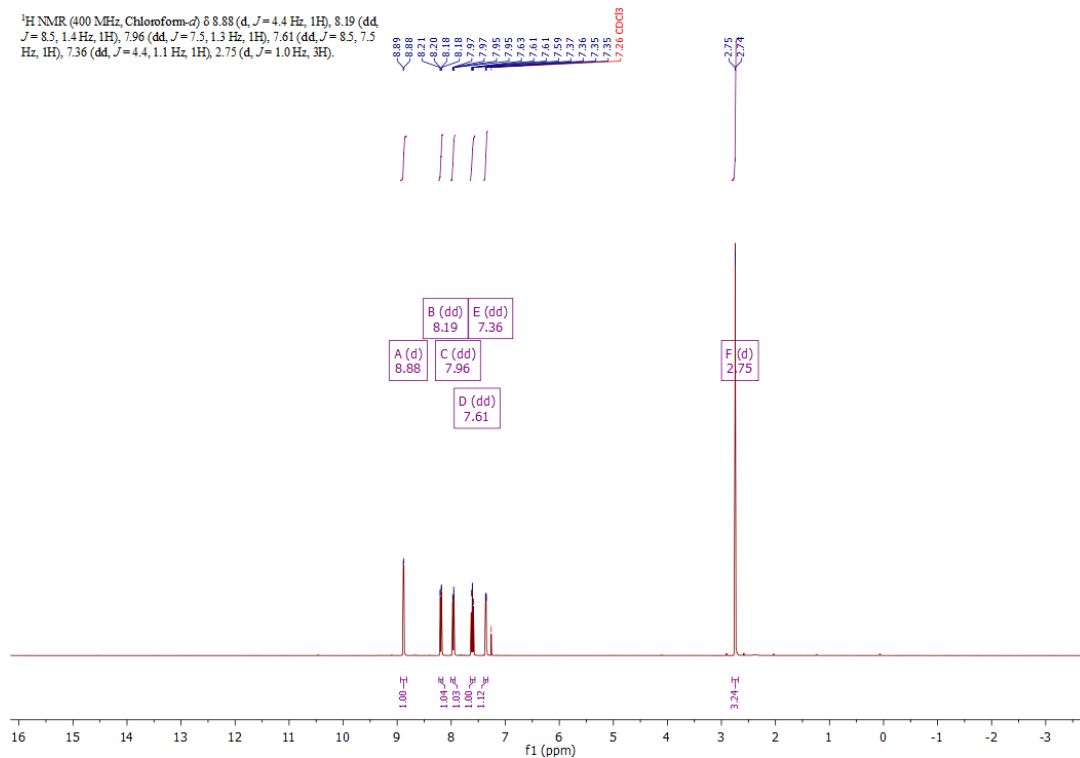
Fig. S12: ¹H NMR spectrum of 4-Me-8-NO₂-qu in CDCl₃.

Fig. S13: Magnification of the ¹H NMR spectrum of 4-Me-8-NO₂-qu in CDCl₃.

35

¹³C NMR (101 MHz, CDCl₃) δ 152.3, 149.1, 144.9, 139.5, 129.3, 128.0, 125.1, 123.6, 123.1, 19.01.
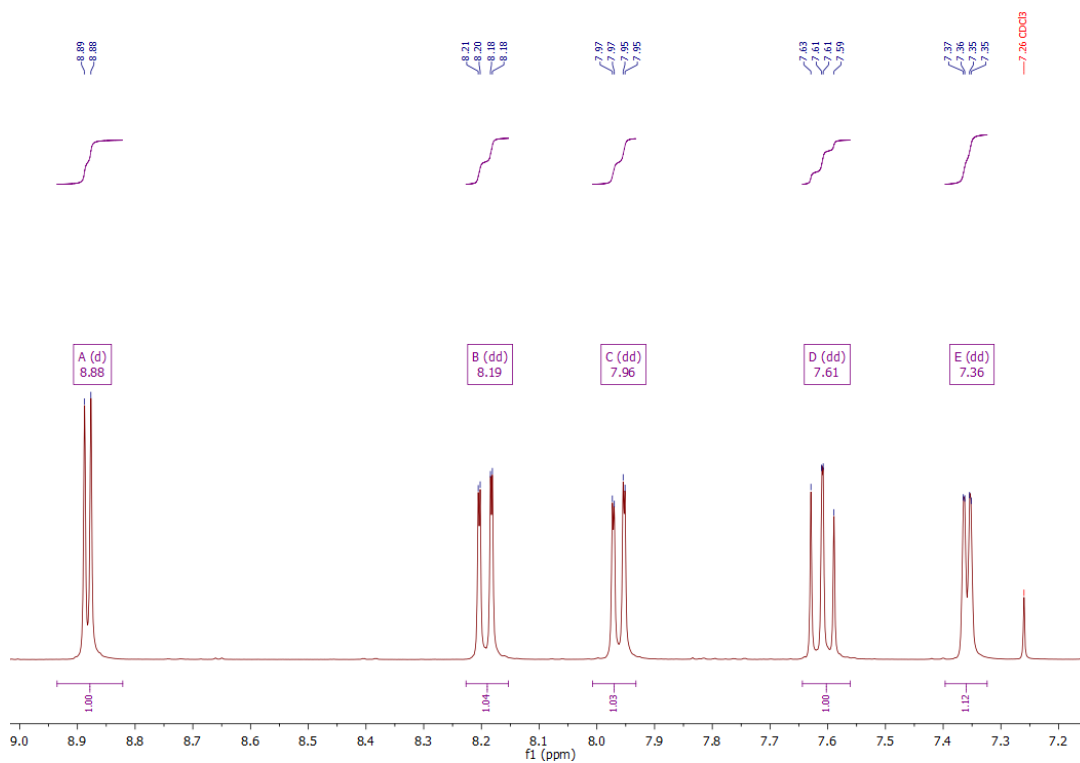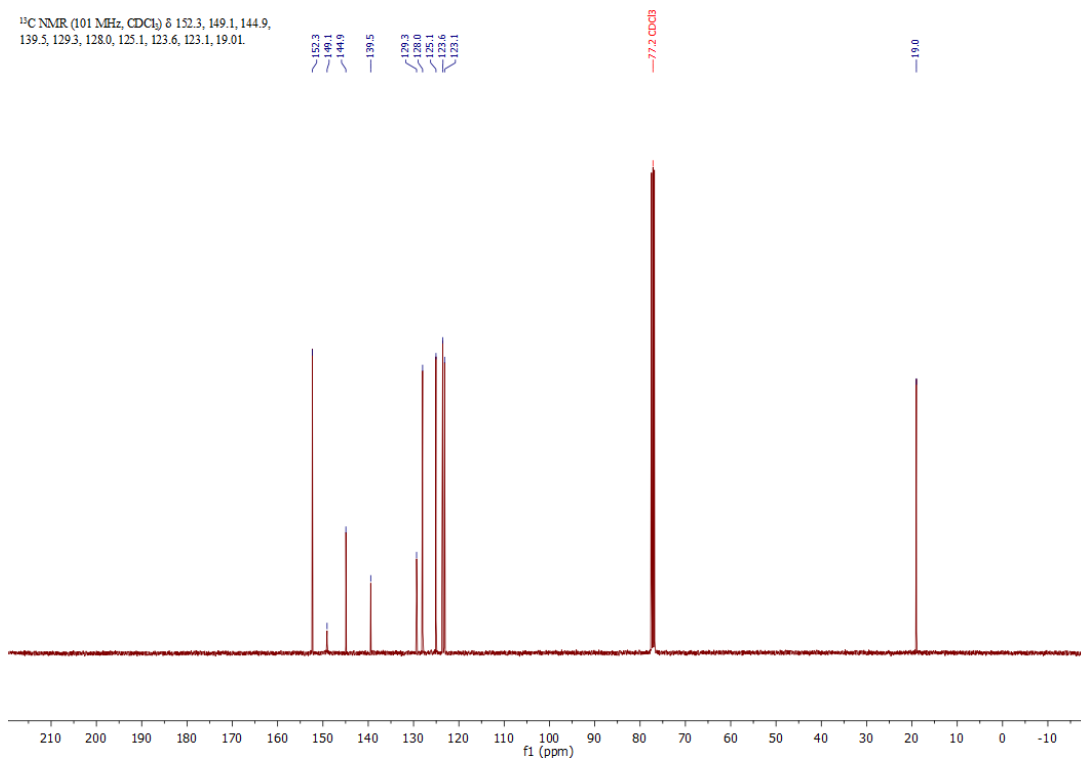
Fig. S14: ^{13}C{^{1}H} NMR spectrum of 4-Me-8-NO₂-qu in CDCl₃.
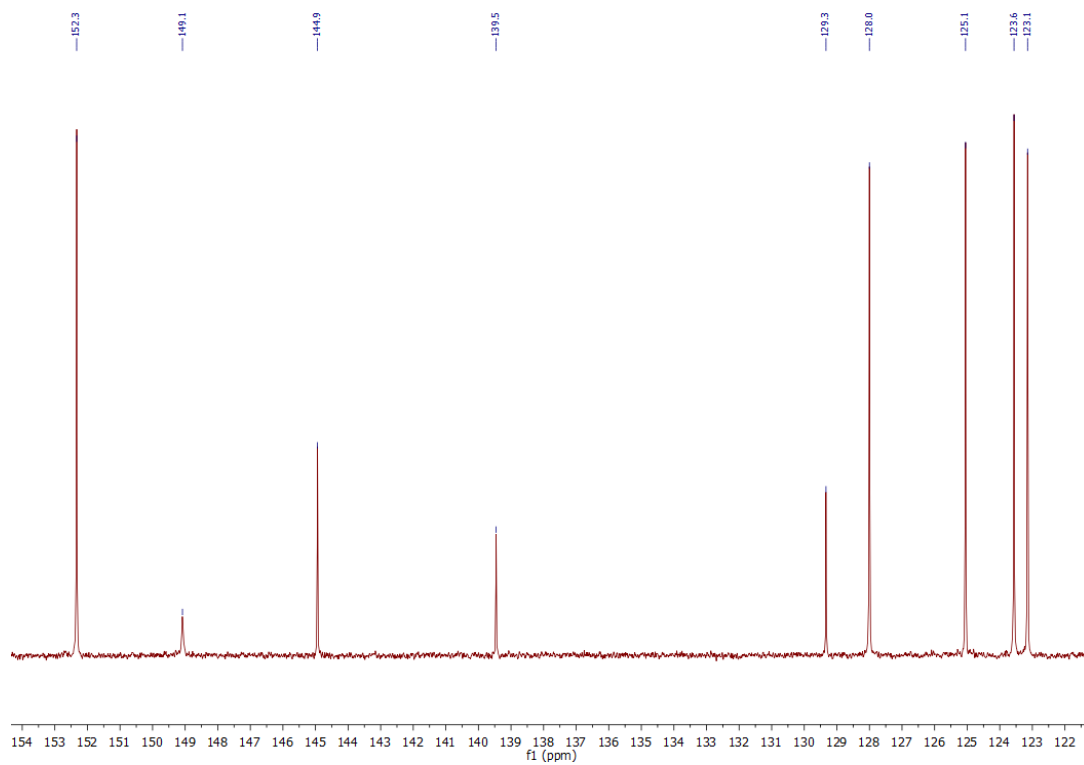
Fig. S15: Magnification of the ^{13}C{^{1}H} NMR spectrum of 4-Me-8-NO₂-qu in CDCl₃.

36

2.6.1.2   4-Methyl-8-aminoquinoline (4-Me-8-NH₂-qu)

¹H NMR (400 MHz, Chloroform-*d*) δ 8.62 (d, *J* = 4.3 Hz, 1H), 7.35 (dd, *J* = 8.4, 7.2 Hz, 1H), 7.29 (dd, *J* = 8.4, 1.5 Hz, 1H), 7.20 (dd, *J* = 4.4, 1.0 Hz, 1H), 6.93 (dd, *J* = 7.2, 1.5 Hz, 1H), 5.01 (s, 2H), 2.65 (d, *J* = 0.9 Hz, 3H).
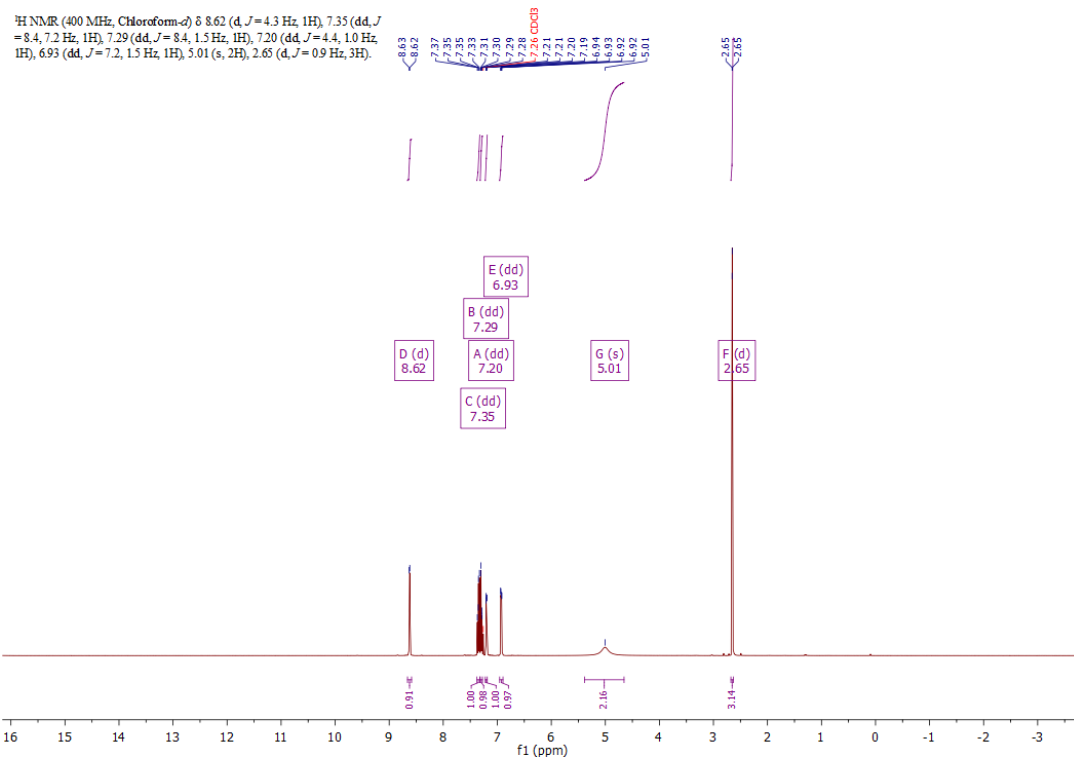
Fig. S16: ¹H NMR spectrum of 4-Me-8-NH₂-qu in CDCl₃.

Fig. S17: Magnification of the ¹H NMR spectrum of 4-Me-8-NH₂-qu in CDCl₃.

^{13}C NMR (101 MHz, CDCl$_3$) δ 147.1, 144.6, 144.5, 138.1, 128.9, 127.2, 122.3, 112.2, 110.1, 19.1.
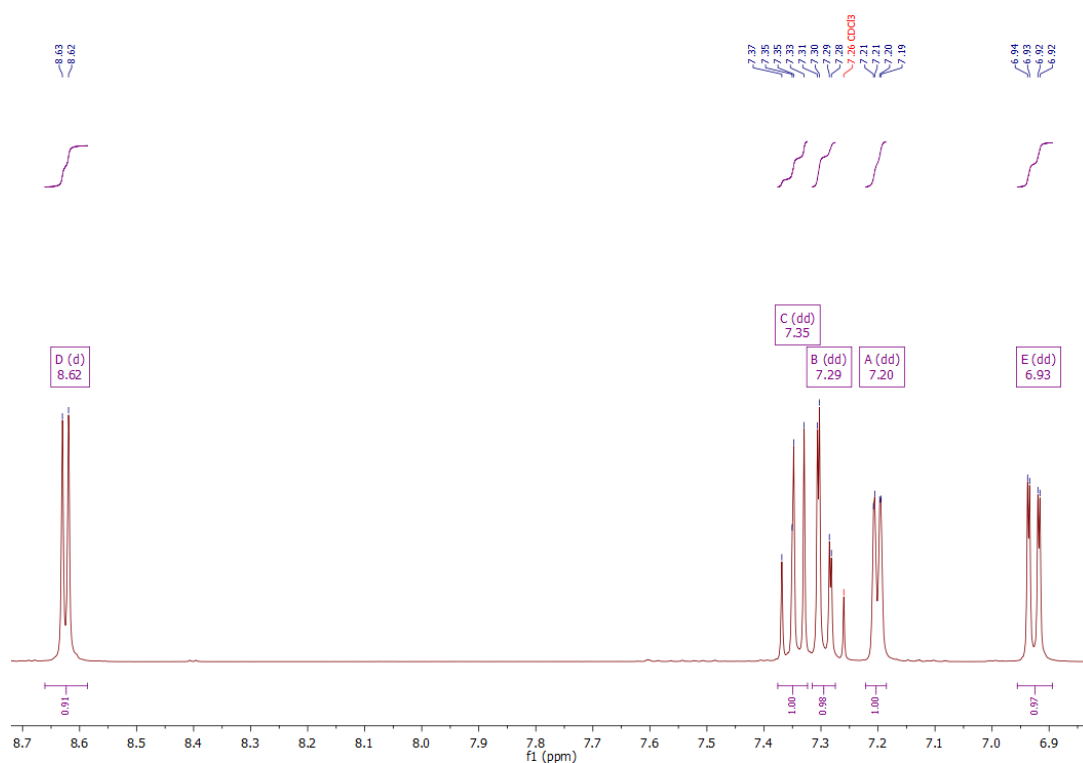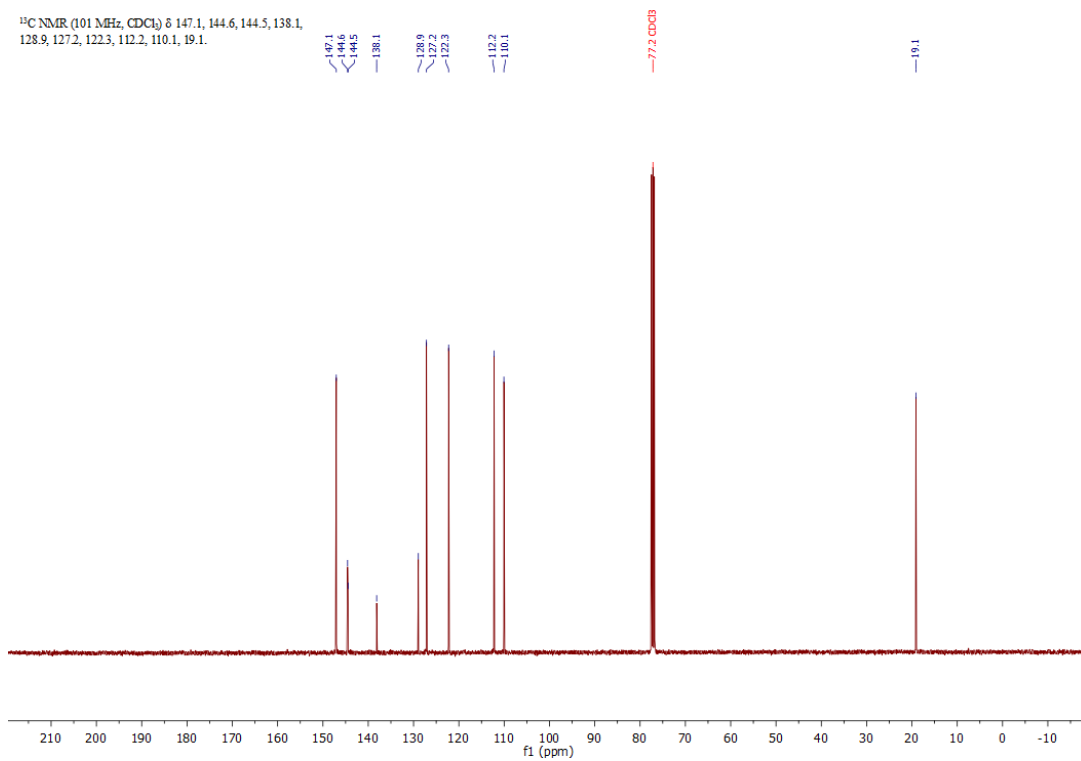
Fig. S18: ^{13}C{^{1}H} NMR spectrum of 4-Me-8-NH$_2$-qu in CDCl$_3$.
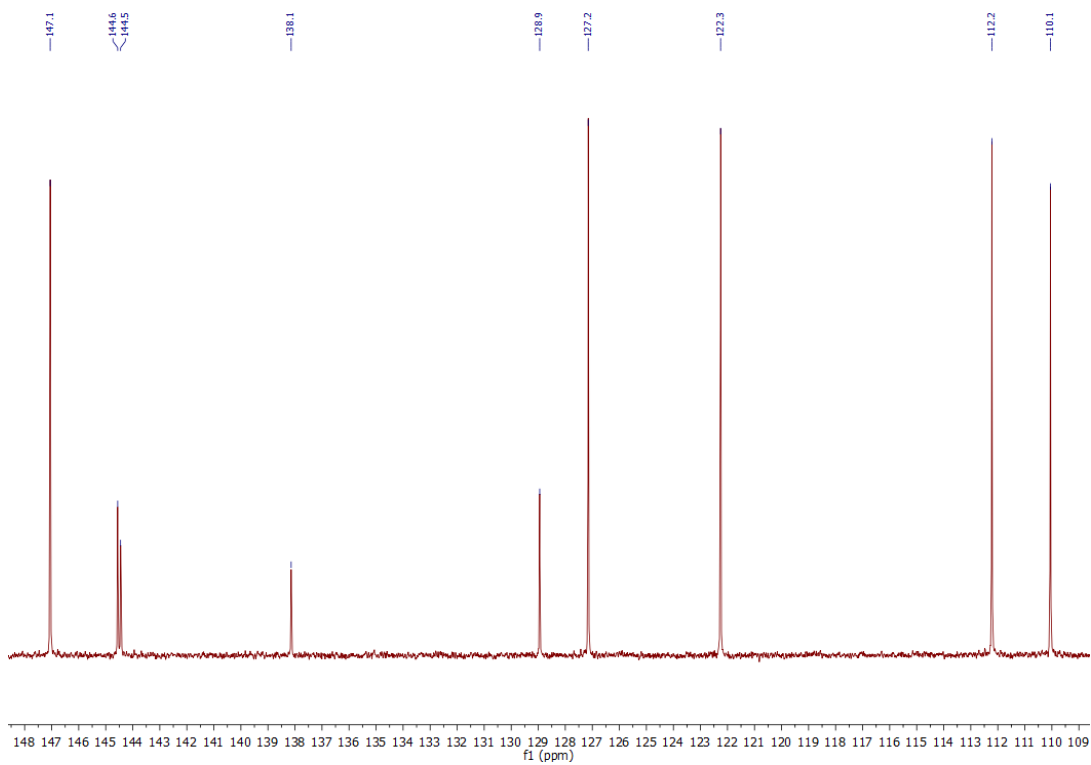
Fig. S19: Magnification of the ^{13}C{^{1}H} NMR spectrum of 4-Me-8-NH$_2$-qu in CDCl$_3$.

2.6.1.3 TMG4Mequ (L7)

^{1}H NMR (400 MHz, Chloroform-d) δ 8.48 (d, J = 4.3 Hz, 1H), 7.20 (dd, J = 8.3, 1.8 Hz, 1H), 7.16 (dd, J = 8.3, 7.0 Hz, 1H), 6.87 (dd, J = 4.3, 1.1 Hz, 1H), 6.64 (dd, J = 7.0, 1.8 Hz, 1H), 2.47 (s, 12H), 2.39 (d, J = 1.0 Hz, 3H).
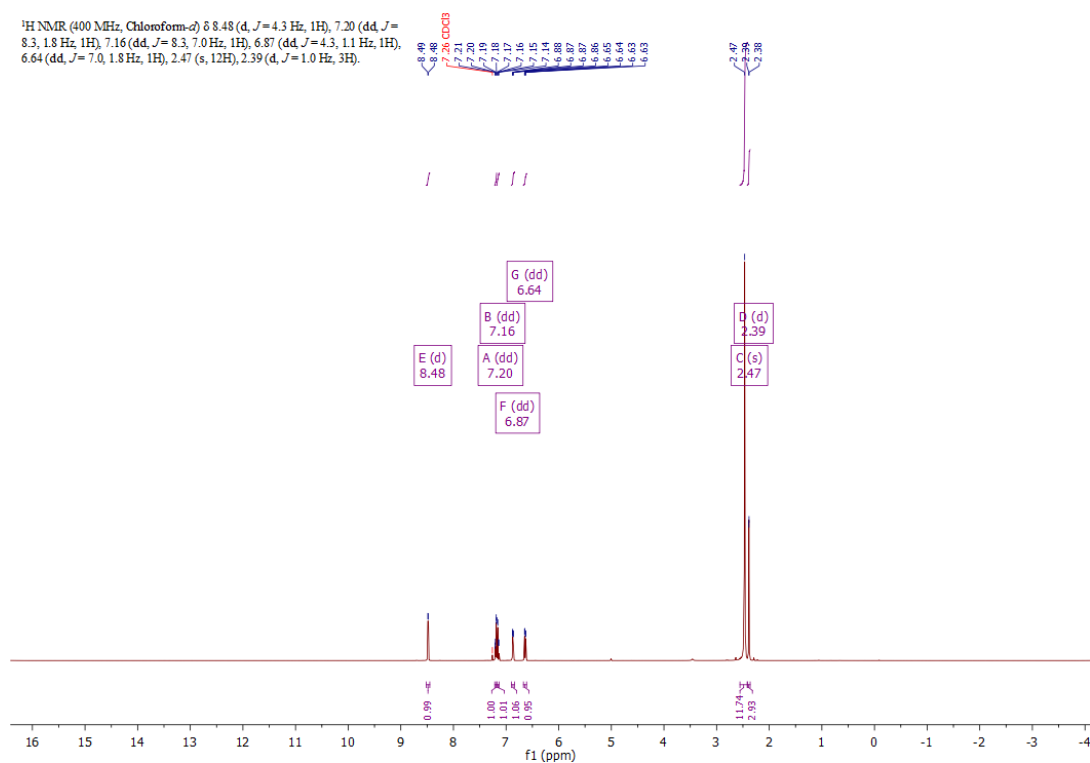
Fig. S20: ^{1}H NMR spectrum of TMG4Mequ (**L7**) in CDCl$_3$.
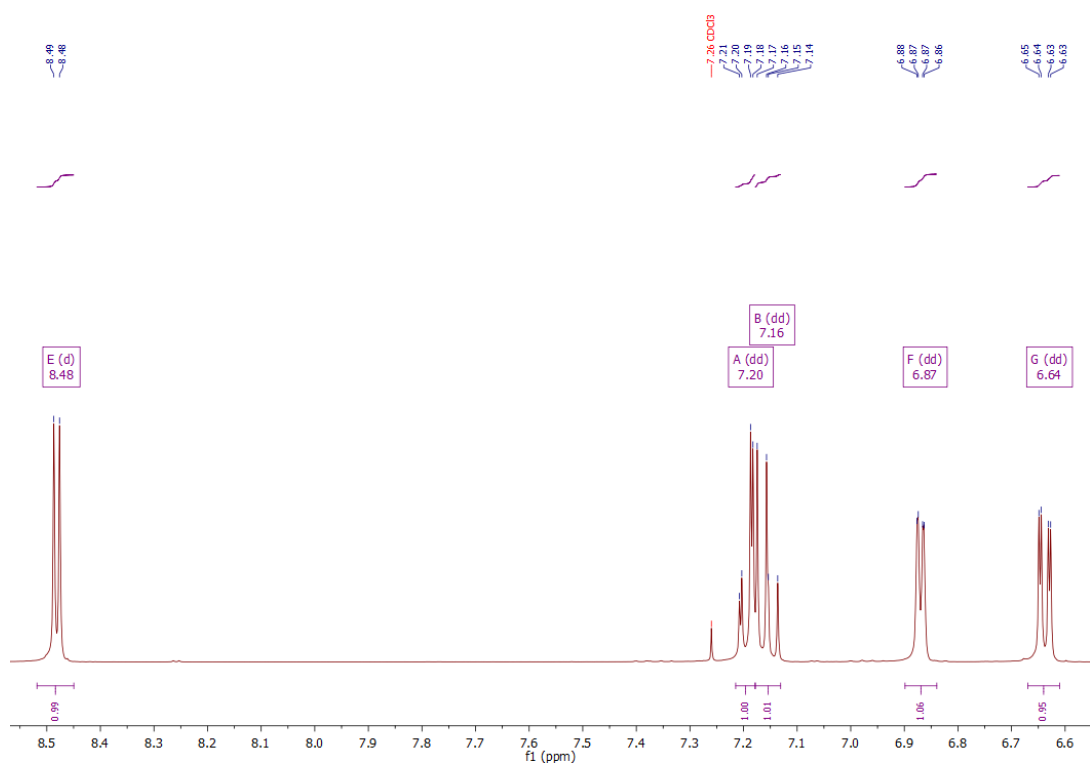
Fig. S21: Magnification of the ^{1}H NMR spectrum of TMG4Mequ (**L7**) in CDCl$_3$.
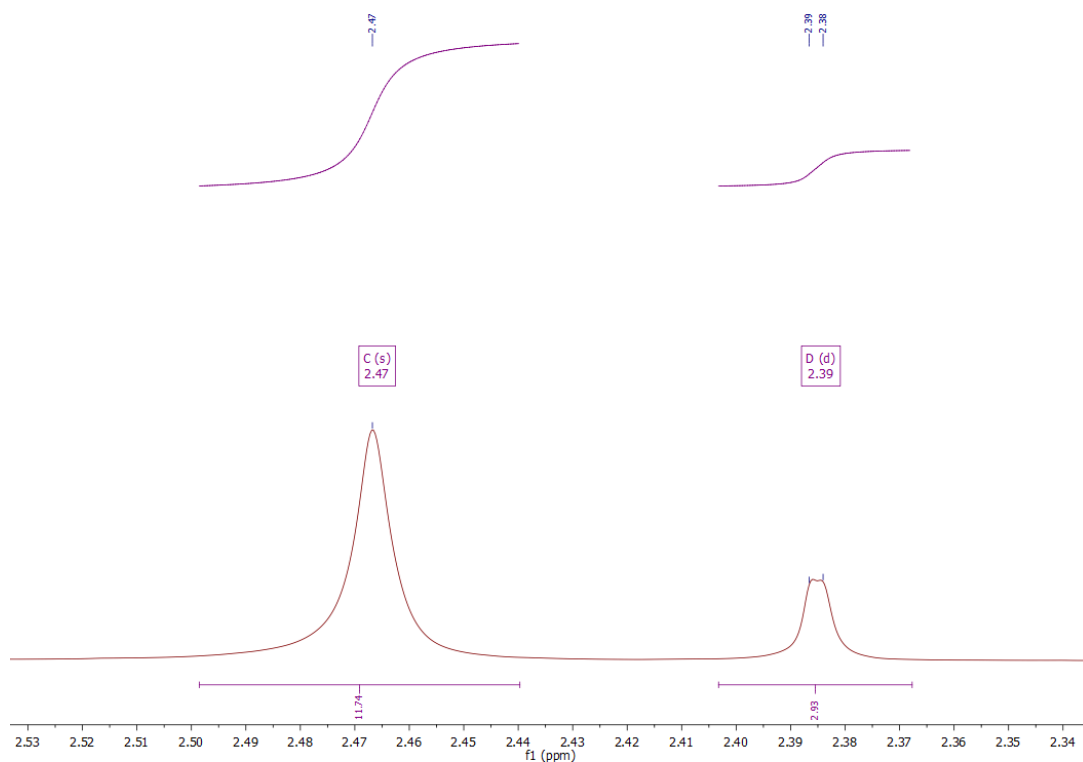
Fig. S22: Magnification of the ^{1}H NMR spectrum of TMG4Mequ (**L7**) in CDCl$_3$.

^{13}C NMR (101 MHz, CDCl$_3$) δ 160.9, 150.2, 147.6, 143.1, 142.2, 128.8, 126.3, 121.0, 118.3, 114.1, 39.0, 18.6.
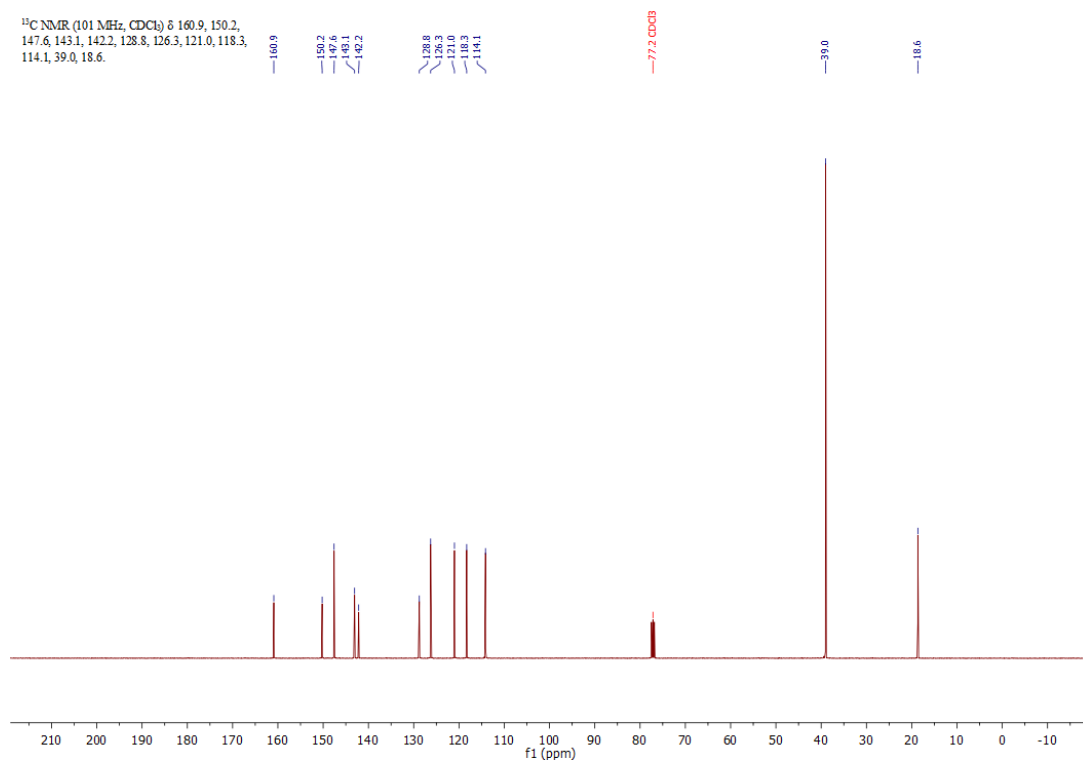
Fig. S23: ^{13}C{^{1}H} NMR spectrum of TMG4Mequ (**L7**) in CDCl$_3$.
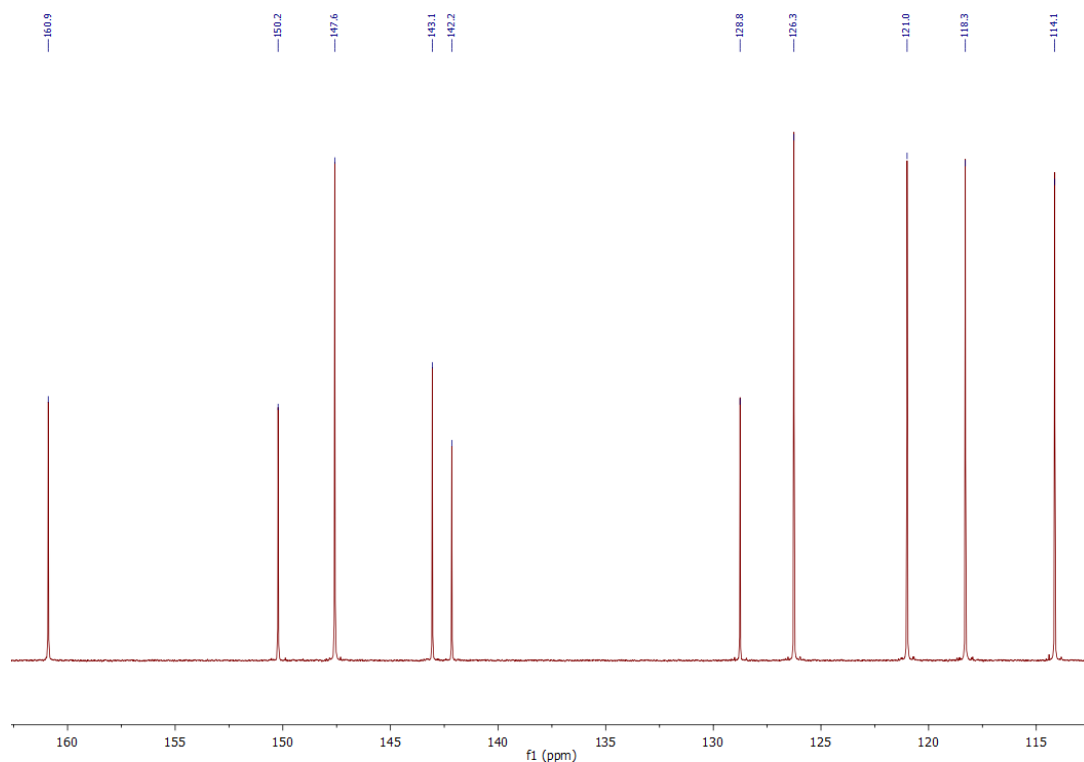
Fig. S24: Magnification of the $^{13}C\{^1H\}$ NMR spectrum of TMG4Mequ (**L7**) in CDCl$_3$.

2.6.1.4 [Cu(TMG4Mequ)₂]PF₆ (C11−PF₆)

^{1}H NMR (400 MHz, MeCN-d3) δ 8.39 (s, 1H), 7.74 − 7.46 (m, H), 7.34 (s, 1H), 6.89 (s, 1H), 2.69 (s, 3H), 2.49 (s,12H).
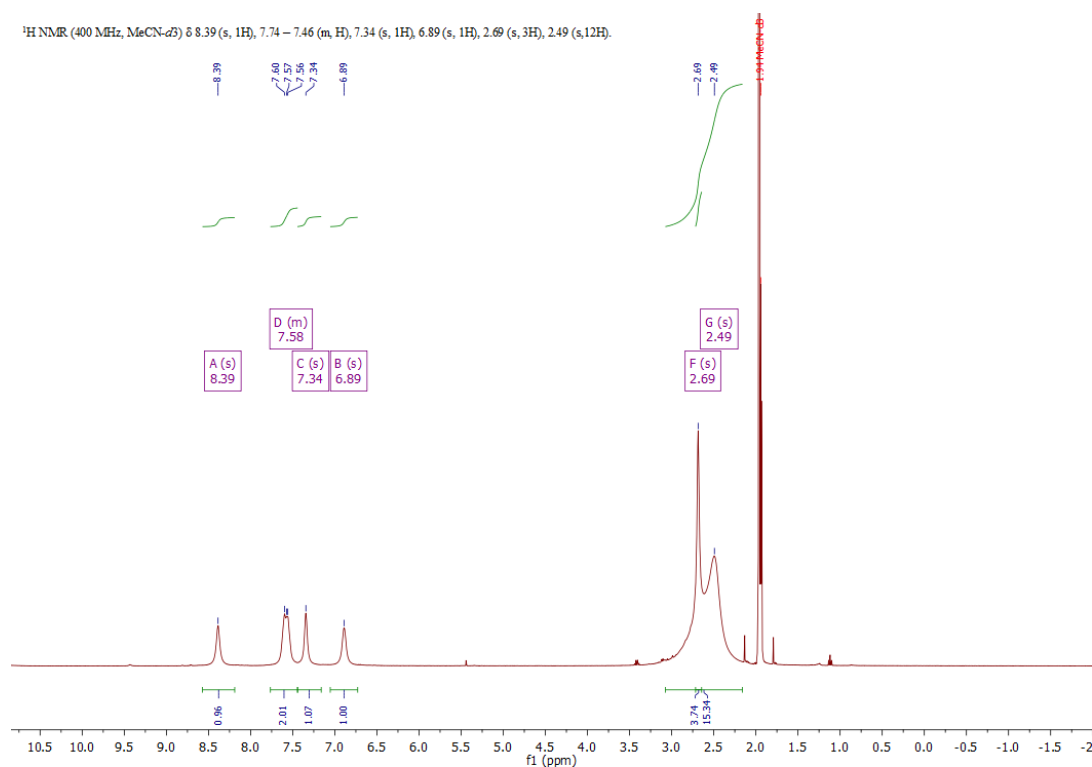
Fig. S25: ^{1}H NMR spectrum of [Cu(TMG4Mequ)₂]PF₆ (**C11−PF₆**) in MeCN-d3 (due to the limited solubility in MeCN and other solvents, it was not possible to measure NMR spectra with a better S/N ratio).
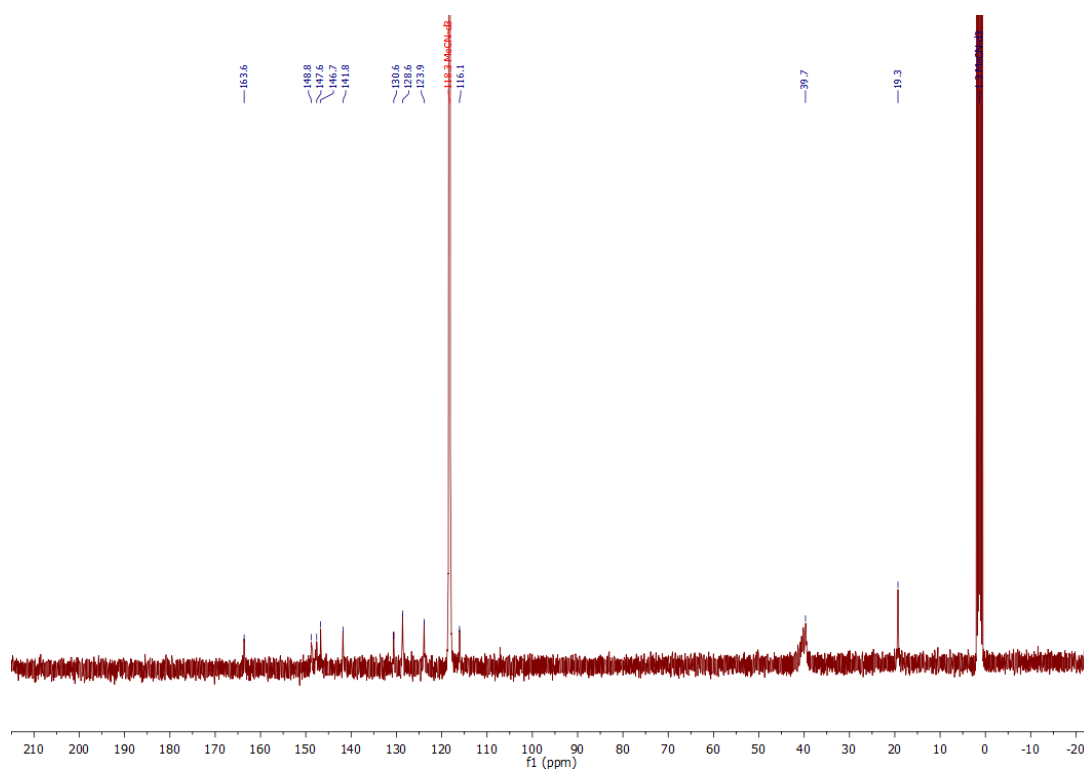
41
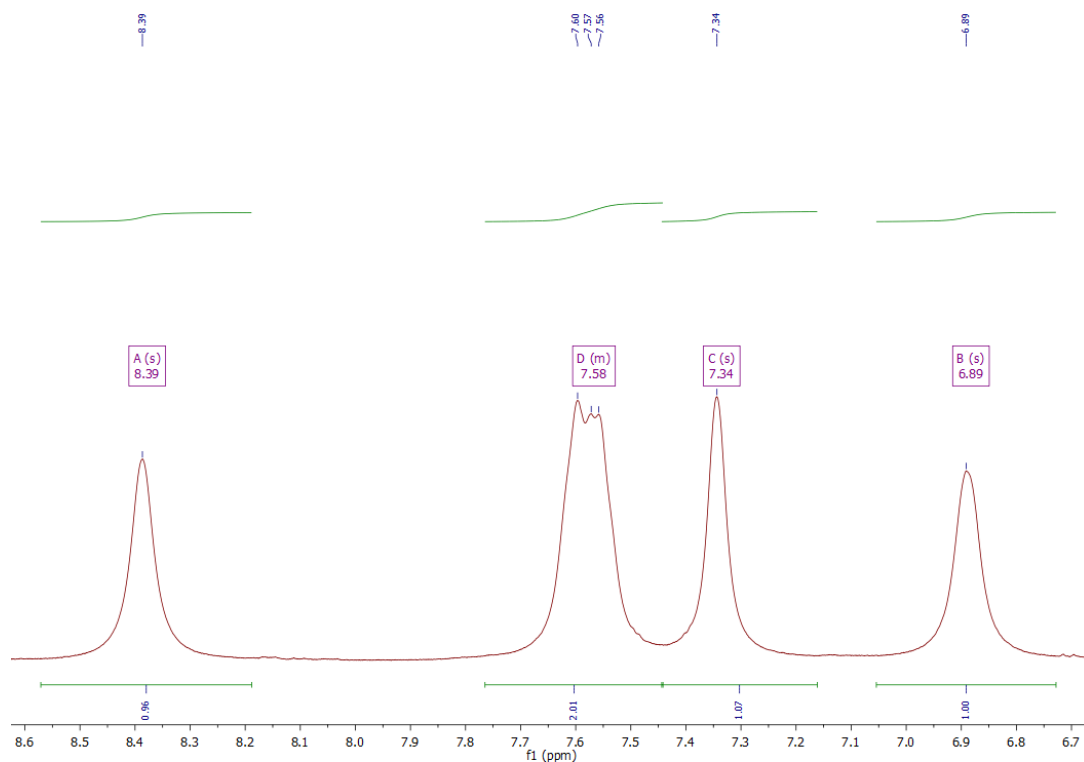
Fig. S26: Magnification of the ^{1}H NMR spectrum of [Cu(TMG4Mequ)$_2$]PF$_6$ (**C11−PF$_6$**) in MeCN-*d*3 (due to the limited solubility in MeCN and other solvents, it was not possible to measure NMR spectra with a better S/N ratio).
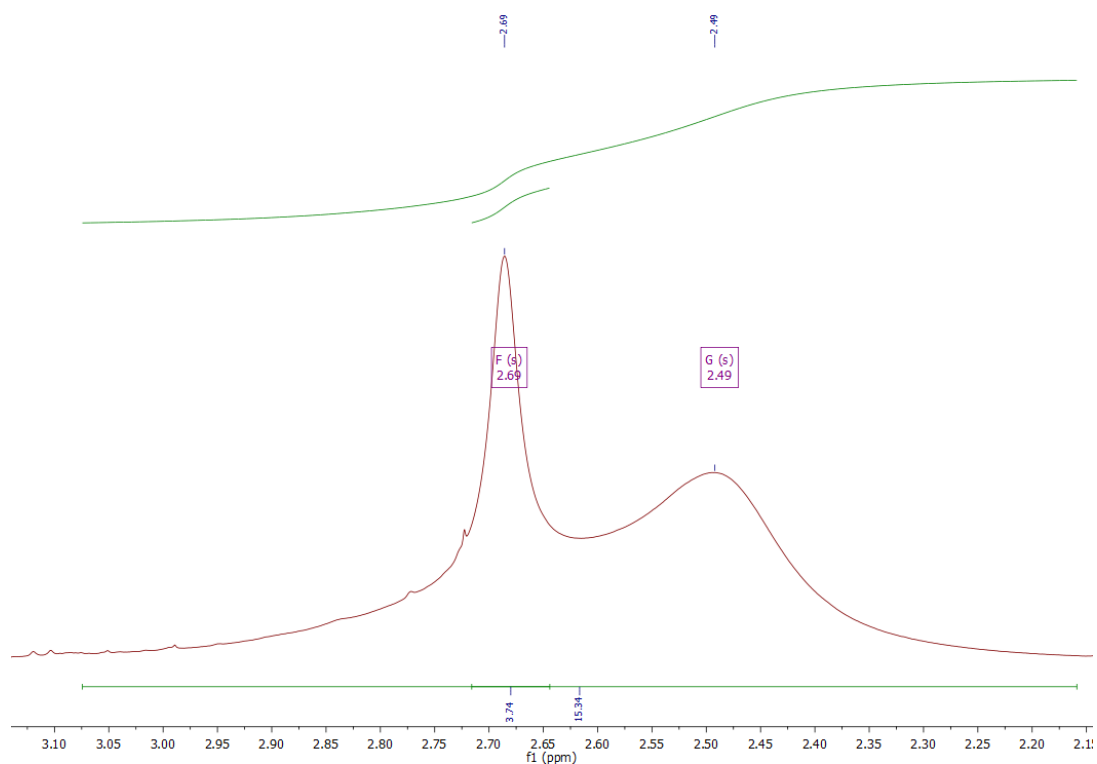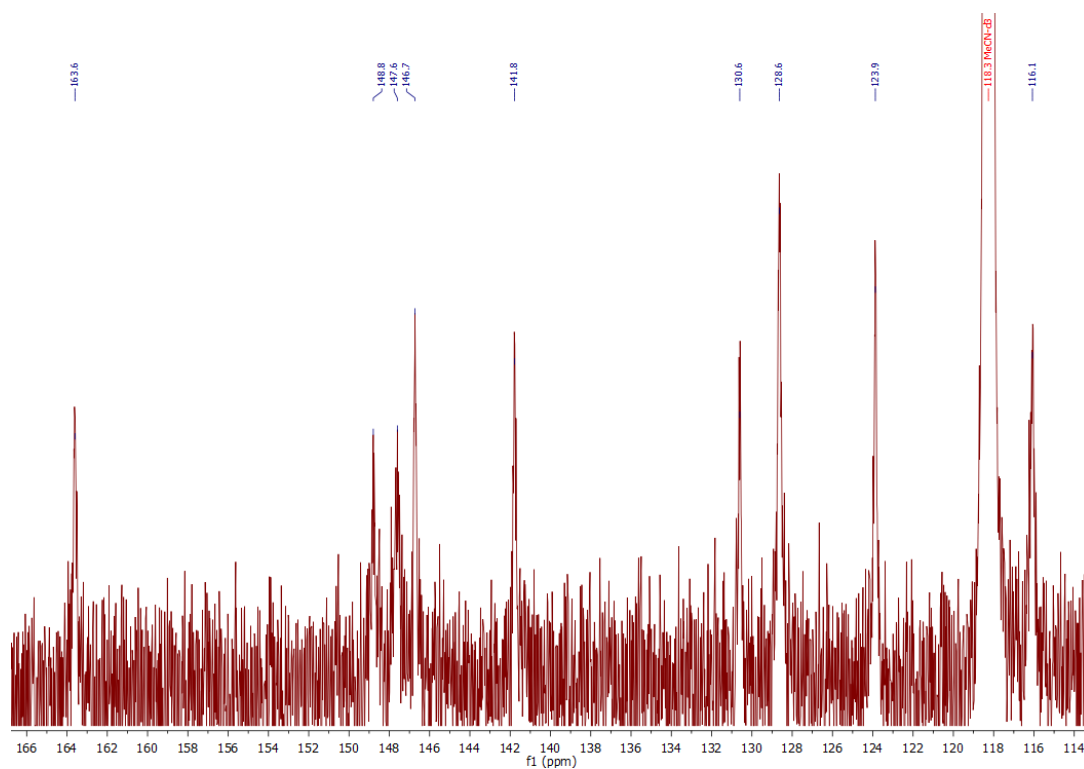

Fig. S27: Magnification of the ^{1}H NMR spectrum of [Cu(TMG4Mequ)$_2$]PF$_6$ (**C11−PF$_6$**) in MeCN-*d*3 (due to the limited solubility in MeCN and other solvents, it was not possible to measure NMR spectra with a better S/N ratio).

Fig. S28: $^{13}C\{^1H\}$ NMR spectrum of [Cu(TMG4Mequ)$_2$]PF$_6$ (**C11–PF$_6$**) in MeCN-*d*3 (due to the limited solubility in MeCN and other solvents, it was not possible to measure NMR spectra with a better S/N ratio).

Fig. S29: Magnification of the $^{13}C\{^1H\}$ NMR spectrum of [Cu(TMG4Mequ)$_2$]PF$_6$ (**C11–PF$_6$**) in MeCN-*d*3 (due to the limited solubility in MeCN and other solvents, it was not possible to measure NMR spectra with a better S/N ratio).

43

2.6.2 TMG4Meequ (L8) and corresponding precursors and Cu(I) complex

2.6.2.1 Methyl quinoline-4-carboxylate (4-Mee-qu)

^{1}H NMR (400 MHz, Chloroform-*d*) δ 9.02 (d, *J* = 4.4 Hz, 1H), 8.77 (ddd, *J* = 8.5, 1.4, 0.6 Hz, 1H), 8.18 (ddd, *J* = 8.4, 1.4, 0.7 Hz, 1H), 7.91 (d, *J* = 4.4 Hz, 1H), 7.78 (ddd, *J* = 8.4, 6.9, 1.4 Hz, 1H), 7.67 (ddd, *J* = 8.4, 6.8, 1.4 Hz, 1H), 4.05 (s, 3H).
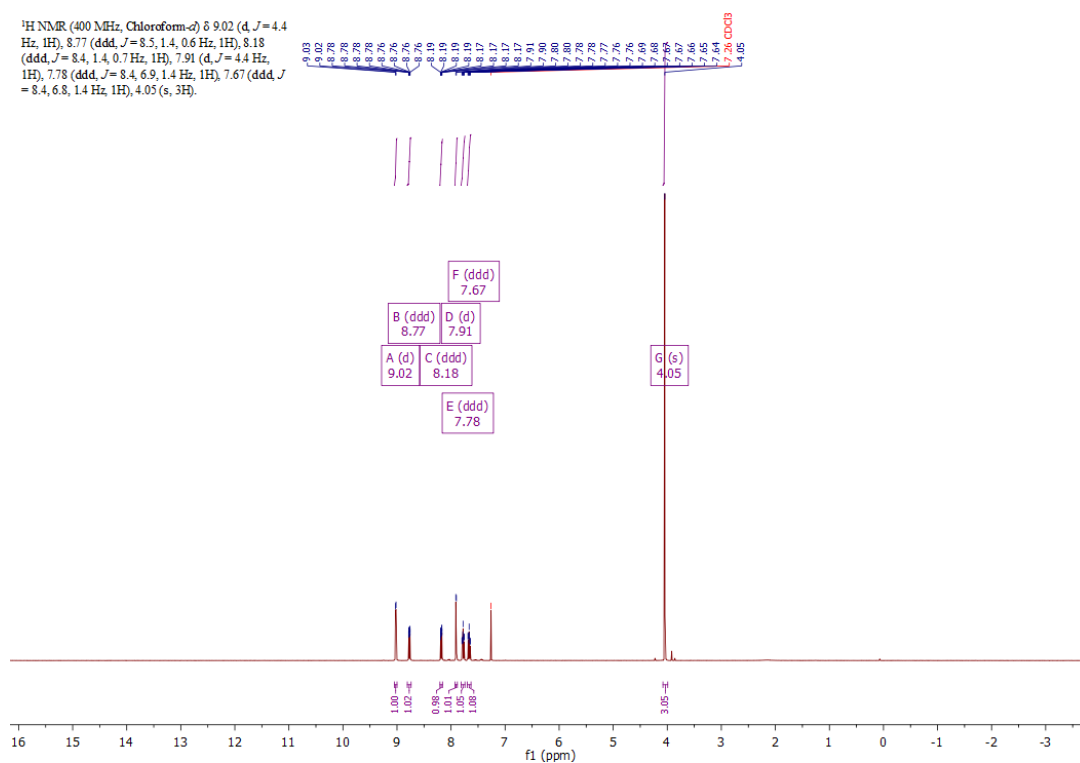
Fig. S30: ^{1}H NMR spectrum of 4-Mee-qu in CDCl$_3$.

Fig. S31: Magnification of the ^{1}H NMR spectrum of 4-Mee-qu in CDCl$_3$.

¹³C NMR (101 MHz, CDCl₃) δ 166.8, 149.9, 149.3, 135.0, 130.2, 129.9, 128.4, 125.8, 125.3, 122.4, 52.9.
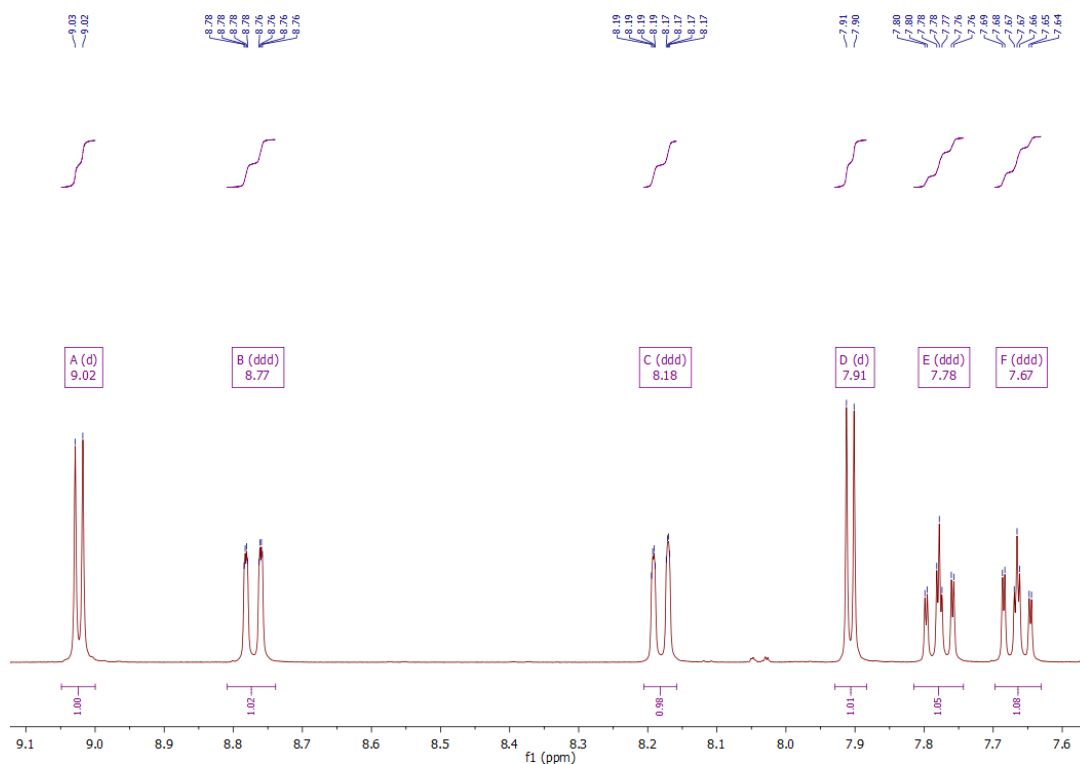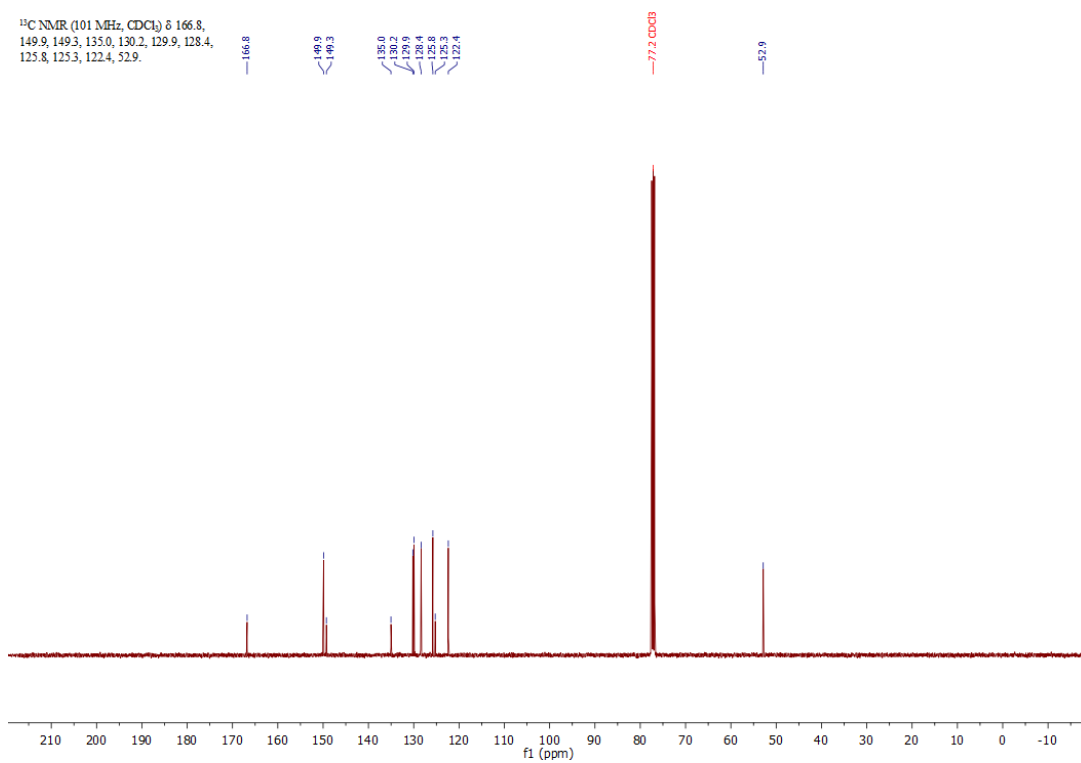
Fig. S32: ¹³C{¹H} NMR spectrum of 4-Mee-qu in CDCl₃.
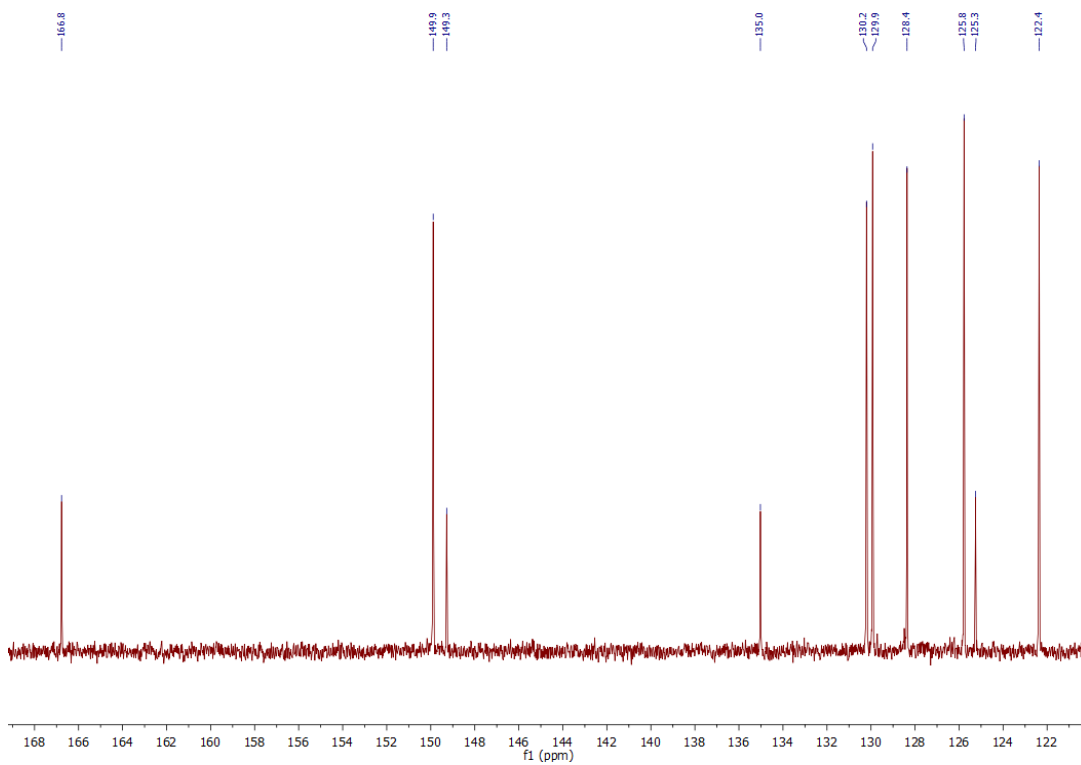
Fig. S33: Magnification of the ¹³C{¹H} NMR spectrum of 4-Mee-qu in CDCl₃.

45

2.6.2.2 Methyl 8-nitroquinoline-4-carboxylate (4-Mee-8-NO₂-qu)

^{1}H NMR (400 MHz, Chloroform-*d*) δ 9.16 (d, *J* = 4.4 Hz, 1H), 9.05 (dd, *J* = 8.8, 1.3 Hz, 1H), 8.06 (d, *J* = 4.4 Hz, 1H), 8.04 (dd, *J* = 7.5, 1.3 Hz, 1H), 7.73 (dd, *J* = 8.8, 7.5 Hz, 1H), 4.07 (s, 3H).
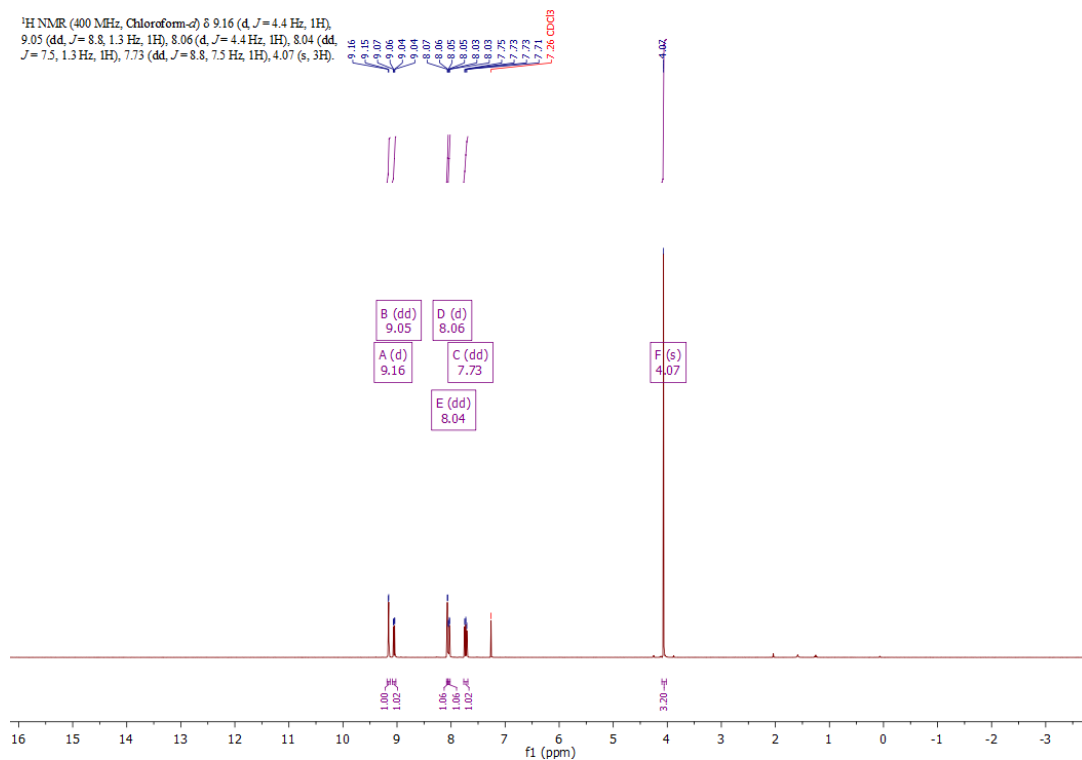
Fig. S34: ^{1}H NMR spectrum of 4-Mee-8-NO₂-qu in CDCl₃.
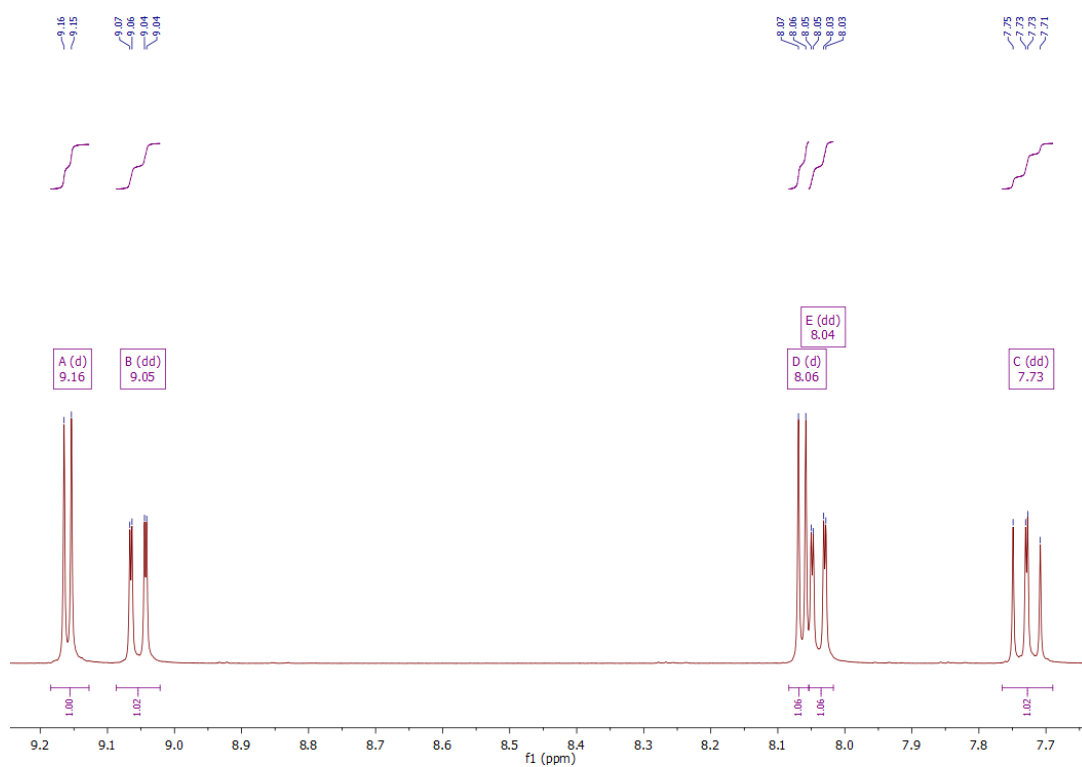
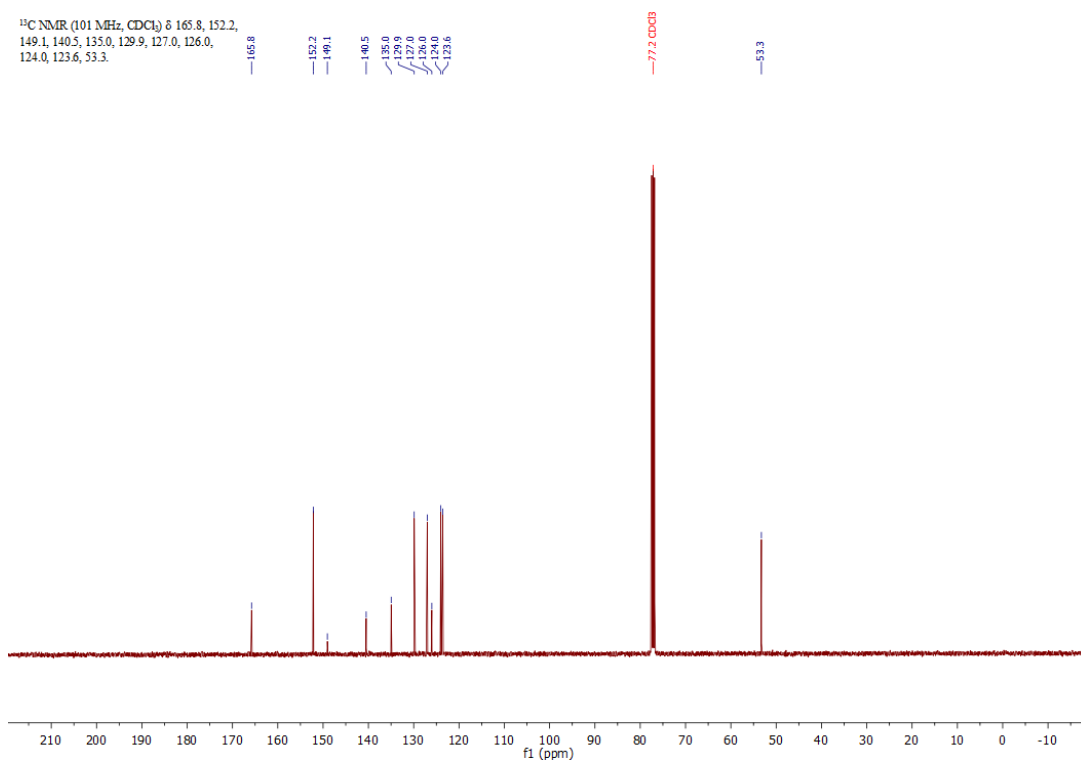Fig. S35: Magnification of the ^{1}H NMR spectrum of 4-Mee-8-NO₂-qu in CDCl₃.
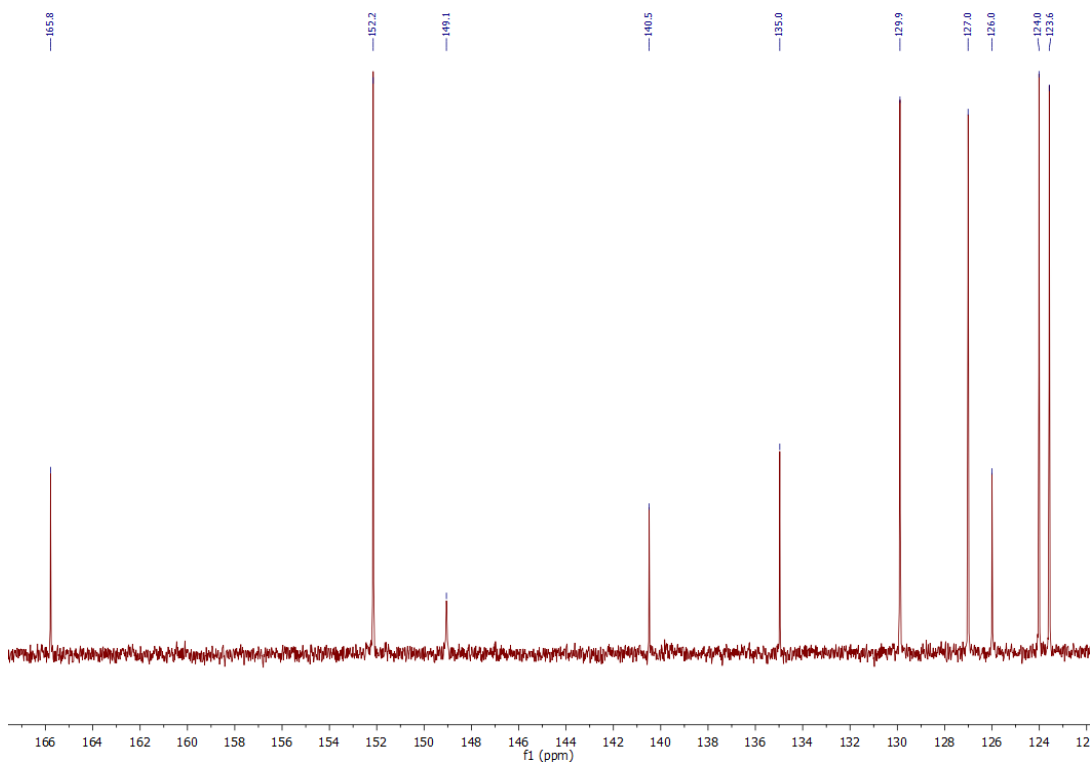
Fig. S36: $^{13}C\{^1H\}$ NMR spectrum of 4-Mee-8-NO_2-qu in $CDCl_3$.

Fig. S37: Magnification of the $^{13}C\{^1H\}$ NMR spectrum of 4-Mee-8-NO_2-qu in $CDCl_3$.

2.6.2.3 Methyl 5-nitroquinoline-4-carboxylate (4-Mee-5-NO₂-qu)

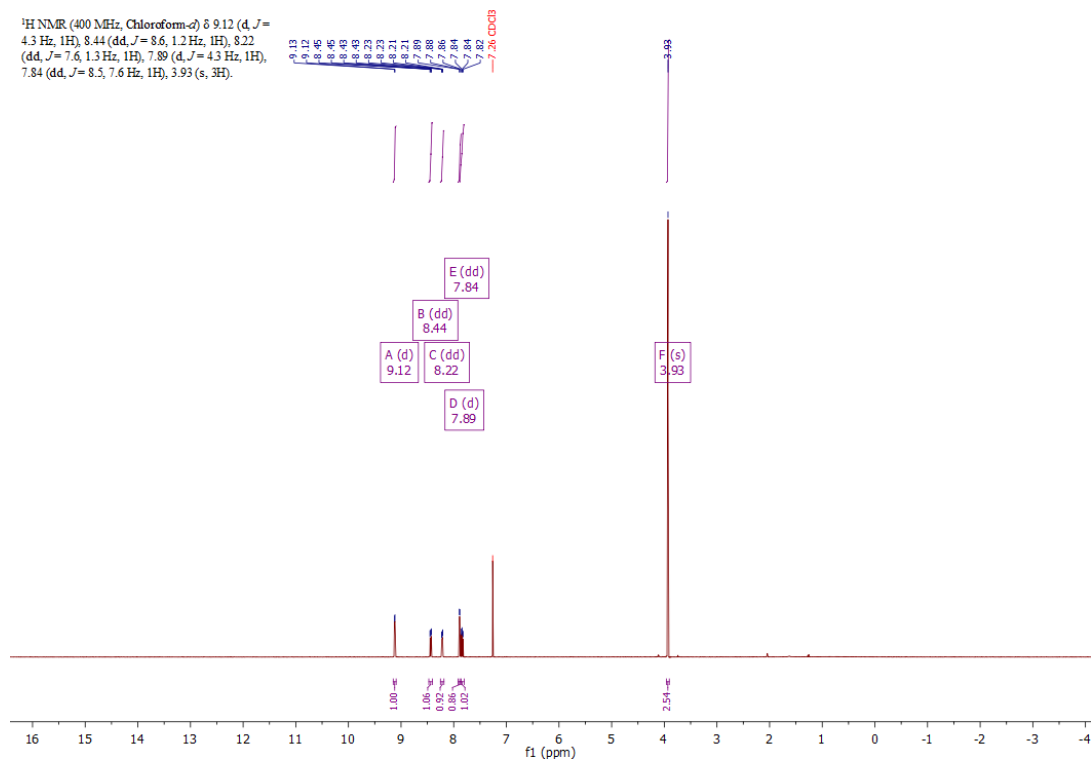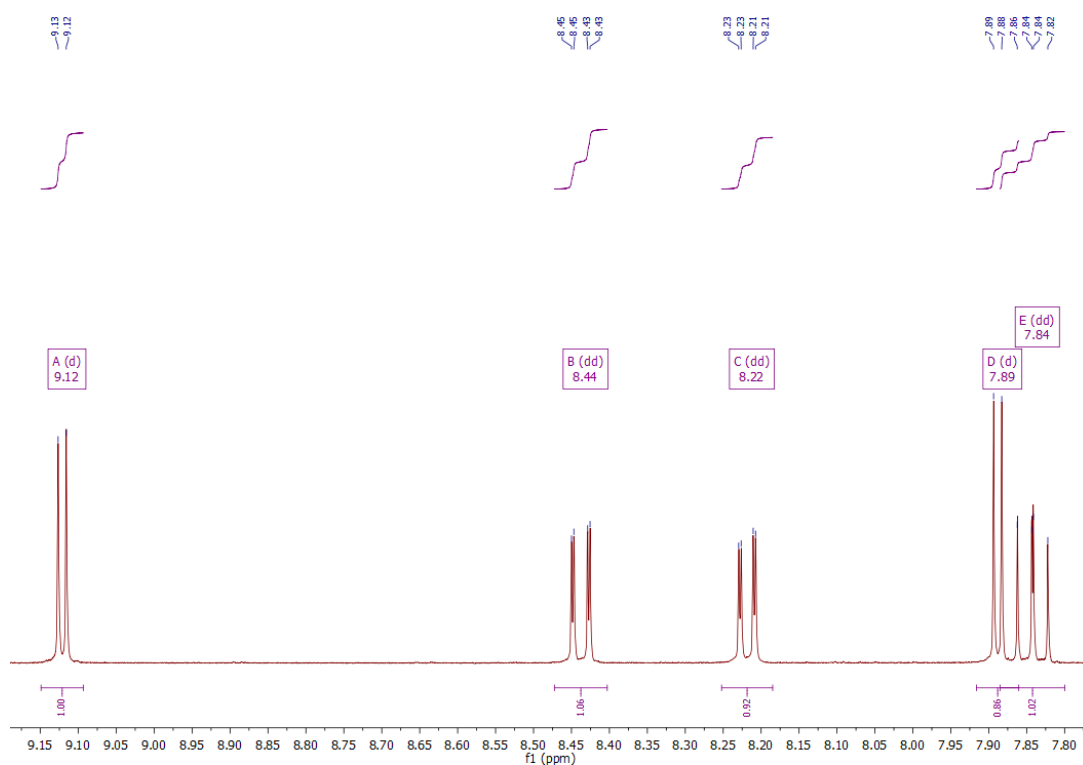1H NMR (400 MHz, Chloroform-*d*) δ 9.12 (d, *J* = 4.3 Hz, 1H), 8.44 (dd, *J* = 8.6, 1.2 Hz, 1H), 8.22 (dd, *J* = 7.6, 1.3 Hz, 1H), 7.89 (d, *J* = 4.3 Hz, 1H), 7.84 (dd, *J* = 8.5, 7.6 Hz, 1H), 3.93 (s, 3H).

Fig. S38: ^{1}H NMR spectrum of 4-Mee-5-NO₂-qu in CDCl₃.

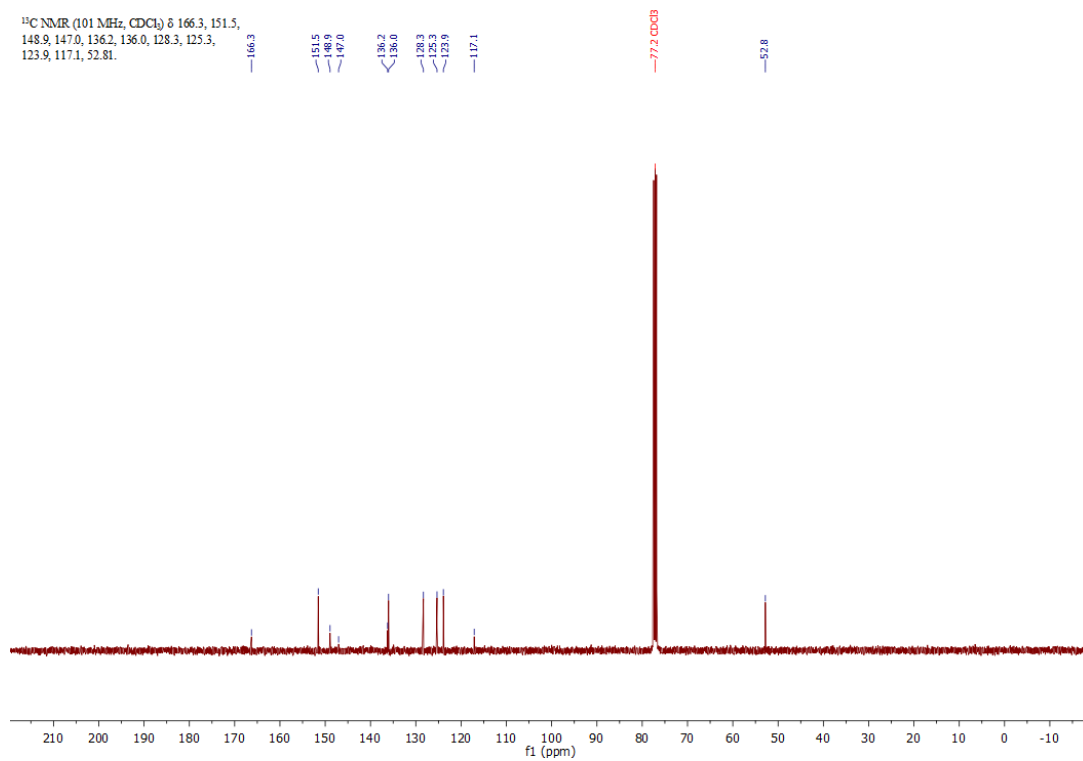Fig. S39: Magnification of the ^{1}H NMR spectrum of 4-Mee-5-NO₂-qu in CDCl₃.

48

¹³C NMR (101 MHz, CDCl₃) δ 166.3, 151.5, 148.9, 147.0, 136.2, 136.0, 128.3, 125.3, 123.9, 117.1, 52.81.

Fig. S40: ¹³C{¹H} NMR spectrum of 4-Mee-5-NO₂-qu in CDCl₃.
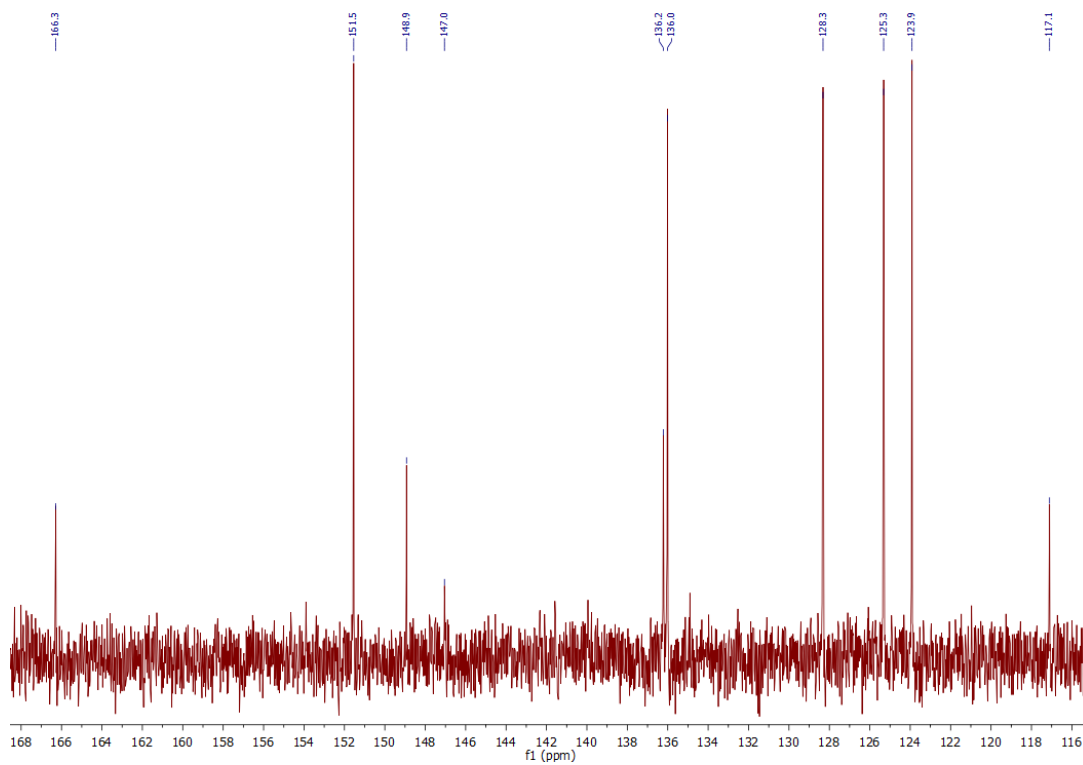
Fig. S41: Magnification of the ¹³C{¹H} NMR spectrum of 4-Mee-5-NO₂-qu in CDCl₃.
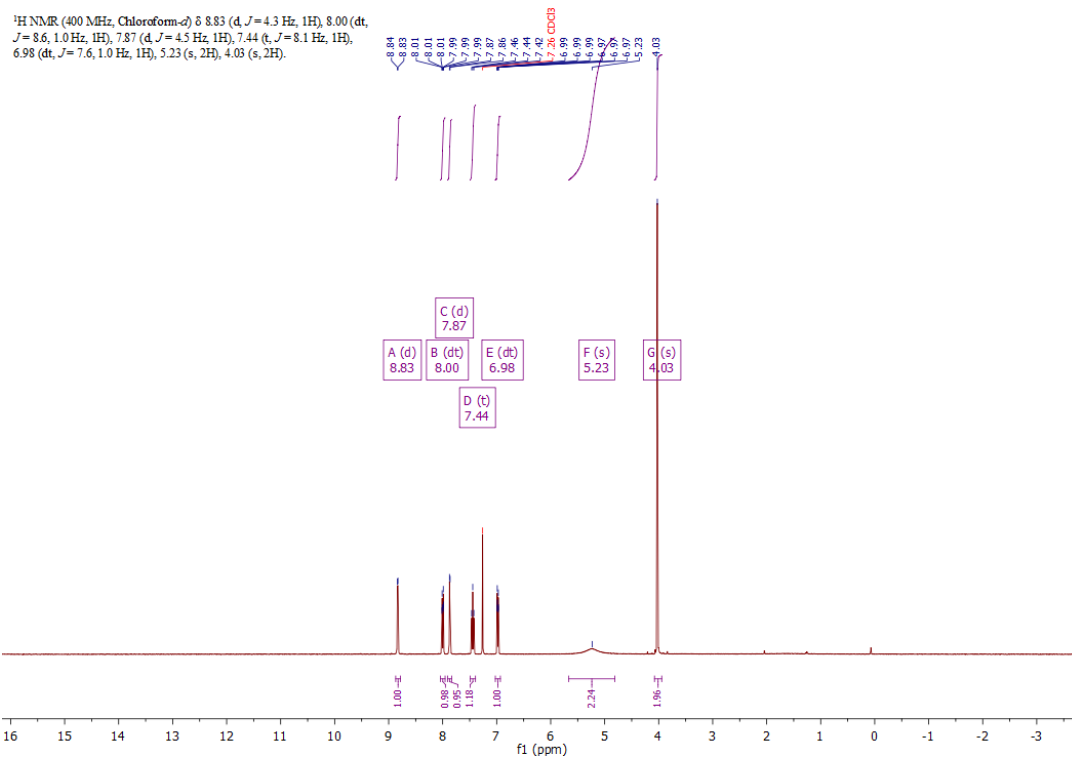
2.6.2.4 Methyl 8-aminoquinoline-4-carboxylate (4-Mee-8-NH₂-qu)
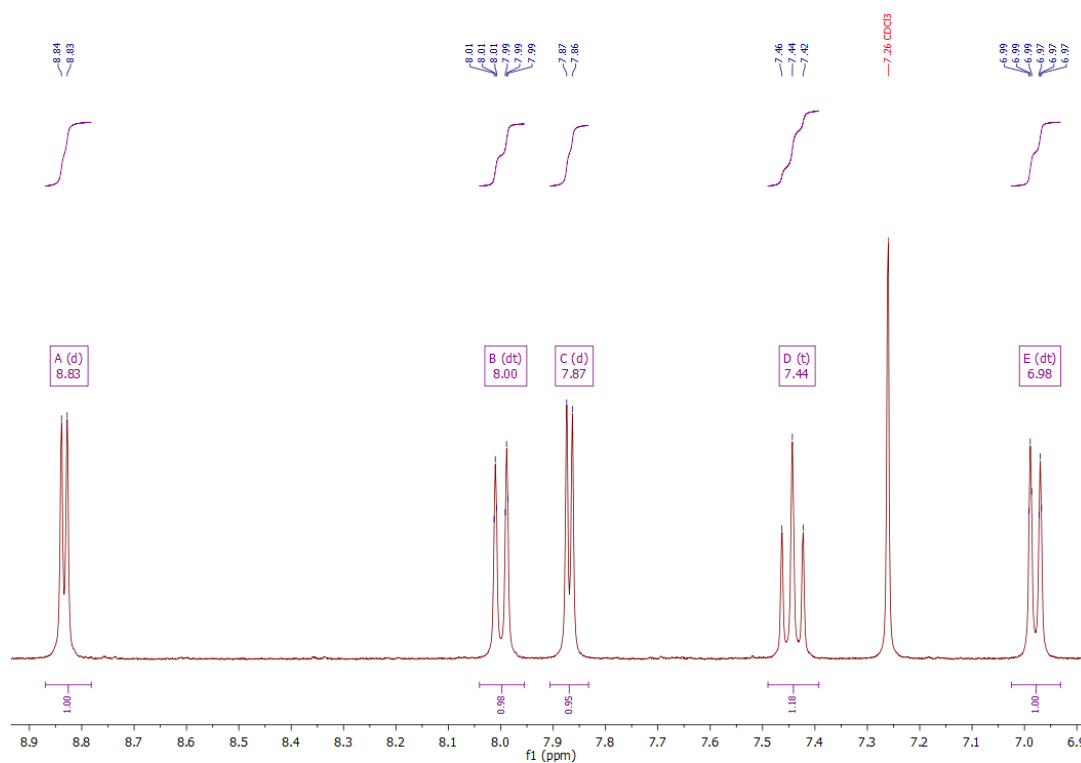
Fig. S42: ¹H NMR spectrum of 4-Mee-8-NH₂-qu in CDCl₃.

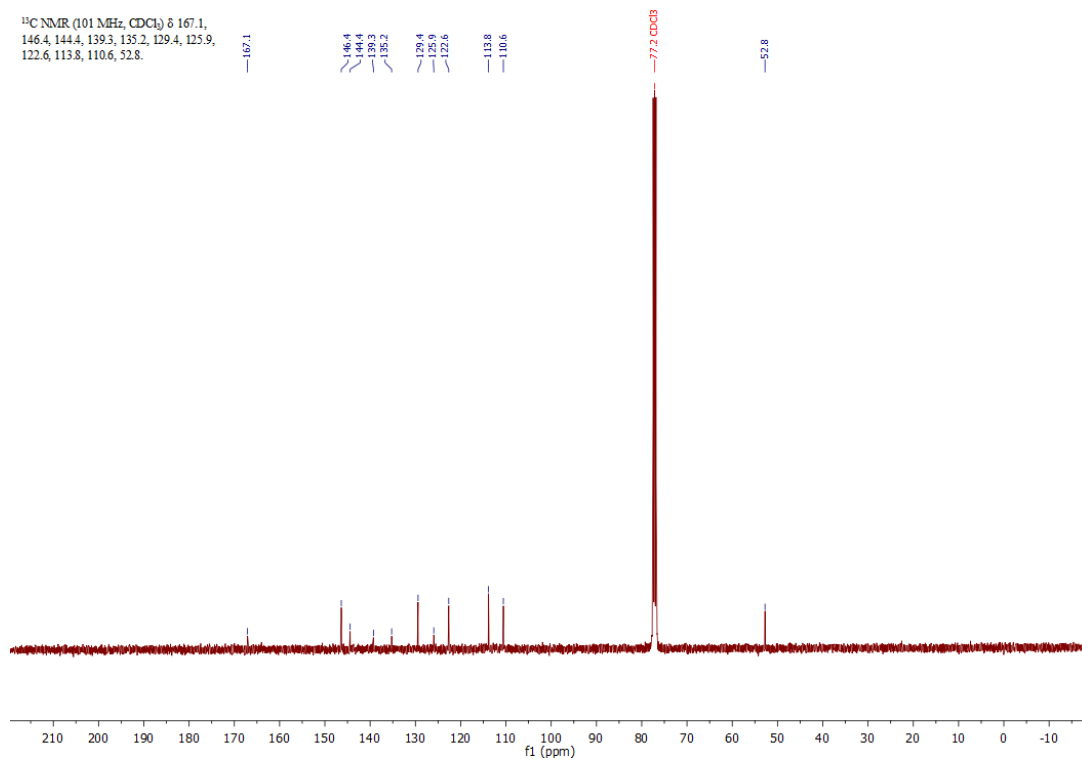Fig. S43: Magnification of the ¹H NMR spectrum of 4-Mee-8-NH₂-qu in CDCl₃.

^{13}C NMR (101 MHz, CDCl$_3$) δ 167.1, 146.4, 144.4, 139.3, 135.2, 129.4, 125.9, 122.6, 113.8, 110.6, 52.8.

Fig. S44: $^{13}C\{^1H\}$ NMR spectrum of 4-Mee-8-NH$_2$-qu in CDCl$_3$.
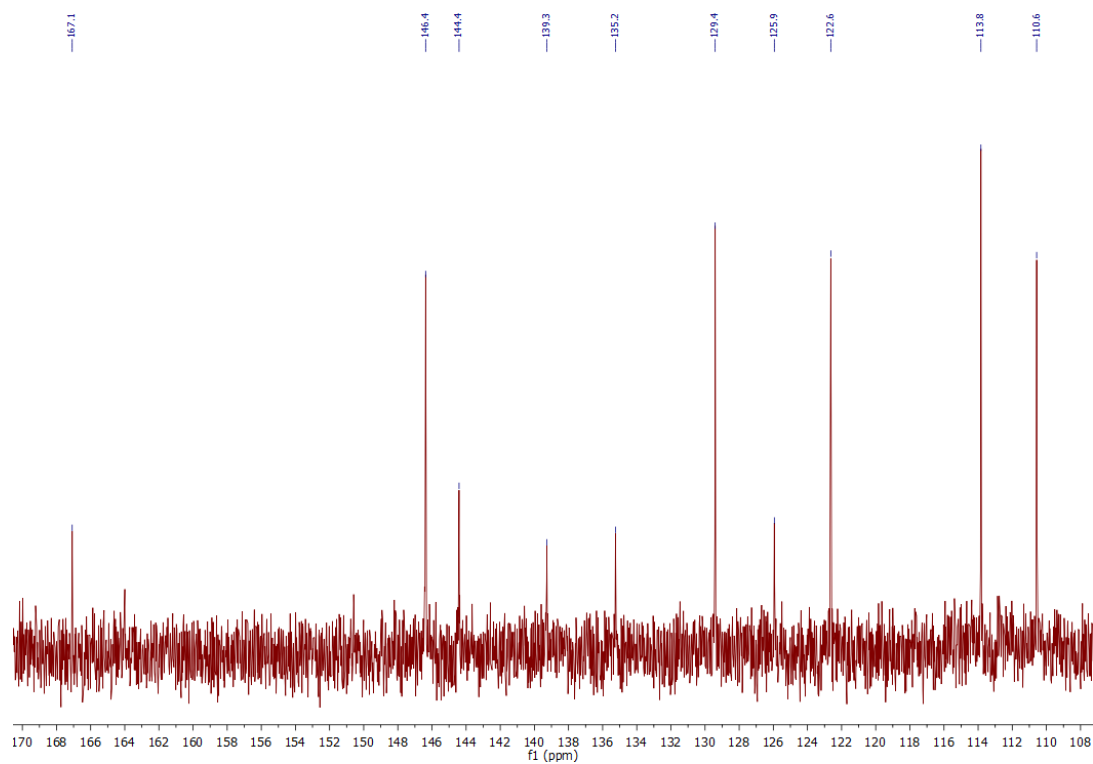

Fig. S45: Magnification of the $^{13}C\{^1H\}$ NMR spectrum of 4-Mee-8-NH$_2$-qu in CDCl$_3$.

2.6.2.5 TMG4Meequ (L8)

^{1}H NMR (400 MHz, Chloroform-*d*) δ 8.90 (d, *J* = 4.3 Hz, 1H), 8.11 (dd, *J* = 8.5, 1.3 Hz, 1H), 7.75 (d, *J* = 4.3 Hz, 1H), 7.47 (dd, *J* = 8.5, 7.5 Hz, 1H), 6.90 (dd, *J* = 7.5, 1.3 Hz, 1H), 4.00 (s, 3H), 2.70 (s, 12H).
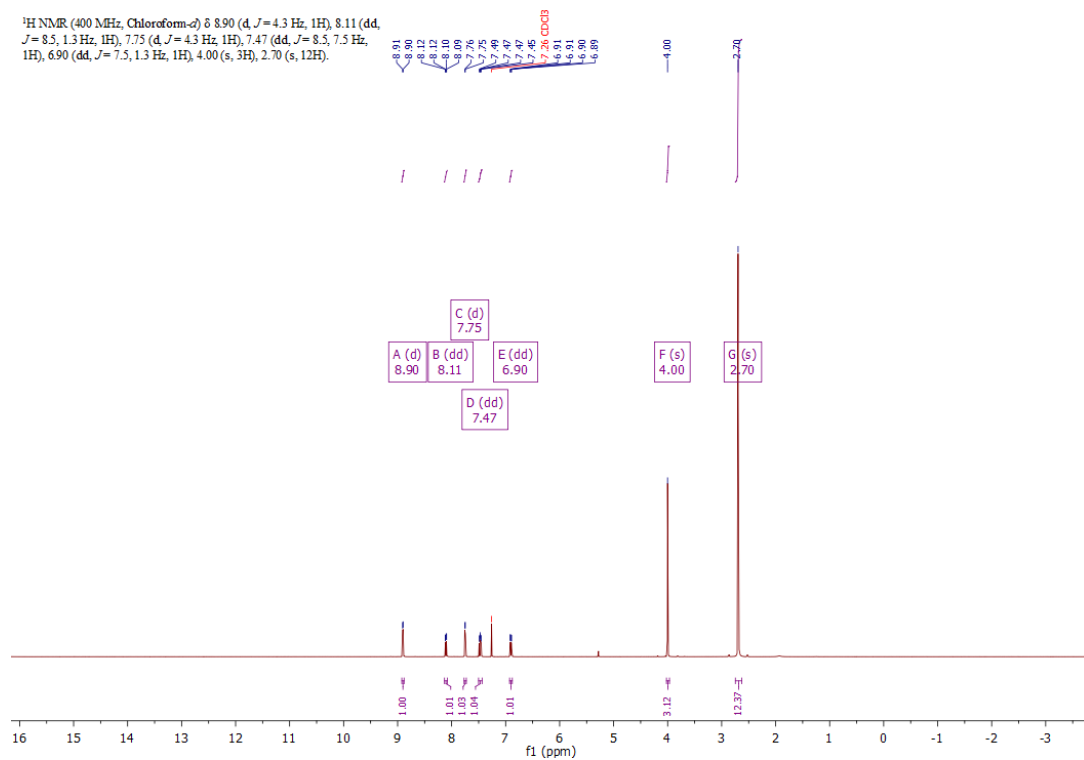

Fig. S46: ^{1}H NMR spectrum of TMG4Meequ (**L8**) in CDCl₃.

Fig. S47: Magnification of the ^{1}H NMR spectrum of TMG4Meequ (**L8**) in CDCl₃.

^{13}C NMR (101 MHz, CDCl$_3$) δ 167.5, 161.9, 150.8, 147.6, 144.0, 134.9, 129.0, 126.2, 121.8, 119.4, 116.2, 52.6, 39.6.
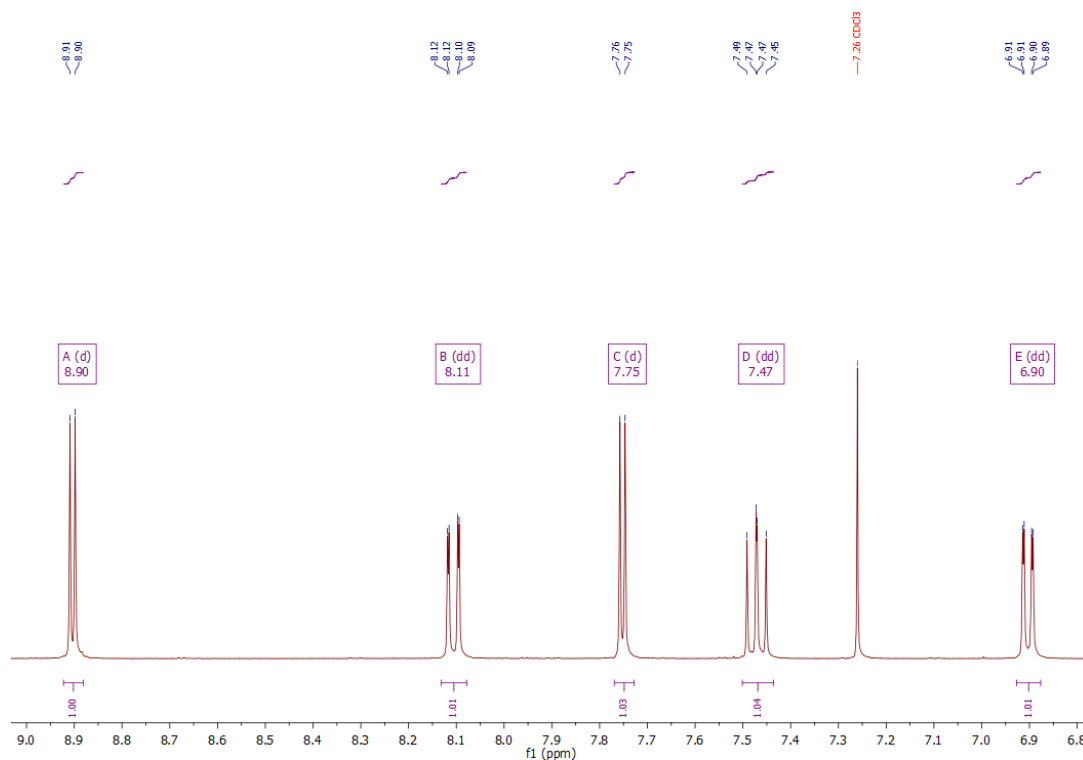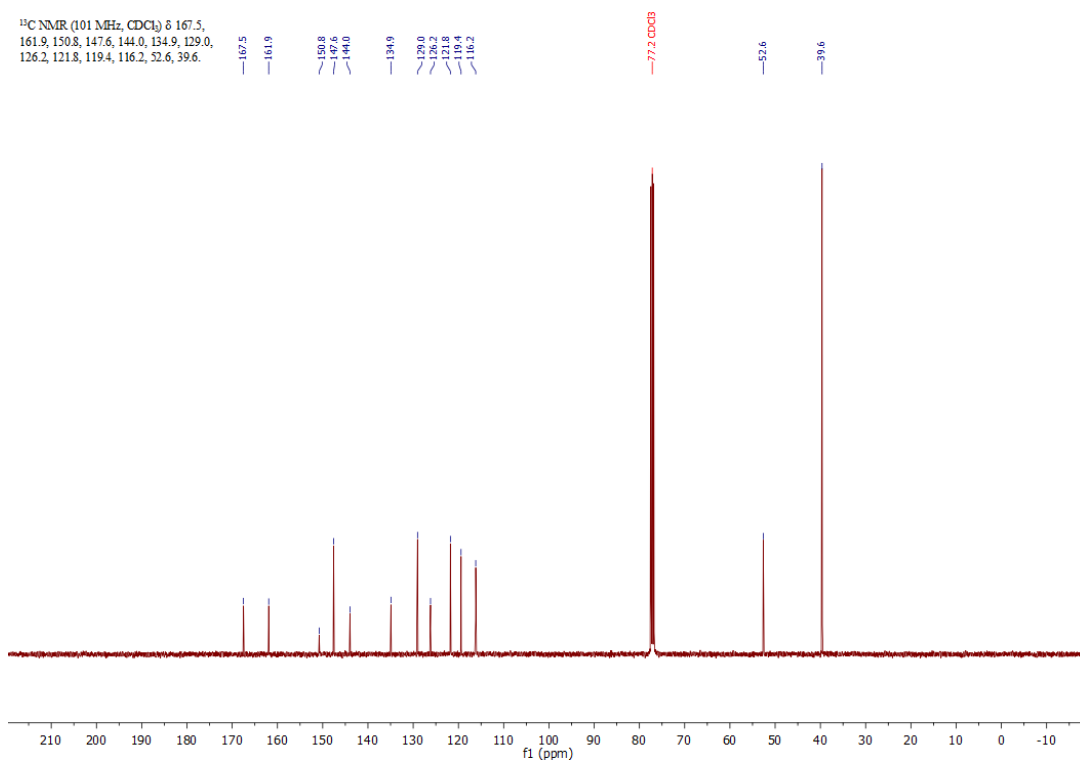
Fig. S48: ^{13}C{^{1}H} NMR spectrum of TMG4Meequ (**L8**) in CDCl$_3$.

Fig. S49: Magnification of the ^{13}C{^{1}H} NMR spectrum of TMG4Meequ (**L8**) in CDCl$_3$.

53

2.6.2.6 [Cu(TMG4Meequ)₂]PF₆ (C13−PF₆)

¹H NMR (400 MHz, MeCN-d3) δ 8.59 (s, 1H), 8.19 (d, J = 8.5 Hz, 1H), 7.97 − 7.88 (m, 1H), 7.64 (t, J = 8.1 Hz, 1H), 6.97 (d, J = 7.6 Hz, 1H), 4.00 (s, 3H), 2.52 (s, 12H).
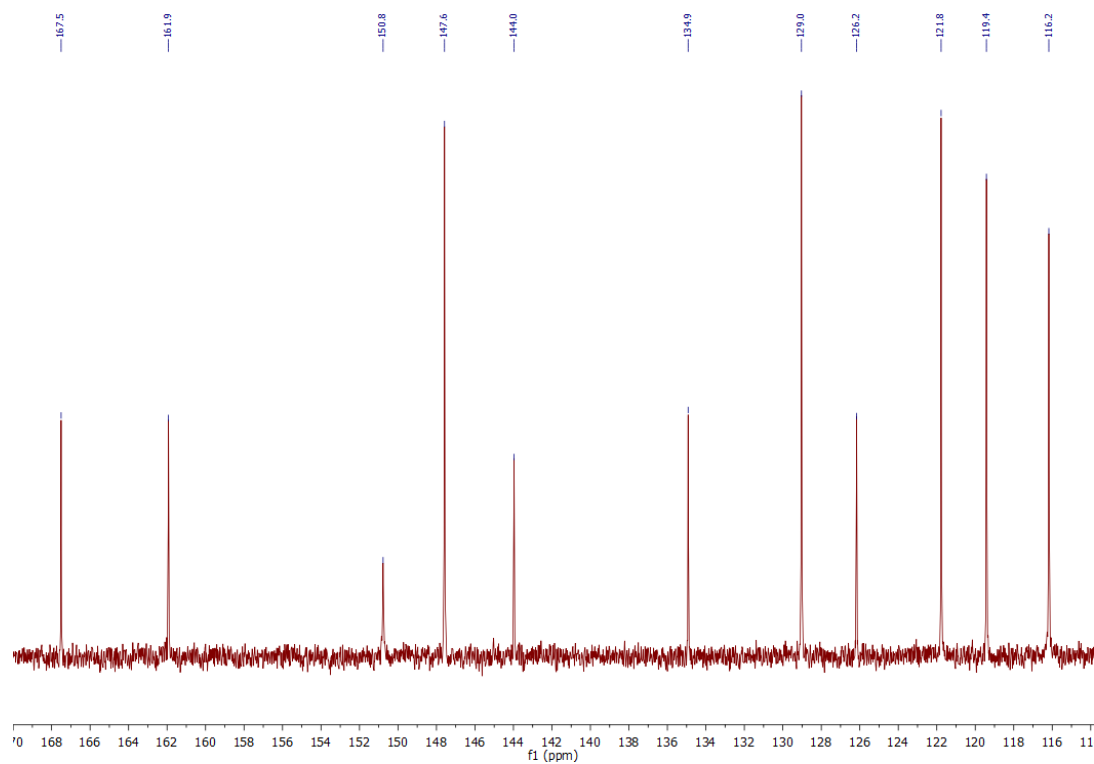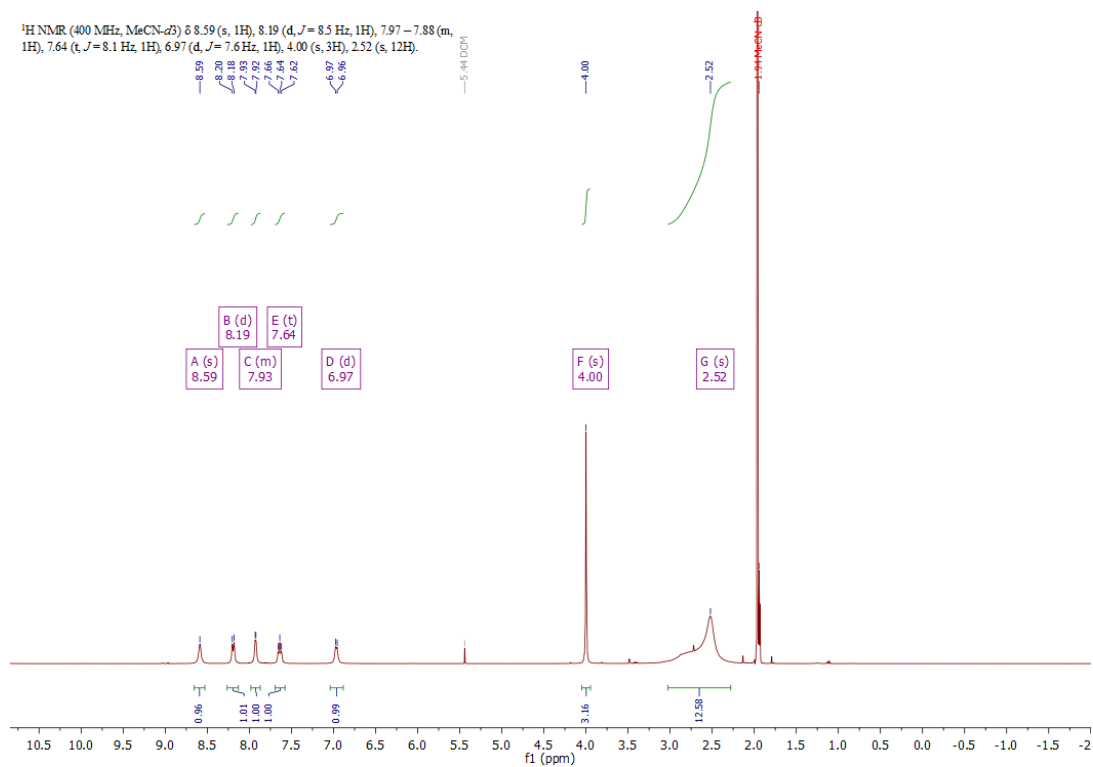
Fig. S50: ¹H NMR spectrum of [Cu(TMG4Meequ)₂]PF₆ (**C13−PF₆**) in MeCN-d3.

Fig. S51: Magnification of the ¹H NMR spectrum of [Cu(TMG4Meequ)₂]PF₆ (**C13−PF₆**) in MeCN-d3.

^{13}C NMR (101 MHz, MeCN-$d3$) δ 167.4, 164.0, 148.7, 146.9, 143.1, 136.3, 130.5, 127.8, 124.8, 118.9, 117.3, 53.6, 39.9.
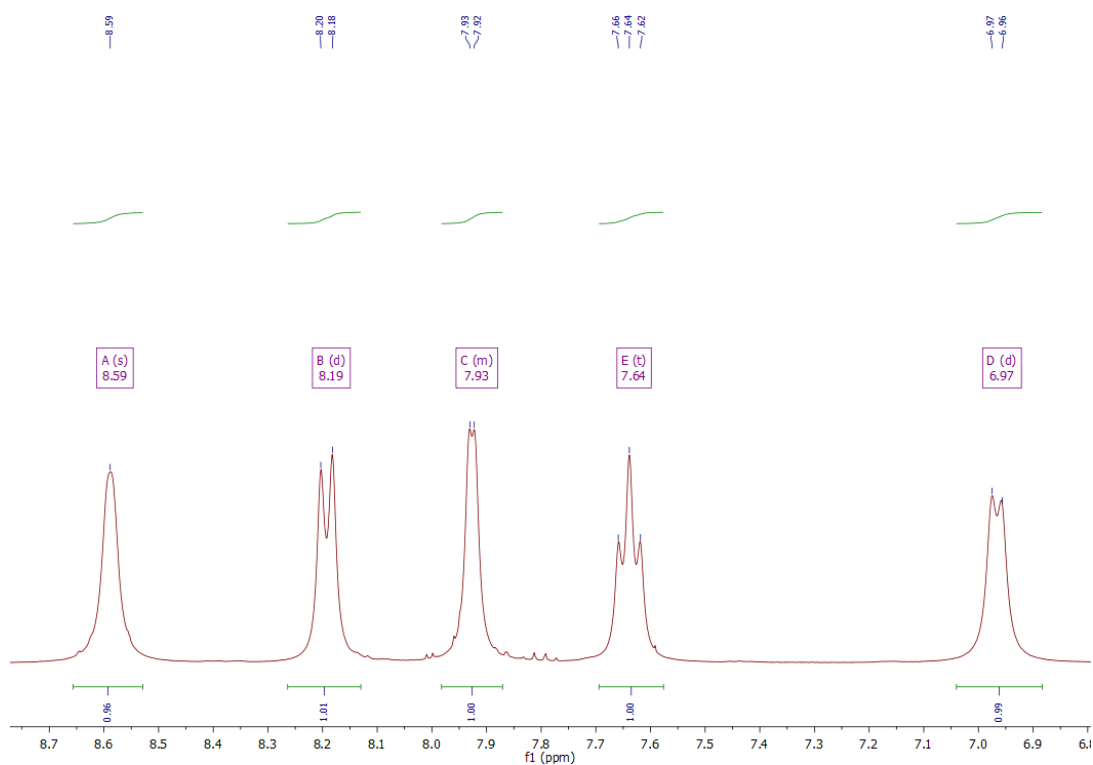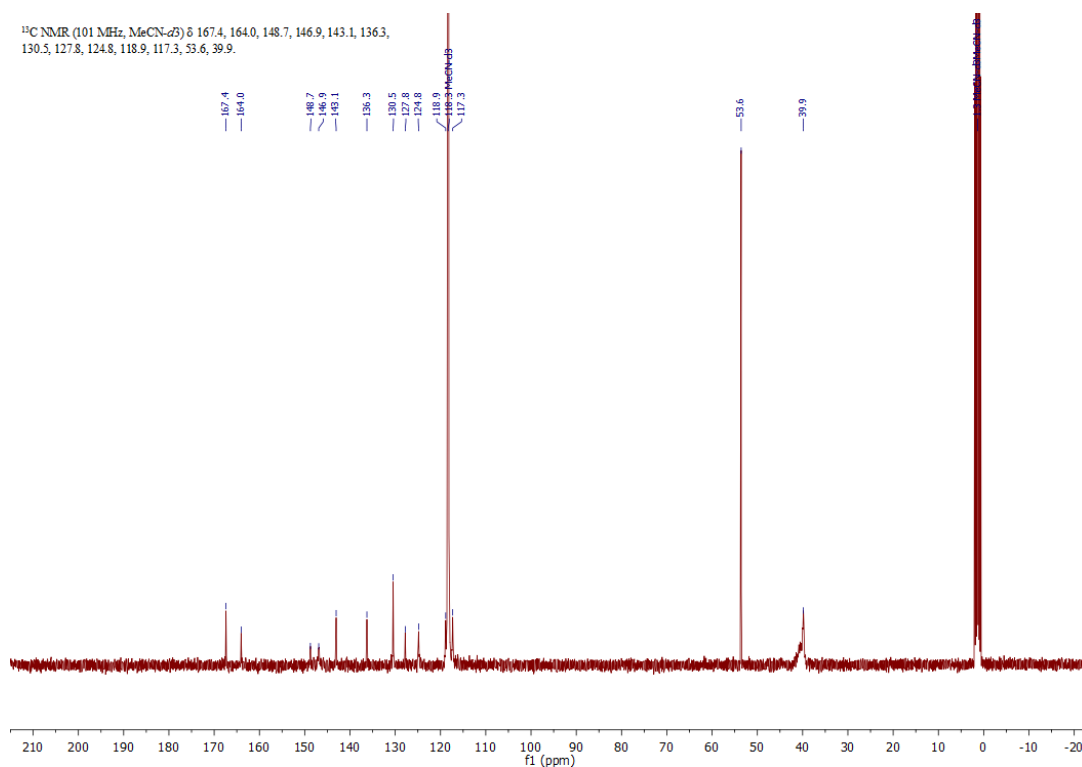
Fig. S52: ^{13}C{^{1}H} NMR spectrum of [Cu(TMG4Meequ)$_2$]PF$_6$ (**C13–PF$_6$**) in MeCN-d3.
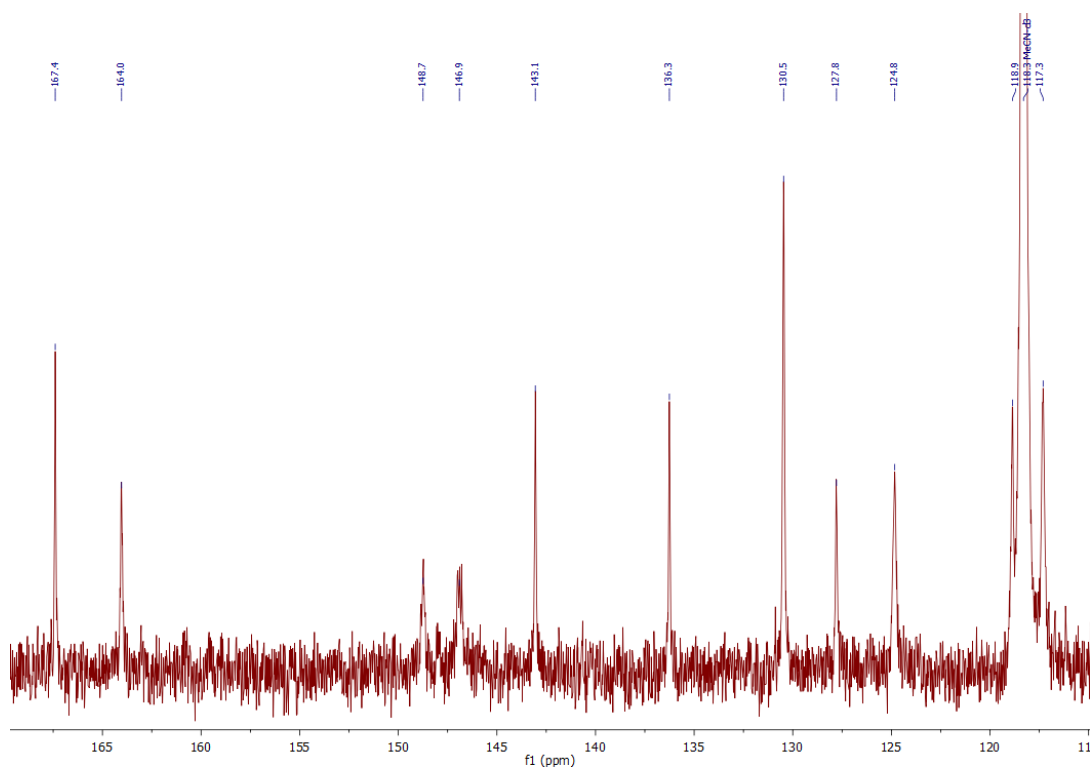
Fig. S53: Magnification of the ^{13}C{^{1}H} NMR spectrum of [Cu(TMG4Meequ)$_2$]PF$_6$ (**C13–PF$_6$**) in MeCN-d3.

55

3 Literature

[1] J. Leonard, B. Lygo, G. Procter, *Praxis der organischen Chemie*. *Ein Handbuch*, Wiley-VCH, Weinheim, **1996**.

[2] a) G. J. Kubas, B. Monzyk, A. L. Crumbliss, *Inorg. Synth.* **1979**, 90; b) B. J. Hathaway, D. G. Holah, A. E. Underhill, *J. Chem. Soc.* **1962**, 2444; c) B. J. Hathaway, D. G. Holah, J. D. Postlethwaite, *J. Chem. Soc.* **1961**, 3215; d) A. Hoffmann, J. Börner, U. Flörke, S. Herres-Pawlis, *Inorg. Chim. Acta* **2009**, *362*, 1185.

[3] W. Kantlehner, E. Haug, W. W. Mergen, P. Speh, T. Maier, J. J. Kapassakalidis, H.-J. Bräuner, H. Hagen, *Liebigs Ann. Chem.* **1984**, *1984*, 108.

[4] G. R. Fulmer, A. J. M. Miller, N. H. Sherden, H. E. Gottlieb, A. Nudelman, B. M. Stoltz, J. E. Bercaw, K. I. Goldberg, *Organometallics* **2010**, *29*, 2176.

[5] P. Tremouilhac, P.-C. Huang, C.-L. Lin, Y.-C. Huang, A. Nguyen, N. Jung, F. Bach, S. Bräse, *Chem. - Methods* **2021**, *1*, 8.

[6] P. Tremouilhac, C.-L. Lin, P.-C. Huang, Y.-C. Huang, A. Nguyen, N. Jung, F. Bach, R. Ulrich, B. Neumair, A. Streit, S. Bräse, *Angew. Chem. Int. Ed.* **2020**, *59*, 22771; *Angew. Chem.* **2020**, *132*, 22960.

[7] *X-Area Pilatus3_SV 1.31.131.0*, STOE, **2017**.

[8] *X-Area Pecipe 1.33.0.0*, STOE, **2015**.

[9] *X-Area Integrate 1.71.0.0*, STOE, **2016**.

[10] *X-Area LANA 1.74.4.0*, STOE, **2017**.

[11] G. M. Sheldrick, *Acta Crystallogr., Sect. A* **2015**, *71*, 3.

[12] G. M. Sheldrick, *Acta Crystallogr., Sect. A* **2008**, *64*, 112.

[13] G. M. Sheldrick, *Acta Crystallogr., Sect. C* **2015**, *71*, 3.

[14] C. B. Hübschle, G. M. Sheldrick, B. Dittrich, *J. Appl. Crystallogr.* **2011**, *44*, 1281.

[15] A. L. Spek, *PLATON, A Multipurpose Crystallographic Tool*, Utrecht University, Utrecht, The Netherlands, **2008**.

[16] A. L. Spek, *Acta Crystallogr., Sect. D* **2009**, *65*, 148.

[17] a) H. Chen, P. Li, M. Wang, L. Wang, *Eur. J. Org. Chem.* **2018**, *2018*, 2091; b) S. Lutun, E. Guichard, B. Hasiak, D. Couturier, *Synth. Commun.* **1999**, *29*, 175.

[18] O. H. Johnson, C. S. Hamilton, *J. Am. Chem. Soc.* **1941**, *63*, 2864.

[19] T. Rösener, A. Hoffmann, S. Herres-Pawlis, *Eur. J. Inorg. Chem.* **2018**, *2018*, 3164.

[20]   S. Herres-Pawlis, A. Neuba, O. Seewald, T. Seshadri, H. Egold, U. Flörke, G. Henkel, *Eur. J. Org. Chem.* **2005**, *2005*, 4879.

[21]   J. Heck, F. Metz, S. Buchenau, M. Teubner, B. Grimm-Lebsanft, T. P. Spaniol, A. Hoffmann, M. A. Rübhausen, S. Herres-Pawlis, *Chem. Sci.* **2022**, *13*, 8274.

[22]   M. J. Frisch, G. W. Trucks, H. B. Schlegel, G. E. Scuseria, M. A. Robb, J. R. Cheeseman, G. Scalmani, V. Barone, G. A. Petersson, H. Nakatsuji, X. Li, M. Caricato, A. V. Marenich, J. Bloino, B. G. Janesko, R. Gomperts, B. Mennucci, H. P. Hratchian, J. V. Ortiz, A. F. Izmaylov, J. L. Sonnenberg, Williams, F. Ding, F. Lipparini, F. Egidi, J. Goings, B. Peng, A. Petrone, T. Henderson, D. Ranasinghe, V. G. Zakrzewski, J. Gao, N. Rega, G. Zheng, W. Liang, M. Hada, M. Ehara, K. Toyota, R. Fukuda, J. Hasegawa, M. Ishida, T. Nakajima, Y. Honda, O. Kitao, H. Nakai, T. Vreven, K. Throssell, J. A. Montgomery Jr., J. E. Peralta, F. Ogliaro, M. J. Bearpark, J. J. Heyd, E. N. Brothers, K. N. Kudin, V. N. Staroverov, T. A. Keith, R. Kobayashi, J. Normand, K. Raghavachari, A. P. Rendell, J. C. Burant, S. S. Iyengar, J. Tomasi, M. Cossi, J. M. Millam, M. Klene, C. Adamo, R. Cammi, J. W. Ochterski, R. L. Martin, K. Morokuma, O. Farkas, J. B. Foresman, D. J. Fox, *Gaussian 16, Revision B.01*, Gaussian, Inc., Wallingford, CT, **2016**.

[23]   a) J. Tao, J. P. Perdew, V. N. Staroverov, G. E. Scuseria, *Phys. Rev. Lett.* **2003**, *91*, 146401; b) V. N. Staroverov, G. E. Scuseria, J. Tao, J. P. Perdew, *J. Chem. Phys.* **2003**, *119*, 12129.

[24]   A. Schäfer, C. Huber, R. Ahlrichs, *J. Chem. Phys.* **1994**, *100*, 5829.

[25]   K. Eichkorn, F. Weigend, O. Treutler, R. Ahlrichs, *Theor. Chem. Acc.* **1997**, *97*, 119.

[26]   F. Weigend, R. Ahlrichs, *Phys. Chem. Chem. Phys.* **2005**, *7*, 3297.

[27]   a) S. Grimme, S. Ehrlich, L. Goerigk, *J. Comput. Chem.* **2011**, *32*, 1456; b) L. Goerigk, S. Grimme, *Phys. Chem. Chem. Phys.* **2011**, *13*, 6670; c) A. Hoffmann, R. Grunzke, S. Herres-Pawlis, *J. Comput. Chem.* **2014**, *35*, 1943.

[28]   a) E. D. Glendening, J. K. Badenhoop, A. E. Reed, J. E. Carpenter, J. A. Bohmann, C. M. Morales, C. R. Landis, F. Weinhold, *NBO 6.0*, Theoretical Chemistry Institute, University of Wisconsin−Madison, Madison, **2013**; b) E. D. Glendening, C. R. Landis, F. Weinhold, *J. Comput. Chem.* **2013**, *34*, 1429; c) F. Weinhold, C. R. Landis, *Valency and Bonding: A Natural Bond Orbital Donor-Acceptor Perspective*, Cambridge University Press, Cambridge, **2005**.

[29]   P. Pracht, F. Bohle, S. Grimme, *Phys. Chem. Chem. Phys.* **2020**, *22*, 7169.

[30] C. Bannwarth, S. Ehlert, S. Grimme, *J. Chem. Theory Comput.* **2019**, *15*, 1652.

[31] F. Neese, *WIREs Comput. Mol. Sci.* **2012**, *2*, 73.

[32] F. Neese, *WIREs Comput. Mol. Sci.* **2022**, *12*, e1606.

[33] a) C. Riplinger, F. Neese, *J. Chem. Phys.* **2013**, *138*, 34106; b) M. Saitow, U. Becker, C. Riplinger, E. F. Valeev, F. Neese, *J. Chem. Phys.* **2017**, *146*, 164105; c) Y. Guo, C. Riplinger, U. Becker, D. G. Liakos, Y. Minenkov, L. Cavallo, F. Neese, *J. Chem. Phys.* **2018**, *148*, 11101; d) Y. Guo, C. Riplinger, D. G. Liakos, U. Becker, M. Saitow, F. Neese, *J. Chem. Phys.* **2020**, *152*, 24116; e) C. Riplinger, B. Sandhoefer, A. Hansen, F. Neese, *J. Chem. Phys.* **2013**, *139*, 134101.

[34] A. Hellweg, C. Hättig, S. Höfener, W. Klopper, *Theor. Chem. Acc.* **2007**, *117*, 587.

[35] V. Barone, M. Cossi, *J. Phys. Chem. A* **1998**, *102*, 1995.

[36] L. Yang, D. R. Powell, R. P. Houser, *Dalton Trans.* **2007**, 955.

[37] V. Raab, K. Harms, J. Sundermeyer, B. Kovacević, Z. B. Maksić, *J. Org. Chem.* **2003**, *68*, 8790.